THE UNIVERSITY OF CHICAGO

ON THE CONSTRUCTION AND DYNAMICS OF KNOTTED FIELDS

A DISSERTATION SUBMITTED TO
THE FACULTY OF THE DIVISION OF THE PHYSICAL SCIENCES
IN CANDIDACY FOR THE DEGREE OF
DOCTOR OF PHILOSOPHY

DEPARTMENT OF PHYSICS

BY
HRIDESH KEDIA

CHICAGO, ILLINOIS
JUNE 2017

To my parents.

"Remember that the fool in the eyes of the gods and the fool in the eyes of man are very different. One who is entirely ignorant of the modes of Art in its revolution or the moods of thought in its progress, of the pomp of the Latin line or the richer music of the vowelled Greeks, of Tuscan sculpture or Elizabethan song may yet be full of the very sweetest wisdom. The real fool, such as the gods mock or mar, is he who does not know himself. I was such a one too long. You have been such a one too long. Be so no more. Do not be afraid. The supreme vice is shallowness. Everything that is realised is right."

– Oscar Wilde, *De Profundis*.

"Life is a mystery." – Sudhir Kedia

TABLE OF CONTENTS

LIST OF FIGURES

LIST OF TABLES

ACKNOWLEDGMENTS

This thesis has had a long gestation period, during which I've had a lot of growing up to do, both as a scientist, and as a human being. Neither would have been possible without my advisor William. William's faith in me, and his fearless enthusiasm gave me permission to make mistakes, and the strength to push forward into unknown territory. I have been deeply influenced by William's way of thinking about science, his emphasis on communicating science clearly, and his honesty with himself. I hope to cultivate these qualities further, as I strive to become a better scientist.

A large part of this thesis came out of work done in collaboration with Daniel Peralta-Salas, whose patient mentoring helped both inspire and reassure me as I needed. Daniel's willingness to listen to my half-baked ideas and teach me about differential forms, helped me feel confident in my mathematical abilities, and attempt calculations I might otherwise have been too intimidated to try.

I am deeply indebted to Paul Wiegmann, whose intuitive way of thinking about abstract mathematical ideas and depth of physical insight continues to amaze and inspire me. Paul's faith in me was a source of constant encouragement, and strength. I always came away from our conversations with a new appreciation for physics, and a rekindled sense of wonder about nature.

I can not thank Arvind Murugan enough. One of our initial conversations near the coffee machine, came a time when I was feeling stuck, and his gentle curiosity and patient listening gave me hope and reassurance. Arvind's approach to biophysics inspired me to study biophysics, and his generosity in helping me learn the ropes in biophysics, is something I will remember and try to emulate.

Conversations with Ari Turner always felt too short, and helped me reach within, and touch the child-like curiosity that is at the core of all scientific endeavor. Ari's sharp insight, and gentle nature, are precious qualities, that I aspire to cultivate.

Being in the company of Professors Sid Nagel, and Tom Witten has nurtured in me, a deep appreciation for the beauty inherent in everyday phenomena, and and has inspired me to strive for simplicity in my understanding of nature. Each time I have felt uncertain about whether physics was the right path for me, and whether I belonged in the physics department, I looked to Sid and Tom, and knew for certain that I wanted to become more like them.

I am thankful to all the professors in the department, especially Paul, Sid, Jeff, Heinrich, Tom, Arvind, and Suri, for their kindness, encouragement, and helpful advice. It has been a joy to be in a place with so many people I looked up to. During the course of this work, I have been nourished by the kindness of many people, had many intellectually nurturing conversations, and have formed friendships which I believe will last for a lifetime.

I am deeply grateful to Amith Darbal, whose love and sense of humor have saved my life in many ways. I have been extremely fortunate to have met Erik Thiede, who taught me how to lift weights and more importantly what it means to be true to oneself. Our friendship continues to nourish me in new and unexpected ways. This work owes a lot to Vishal Soni, who helped me deal with self-doubt, regularly challenged my assumptions, infused warmth in our shared space with his fearless sense of humor and the deep love that he exudes. Stéphane's generosity, and his free-spirited nature often gave me a breath of fresh air, when I needed it the most. Yuval's kindness and patience, made Hyde Park feel more like home, and his company made scientific writing almost pleasurable. I am grateful to Martin for introducing me to improv, and for his constant support. It has been a joy to share an office with Lisa, who has seen me through thick and thin. I am grateful to all the members of the soft matter journal club, which helped reinvigorate my curiosity, and motivated me to become a better physicist. I am deeply grateful to Josh Singh, to all the wonderful people I've met at the Mankind Project, and to Mike Pietrus.

Katie Klymko has been a special friend, whose uninhibited compassion, and capacity for

striving constantly amaze me, and reaffirm my faith in humanity. I am thankful to Johannes Knebel, and Archishman Raju, for their encouragement, and friendship. I was fortunate to have met many wonderful people at the Boulder School, memories of which always make me smile. I am grateful to Katherine Linzer and her family for their support and encouragement.

This work has received support from the improv community in Chicago, and has indulgently fed on the music of many soulful blues, and jazz musicians. I owe a special debt to Regina Carter, whose music lubricated much of this journey.

To all the people I have crossed paths with: every kind word, every understanding nod, every smile, has made a difference to me.

This work is dedicated to my parents for their love, and patience.

ABSTRACT

Representing a physical field in terms of its field lines has often enabled a deeper understanding of complex physical phenomena, from Faraday's law of magnetic induction [1], to the Helmholtz laws of vortex motion [2], to the free energy density of liquid crystals [3] in terms of the distortions of the lines of the director field. At the same time, the application of ideas from topology—the study of properties that are invariant under continuous deformations—has led to robust insights into the nature of complex physical systems from defects in crystal structures [4, 5], to terrestrial magnetism [6], to topological conservation laws [7, 8, 9].

The study of knotted fields, physical fields in which the field lines encode knots, emerges naturally from the application of topological ideas to the investigation of the physical phenomena best understood in terms of the lines of a field. A knot—a closed loop tangled with itself which can not be untangled without cutting the loop—is the simplest topologically non-trivial object constructed from a line.

Remarkably, knots in the vortex (magnetic field) lines of a dissipationless fluid (plasma), persist forever as they are transported by the flow, stretching and rotating as they evolve. Moreover, deeply entwined with the topology-preserving dynamics of dissipationless fluids and plasmas, is an additional conserved quantity—helicity, a measure of the average linking of the vortex (magnetic field) lines in a fluid (plasma)—which has had far-reaching consequences for fluids and plasmas. Inspired by the persistence of knots in dissipationless flows, and their far-reaching physical consequences, we seek to understand the interplay between the dynamics of a field and the topology of its field lines in a variety of systems.

While it is easy to tie a knot in a shoelace, tying a knot in the the lines of a space-filling field requires contorting the lines everywhere to match the knotted region. The challenge of analytically constructing knotted field configurations has impeded a deeper understanding of the interplay between topology and dynamics in fluids and plasmas. We begin by analytically constructing knotted field configurations which encode a desired knot in the lines of the field,

and show that their helicity can be tuned independently of the encoded knot.

The nonlinear nature of the physical systems in which these knotted field configurations arise, makes their analytical study challenging. We ask if a linear theory such as electromagnetism can allow knotted field configurations to persist with time. We find analytical expressions for an infinite family of knotted solutions to Maxwell's equations in vacuum and elucidate their connections to dissipationless flows. We present a design rule for constructing such persistently knotted electromagnetic fields, which could possibly be used to transfer knottedness to matter such as quantum fluids and plasmas.

An important consequence of the persistence of knots in classical dissipationless flows is the existence of an additional conserved quantity, helicity, which has had far-reaching implications. To understand the existence of analogous conserved quantities, we ask if superfluids, which flow without dissipation just like classical dissipationless flows, have an additional conserved quantity akin to helicity. We address this question using an analytical approach based on defining the particle relabeling symmetry—the symmetry underlying helicity conservation—in superfluids, and find that an analogous conserved quantity exists but vanishes identically owing to the intrinsic geometry of complex scalar fields. Furthermore, to address the question of a "classical limit" of superfluid vortices which recovers classical helicity conservation, we perform numerical simulations of *bundles* of superfluid vortices, and find behavior akin to classical viscous flows.

CHAPTER 1

INTRODUCTION

Understanding physical phenomena in terms of the lines of a physical field has a long history of successful practice, dating back to the work of Faraday [10, 11, 12, 1], and Maxwell [13, 14, 15, 16]. The concept of lines of force, invented by Faraday [1], provided the basis for his law of electromagnetic induction, and eventually inspired Maxwell's theory of electromagnetism [14]. The basic idea of representing the entities of physical interest in a system, in terms of the lines of a field has found application in a myriad of ways including force chains in granular materials [17, 18, 19], dislocation lines in crystals [20, 21], lines of the director field in liquid crystals [3, 22], lines of the magnetic field in plasmas [23, 24], vortex lines in a fluid [2, 25], and lines of the electric and magnetic fields in light [26, 27], to name a few.

At the same time, the application of ideas from topology—the study of properties that are invariant under continuous deformations—has yielded robust insights into a variety of complex physical phenomena, including the quantum hall effect [28], electronic properties of topological insulators [29, 30], mechanical properties of topological metamaterials [31, 32, 33], defect structures observed in liquid crystals [5, 34, 35, 36, 37], the design of optical vortices in light beams [38, 39], and the dynamics of fluids [9, 40] and plasmas [8, 41, 42, 43]. The physical properties of a system which arise from an underlying topological invariant—a property that is invariant under continuous deformations such as the genus of a closed surface, or the linking number between two closed loops—are intrinsically robust to smooth perturbations of the system, and therefore lead to insights which are unchanged in the presence of disorder, and independent of the details of a system.

The simplest topologically non-trivial object formed from a line is a knot: a closed loop tangled with itself, which retains its identity under any smooth transformation such as stretching or rotating, and can be untangled only by cutting the loop. The application of topological concepts to the study of physical phenomena which are best understood in terms

of the lines of a field, leads naturally to the study of knotted fields.

Recent experimental advances have enabled the creation of knots in a variety of systems: in the vortex lines of a fluid using 3D-printed wings in the shape of knots [44], in the defect lines of the director field in nematic liquid crystals using colloidal micro-particles and highly focused laser tweezers [45], and in the lines of darkness in optical beams by matching a slice of the theoretically constructed knotted optical field [38].

The possible existence of knotted field configurations in nature and the recent technological advances in the design of such knotted fields in experiment, lead naturally to the question of how such knotted fields evolve with time. Remarkably, knots in the vortex lines of an idealized dissipationless flow (Euler flow) never never untie themselves, stretching and rotating as they are transported by the flow, a consequence of the Helmholtz laws of vortex motion [2]. This remarkable fact served as inspiration for Lord Kelvin's vortex atom hypothesis [25], which in turn led to the birth of mathematical knot theory [46, 47, 48]. Almost a century later, it was shown [23, 24] that knots in the magnetic field lines of an infinitely conducting plasma also persist forever, evolving like unbreakable elastic filaments frozen into the flow of the plasma.

Furthermore, intimately related to the topology preserving dynamics of Euler flows and infinitely conducting plasmas, is the existence of an extra conserved quantity: helicity [8, 9]. Helicity is a measure of the average linking of vortex (magnetic field) lines in a fluid (plasma) and its conservation imposes a strong topological constraint on the motion of vortex lines (magnetic field lines) in a fluid (plasma), having far-reaching consequences. In particular, helicity conservation has been fundamental to the development of turbulent dynamo theory [49, 50, 51], the stability and relaxation of plasmas [52, 53, 54, 55], and vortex dynamics in fluids [9, 56, 57].

In the study of knotted fields, a natural question arises: what kinds of knotted field configurations are allowed? Tying a knot in a shoelace is a relatively simple affair, however

tying a knot in the lines of a space-filling vector field requires the lines everywhere to twist to conform to the knot at the center. To better understand the allowed knotted configurations of vortex lines in a fluid or the magnetic field lines in a plasma, we begin by constructing knotted field configurations with controllable helicity [58].

The study of the dynamics of knotted field configurations in fluids and plasmas is challenging owing to their inherent nonlinearity. To analytically study the dynamics of knotted field configurations, we ask if knots in the lines of an electric (magnetic) field can be preserved by Maxwell's equations in vacuum—a linear theory. We find an infinite family of knotted solutions [59] to Maxwell's equations, encoding all torus knots and links, which persist forever. We then consider the constraints on designing such knotted Maxwell fields, and find a sufficient initial condition required for such knots to persist with time [60].

To gain a deeper understanding into the conservation of helicity, we study if an analogous conserved quantity exists in superfluids which flow without dissipation just like Euler flows. We address [61] the question of a "superfluid helicity" using an analytical approach based on defining the particle relabeling symmetry in superfluid flows. Furthermore, we use numerical simulations to demonstrate that *bundles* of superfluid vortices evolve coherently and recover the "classical limit" of superfluid flows, but their evolution is more akin to vortices in classical viscous flows.

The work presented in the following chapters is based on the following references: [58, 59, 60, 61].

CHAPTER 2

WEAVING KNOTTED VECTOR FIELDS

This chapter is based on the work presented in [58].

2.1 Introduction

The idea that a physical field—such as a magnetic field—could be weaved into a knotty texture, has fascinated scientists ever since Lord Kelvin conjectured that atoms were in fact vortex knots in the aether. Since then, topology has emerged as a key organizing principle in physics, and knottiness is being explored as a fundamental aspect of classical and quantum fluids [9, 62, 44, 56, 63, 64, 65, 66], magnetic fields in light and plasmas [67, 68, 26, 69, 27, 70, 71, 72, 73, 74, 59], liquid crystals [45, 37, 75, 76], optical fields [77, 38], nonlinear field theories [78, 79, 80, 81], wave chaos [82], and superconductors [83, 84].

In particular, helicity—a measure of average linking of field lines—is a conserved quantity in ideal fluids [2, 85] and plasmas [8, 41, 24]. Helicity thus places a fundamental topological constraint on their evolution [9, 68], and plays an important role in turbulent dynamo theory [86, 87, 49], magnetic relaxation in plasmas [43, 88, 89], and turbulence [90, 91]. Beyond fluids and plasmas, helicity conservation leads to a natural connection between the minimum energy configurations of knotted magnetic flux tubes [68, 88, 92], and tight knot configurations [93, 94], and tentatively with the spectrum of mass-energies of glueballs in the quark-gluon plasma [95, 96, 97].

Knotted field configurations provide a natural setting for studying helicity, but more subtlety is required to tie a knot in the lines of a vector field than in a shoelace: all the streamlines of the entire space-filling field must twist to conform to the knotted region. The difficulty of constructing knotted field configurations with controlled helicity makes it challenging to understand the role of helicity in the evolution of knotted structures [9, 68, 69].

In this chapter, based on [58], we show how to explicitly construct knotted, divergence-free vector fields with a wide range of topologies which have finite-energy and tunable helicity, and give a systematic prescription for calculating the helicity of these knotted fields.

Studying the dynamics of these knotted field configurations in fluids and plasmas may deepen our understanding of helicity, give insights into the longstanding problem of 'magnetic relaxation under topological constraints' [98], and help understand the stability of plasmas in knotatrons – magnetic confinement devices in the shape of knots [99].

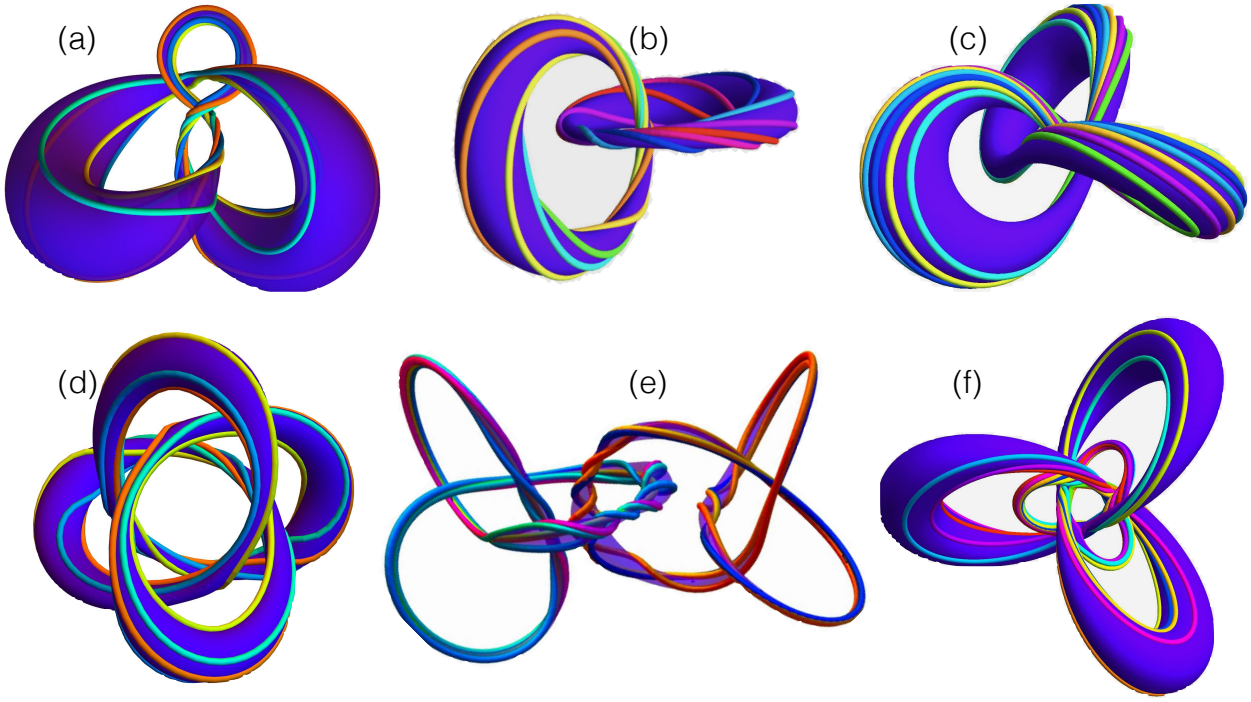

Figure 2.1: Knotted structures encoded in the level sets of the complex scalar fields $\psi = P(u, u^*, v, v^*)/Q(u, u^*, v, v^*)$, where (u, v) are functions of (x, y, z) (see Eq. (2.3)). (**a**) Figure-8 knots: $\psi = v/\left(64u^3 - 12u(3 - 2v^2 + 2v^{*2}) + (14v^2 + 14v^{*2} - v^4 + v^{*4})\right)$. (**b**) Linked rings: $\psi = u^2/\left(u^2 - v^2\right)$. (**c**) Trefoil knots: $\psi = u^3/\left(u^3 + v^2\right)$. Level curves of ψ encode torus knots and links when $Q(u, v)$ is of Brieskorn form [100]: $u^p + v^q$. (**d**) Figure-8 knots (symmetric): $\psi = u/\left(64v^3 - 12v(3 + 2u^2 - 2u^{*2}) - (14u^2 + 14u^{*2} + u^4 - u^{*4})\right)$. (**e**) Linked trefoil knots, constructed from 2 copies of the Milnor polynomial for a trefoil knot. (**f**) $C^{2,3}_{3,2}$ cable knots: $\psi = (u\, v)\,/\left(v^4 - 2u^3\, v^2 - 2iu^3\, v + u^6 + \frac{1}{4}u^3\right)$.

A classical problem from mathematics is the study of knots and links as nodal lines (zeros)

of complex scalar fields [101, 100, 102, 38, 103]. In fact, the level sets of a complex scalar field can give rise to collections of knotted curves that smoothly intertwine to fill up space. Well-known examples are the Hopf fibration [26, 104, 105, 27, 70, 106], Seifert fibrations [107, 71] and Milnor fibrations [100, 38, 39]. Many knots can be embedded as the nodal lines of complex scalar fields, in the family of lemniscate knots and their generalizations [108], which includes all torus knots and links [101], the figure-8 knot and generalizations [38] (including the borromean rings and Turk's head knot), cable knots [109], and links of any of these.

Some representative examples of knotted complex scalar fields are illustrated in Fig. 2.1, where the level curves wind around knotted or linked tori, encoding the Hopf link (Fig. 2.1(b)), the trefoil knot (Fig. 2.1(c)), the figure-8 knot [38] (Fig. 2.1(a),(d)), a link of two trefoils (Fig. 2.1(e)) and a cable knot (Fig. 2.1(f)). In all of these examples, the level curves of the complex scalar field ψ, for any complex value of ψ, organize around a core set of lines where $\psi = 0\,,\,\infty$ (zeros and poles of ψ). Our construction of knotted vector fields follows from such knotted complex scalar fields, based on [101, 108, 81], where the level curves of constant complex amplitude are collections of knotted curves filling up space.

A vector field tangent to the level curves of a complex scalar field ψ is given simply by the the cross product $-i\nabla\psi^* \times \nabla\psi = \nabla \times \mathrm{Im}\,(\psi^*\nabla\psi)$. A vector field with the same flow lines is

$$\mathbf{B} = \frac{1}{2\pi i}\frac{\nabla\psi^* \times \nabla\psi}{(1+\psi\,\psi^*)^2}. \tag{2.1}$$

This field is smooth everywhere, divergence-free ($\nabla\cdot\mathbf{B} = 0$) and has finite energy ($\int \mathrm{d}^3x\,|\mathbf{B}|^2 < \infty$). This vector field arises in a variety of different contexts, and was used previously to construct knotted initial states for electromagnetic fields [26, 71], and topological solitons in ideal magnetohydrodynamics [67].

Since the flow lines of $\mathbf{B}$ (i.e. the level sets of ψ) can clearly be knotted, it is natural to suppose that such fields have nontrivial helicity. Explicitly calculating the helicity $\mathcal{H} =$

$\int \mathrm{d}^3x\, \mathbf{A}\cdot\mathbf{B}$ requires the choice of a vector potential $\mathbf{A}$ such that $\nabla\times\mathbf{A}=\mathbf{B}$. A natural candidate,

$$\mathbf{A}=\frac{1}{4\pi i}\frac{(\psi^*\,\nabla\psi-\psi\,\nabla\psi^*)}{(1+\psi^*\,\psi)}, \tag{2.2}$$

suggests that the helicity of the knotted vector field $\mathbf{B}$ vanishes. We will show that $\mathbf{A}$ in Eq. (2.2) has a singular part which can be systematically removed, leading to a nonsingular vector potential which allows explicit calculation of the helicity of all these knotted fields.

The helicity of the resulting knotted vector field can be computed explicitly, and may be varied without changing the underlying knotted structure. Furthermore, these fields may be restricted to the interior of knotted flux tubes [1], whose helicity can be calculated exactly. Lastly, we construct knotted fields with vanishing total helicity, but non-vanishing helicity in the interior of knotted flux tubes—tori tangent to the lines of $\mathbf{B}$.

2.2 Knotted fields from Rational maps

Rational maps have found success in approximating certain minimum energy solutions of the Skyrme model [111], and this technique was extended by Sutcliffe [81] to approximate knotted solutions of the Skyrme-Faddeev model. The knotted vector field construction described here is based on rational maps of similar form. A rational map is defined as the ratio of two complex-valued polynomials $\psi=P(u,u^*,v,v^*)/Q(u,u^*,v,v^*)$, where the nodal lines (zeros) of $Q(u,u^*,v,v^*)$ have the form of the desired knot, and $P(u,u^*,v,v^*)$ is chosen to encode the desired helicity (Fig. (2.4)). Here, as in Fig. 2.1, (u,v) are complex coordinates on S^3 which stereographically project to coordinates (x,y,z) in $\mathbb{R}^3$ by

$$u=\frac{2(x+i\,y)}{1+r^2}\,,\; v=\frac{2z+i\,(r^2-1)}{1+r^2}, \tag{2.3}$$

1. helicity in these flux tubes is gauge invariant [9, 110] because $\mathbf{B}\cdot\hat{\mathbf{n}}=0$ on the surface of these flux tubes, ie. they are magnetic surfaces

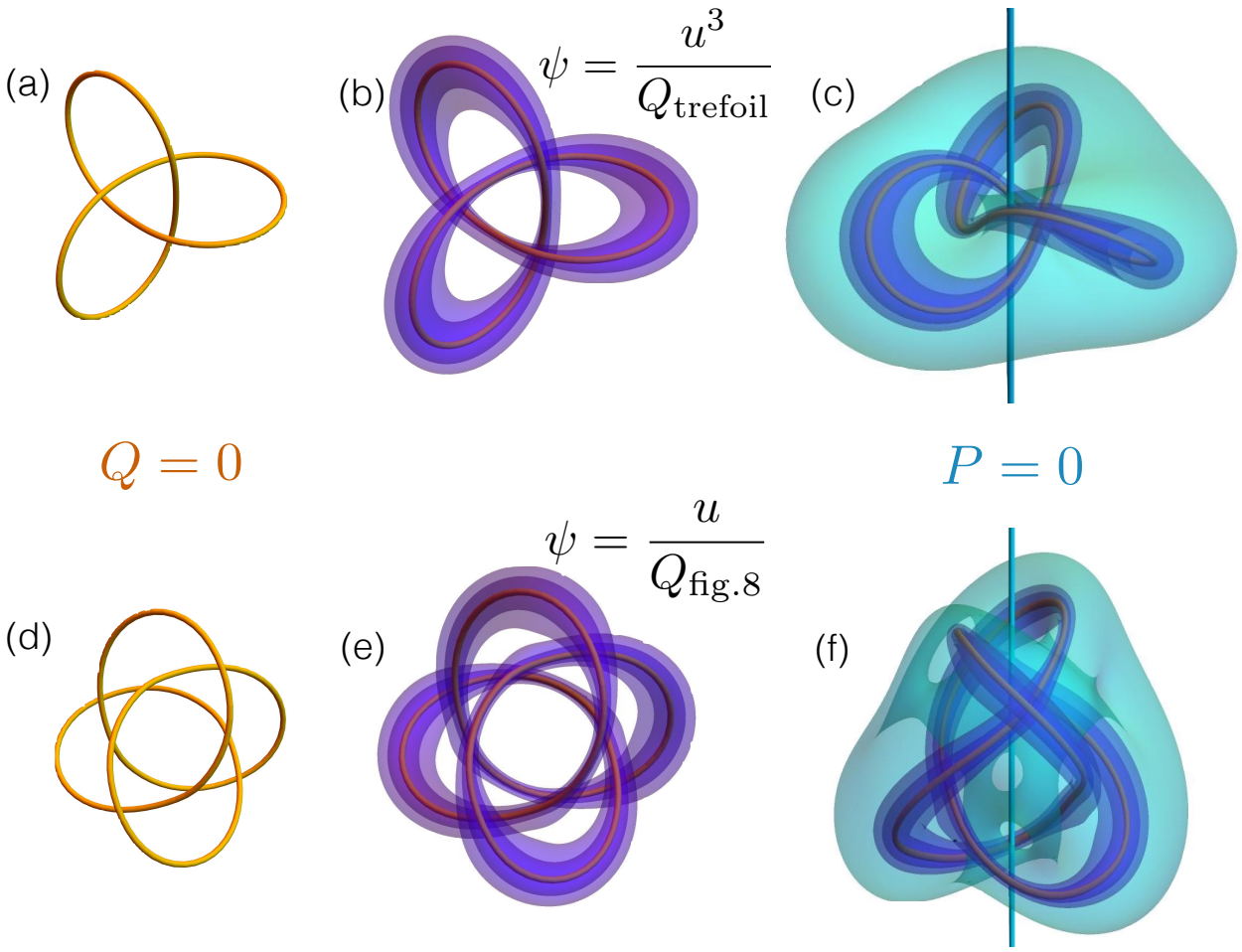

Figure 2.2: Organization of the lines of **B** around lines where $\psi = P(u,v)/Q(u,v)$ is 0 or ∞. (**a**), (**d**) $Q = 0$ corresponds to the trefoil and figure-8 knots. $Q_{\text{trefoil}} = u^3 + v^2$, $Q_{\text{fig-8}} = 64v^3 - 12v(3 + 2u^2 - 2u^{*2}) - (14u^2 + 14u^{*2} + u^4 - u^{*4})$. (**b**),(**e**) The lines of **B** are tangent to nested knotted tori (blue) organized around the knots where $Q = 0$. (**c**),(**f**) $P(u,v) = 0$ corresponds to the z-axis. The lines of **B** are tangent to nested tori (cyan) organized around $P(u,v) = 0$.

where $r^2 = x^2 + y^2 + z^2$, and (u^*, v^*) denote complex conjugates of (u, v).

Such ψ automatically give rise to a vector field **B** as in Eq. (2.1), whose flow lines coincide with the level curves of ψ. The core set of lines that organize the flow lines of **B** are the zeros of P and Q (see Fig. 2.2). A wide variety of knotted fields **B** can be constructed from rational maps ψ by encoding the desired knot in the zeros of $Q(u, u^*, v, v^*)$ as shown in the Appendix. The above map from S^3 to $\mathbb{R}^3$: $(u, v) \to (x, y, z)$ is not unique. Other possible

choices of stereographic projections are obtained by transformations of the above complex functions $u(x,y,z)$, $v(x,y,z)$ in Eq. (2.3) under translations, rotations and reflections of the x,y,z axes. These choices of the projections result in corresponding translations, rotations and reflections of the knotted field constructed from $\psi = P(u,u^*,v,v^*)/Q(u,u^*,v,v^*)$.

2.2.1 Structure of knotted field lines

. We rewrite $\mathbf{B}$ using Euler potentials [112, 113, 114, 115]:

$$\mathbf{B} = \nabla\left(\frac{\psi\,\psi^*}{1+\psi\,\psi^*}\right)\times\frac{1}{4\pi i}\nabla\log\left(\frac{\psi}{\psi^*}\right) = \frac{1}{2\pi}\nabla\chi\times\nabla\eta \tag{2.4}$$

where $\chi = (\psi\,\psi^*)\,/\,(1+\psi\,\psi^*)$, $\chi\in[0,1]$ and $\eta = \frac{1}{2i}\log(\psi/\psi^*)$, $\eta\in[0,2\pi)$. We note that as $r\to\infty$, $|\nabla\chi|\sim O(1/r)$, $|\nabla\eta|\sim O(1/r)$, so that the energy density $|\mathbf{B}|^2\sim O(1/r^4)$ and the energy of all such fields, as the square integral of $\mathbf{B}$, is finite.

The lines of $\mathbf{B}$ are tangent to surfaces of constant χ and Seifert surfaces of constant η (see Fig. 2.3), which can be considered as a generalization of the surfaces of constant $\rho\,(\leftrightarrow\chi)$ and constant $\phi\,(\leftrightarrow\eta)$ in cylindrical coordinates (ρ,ϕ,z), with the knot $Q=0$ replacing the z-axis.

The surfaces of constant χ are knotted tori, nested inside one another (Fig. 2.3), with smaller values of χ corresponding to larger tori, and the largest value $\chi=1$ corresponding to the knot $Q=0$ at the center of the tori (Fig. 2.2(a),(d)). Isosurfaces of smaller χ are increasingly bigger knotted tori, eventually colliding to give tori organized around $P=0$, as shown in Fig. 2.2(c),(f) in cyan, which converge to the lines $P=0$ as $\chi\to 0$.

By contrast, η is constant on Seifert surfaces for the core set of lines: $P=0\,,\,Q=0$. Seifert surfaces for $Q=0$ are shown in Fig. 2.3. Since η is well-defined only in a multiply-connected volume which excludes the core set of lines, the helicity of $\mathbf{B}$ can be non-vanishing [116], in spite of being expressible in terms of Euler potentials.

2.3 Helicity of knotted fields

A smooth vector potential $\mathbf{A}$ satisfying $\nabla \times \mathbf{A} = \mathbf{B}$ is needed to calculate the helicity $\mathcal{H} = \int \mathrm{d}^3x\, \mathbf{A} \cdot \mathbf{B}$ of these knotted fields explicitly. We now give a general prescription for computing such a vector potential, starting by rewriting $\mathbf{A}$ in Eq. (2.2) as

$$\mathbf{A} = \frac{1}{4\pi i} \left(\frac{\psi\, \psi^*}{1 + \psi\, \psi^*} \right) \nabla \log \left(\frac{\psi}{\psi^*} \right). \tag{2.5}$$

Substituting $\psi = P(u, u^*, v, v^*)/Q(u, u^*, v, v^*)$ gives

$$\mathbf{A} = \frac{1}{4\pi i} \times \left[\frac{|P|^2 \nabla \log \left(\frac{P}{P^*} \right) + |Q|^2 \nabla \log \left(\frac{Q}{Q^*} \right)}{|P|^2 + |Q|^2} - \nabla \log \left(\frac{Q}{Q^*} \right) \right] \tag{2.6}$$

The last term containing $\nabla \log (Q/Q^*)$ is singular at $Q = 0$. Since $|Q|^2 \nabla \log(Q/Q^*) = Q^* \nabla Q - Q \nabla Q^*$, this term in the fraction is smooth and nonsingular.

Hence the singular gauge transformation $\tilde{\mathbf{A}} = \mathbf{A} + (1/4\pi i) \nabla \log (Q/Q^*)$, removes the singularity in $\mathbf{A}$, allowing the helicity to be computed directly. The vector potential $\tilde{\mathbf{A}}$ is smooth everywhere, giving the correct helicity $\mathcal{H} = \int \mathrm{d}^3x\, \tilde{\mathbf{A}} \cdot \mathbf{B}$, which is equal to the Hopf invariant of the map ψ [117, 81] by the Whitehead integral formula. Hence we can explicitly compute the helicity [2] of arbitrary knotted fields $\mathbf{B}$ and therefore, the Hopf invariant of arbitrary rational maps.

Surfaces of constant $\log (Q/Q^*)$ yield explicit expressions for Seifert surfaces of the knot $Q(u, u^*, v, v^*) = 0$ (see Fig. 2.3), and could be used to generate initial wave-functions describing knotted vortices in superfluids and Bose-Einstein condensates.

The simplest illustration of our construction is given by the Hopf map [26, 104, 105, 27, 106] $\psi = u/v$. The vector potential given by Eq. (2.5) has a singularity at $v = 0$

2. Mathematically, $\psi(u, v)$ takes its value on the complex projective plane, $\mathbb{CP}^1$ (i.e. the complex numbers with the point at ∞), which is homeomorphic to the 2-sphere S^2: in this sense, helicity can be understood as the topological degree of the map $S^3 \to S^2$.

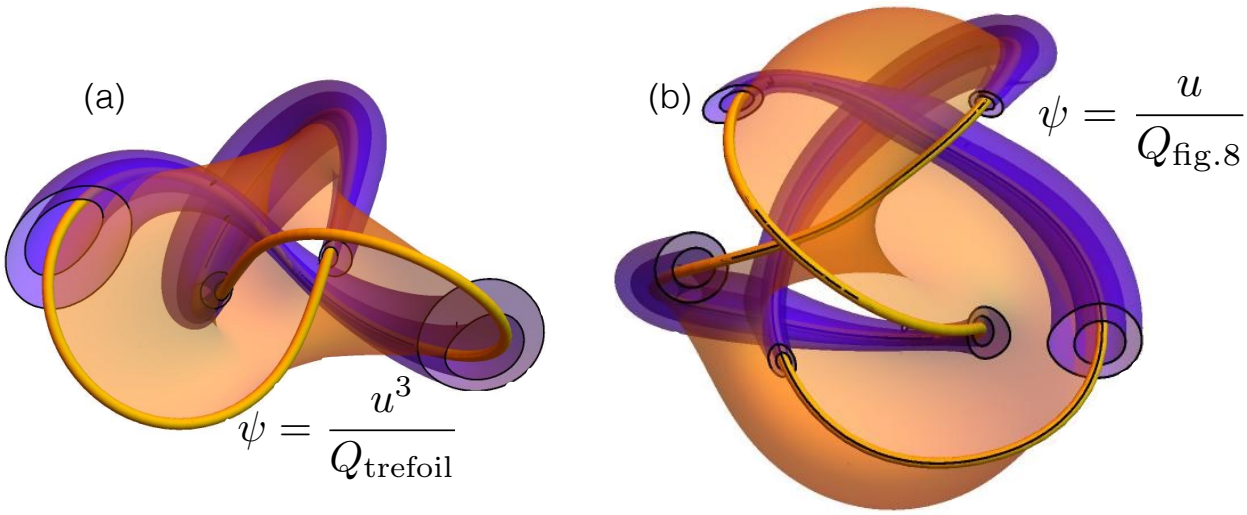

Figure 2.3: Knotted field structures: knotted flux surfaces (blue) are surfaces of constant χ, and Seifert surfaces for $Q(u, u^*, v, v^*) = 0$ (orange) are surfaces of constant $\log(Q/Q^*)$. (**a**) Trefoil knot with Q_{trefoil}, (**b**) Figure-8 knot with $Q_{\text{fig-8}}$ are defined in Fig. 2.2.

(the unit circle in the xy-plane), which is removed via the singular gauge transformation $\tilde{\mathbf{A}} = \mathbf{A} + (1/4\pi i)\,\nabla \log(v/v^*)$. The new vector potential $\tilde{\mathbf{A}}$ is smooth everywhere, and gives the correct helicity $\mathcal{H} = \int \mathrm{d}^3x\, \tilde{\mathbf{A}} \cdot \mathbf{B} = 1$, equal to the Hopf invariant of the map [117, 81].

2.3.1 Tuning the helicity of a knotted field

The helicity of $\mathbf{B}$ can be tuned without changing the underlying knotted structure encoded in $\mathbf{B}$, as for rational maps [81]. The flow lines of $\mathbf{B}$ contained in the knotted tori of constant χ in the neighborhood of the knot $Q = 0 \iff \chi = 1$, encode knots of the same type as the knot $Q = 0$. However the degree of winding of these lines—and hence the helicity of $\mathbf{B}$—can be controlled by changing $P(u, v)$, as illustrated in Fig. 2.4.

Knotted fields encoding torus knots and links can be constructed from maps $\psi = P(u, v)/Q(u, v)$ with $P(u, v) = u^\alpha\, v^\beta$, $Q(u, v) = u^q + v^p$. The helicity of these fields can be varied without changing the underlying knotted structure by changing α, β in $P(u, v) = u^\alpha\, v^\beta$. The helicity of $\mathbf{B}$, being equal to the Hopf invariant [117, 81] of the map ψ, is $\mathcal{H} = \alpha\, p + \beta\, q$. The lines of the field $\mathbf{B}$ wind more for higher values of α, β as indicated by the higher values of helicity.

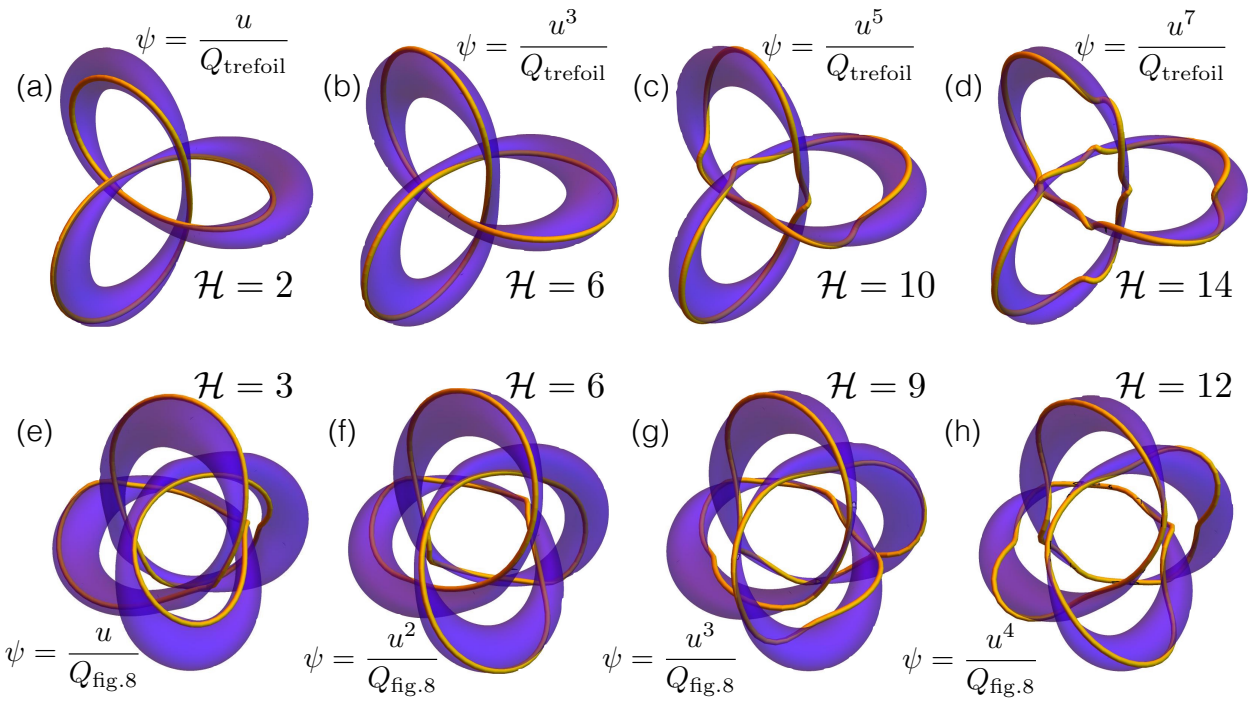

Figure 2.4: Tuning the helicity $\mathcal{H}$ of the knotted field $\mathbf{B}$ by changing P for two fixed knot types (set by $\leftrightarrow Q$). Varying the helicity corresponds to varying amounts of winding of the lines of $\mathbf{B}$. (**a**,**b**,**c**,**d**): Trefoil knots with Q_{trefoil}, (**e**,**f**,**g**,**h**): Figure-8 knots with $Q_{\text{fig-8}}$, with Q functions as defined in Fig. 2.2.

Knotted fields encoding other knot types such as lemniscate knots, cable knots, iterated torus links can be constructed from maps $\psi = u^\alpha/Q(u, u^*, v)$ [118, 38, 108, 109]. Their helicity is given by $\mathcal{H} = \alpha \deg_v(Q)$ where $\deg_v(Q)$ is the highest power of v appearing in $Q(u, u^*, v)$, and can be tuned by changing α.

The helicity of such knotted fields $\mathbf{B}$ can be tuned further to yield negative values by substituting P or Q with their complex conjugates.

2.3.2 Helicity of knotted flux tubes

Knotted flux tubes—magnetic flux tubes in plasmas or vortex tubes in fluids—can be generated by restricting the knotted field $\mathbf{B}$ to the interior of a knotted tube (Fig. 2.3): $\chi > \chi_0$. Such a knotted flux tube contains flux $(1 - \chi_0)$, and its helicity can be calculated as in

[110, 69] to be $\mathcal{H}_{\chi_0} = (1-\chi_0)^2\,\mathcal{H}_{\text{total}}$, as the helicity for a uniformly twisted field with twist equal to $\mathcal{H}_{\text{total}}$.

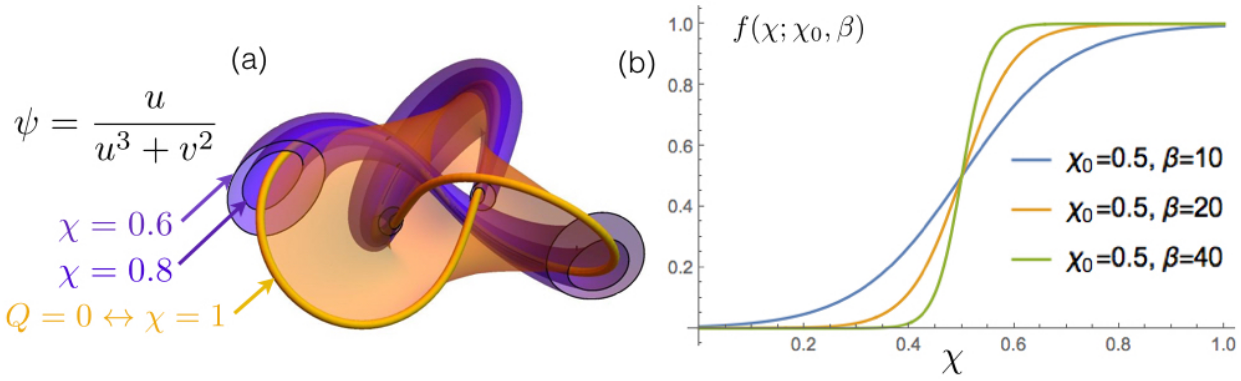

Figure 2.5: (**a**) The lines of **B** are tangent to nested tori (surfaces of constant χ) shown in blue. Also shown is a surface of constant $\log(Q/Q^*)/(4\pi i)$ (orange). (**b**) The smooth function $f(\chi;\chi_0,\beta)$ which is close to 1 in the interior of the knotted torus $\chi = \chi_0$, and smoothly decays to 0 outside. The decay rate is controlled by the choice of β.

To restrict the knotted field **B** to the interior of a knotted tube $\chi = \chi_0$ and decay smoothly outside of the tube ($\chi < \chi_0$), we consider the following function $f(\chi;\chi_0,\beta)$ associated with the Fermi-Dirac distribution:

$$f(\chi;\chi_0,\beta) = \frac{1}{1+\exp(\beta(\chi_0-\chi))} \tag{2.7}$$

as shown in Fig. 2.7(b).

Multiplying the knotted field **B** in Eq. (2.4) by $f(\chi;\chi_0,\beta)$ gives a modified field $\mathbf{B}'$ which decays smoothly outside the knotted tube i.e. for $\chi < \chi_0$:

$$\mathbf{B}' = f(\chi;\chi_0,\beta)\,\nabla\chi\times\nabla\eta \tag{2.8}$$

As shown in Fig. 2.5(b), the choice of β controls the rate of decay of **B** outside the knotted tube $\chi = \chi_0$.

Calculating the helicity of the knotted field $\mathbf{B}'$ in Eq. (2.8) which decays smoothly outside

a knotted tube $\chi = \chi_0$ requires the choice of a smooth vector potential $\mathbf{A'} : \nabla \times \mathbf{A'} = \mathbf{B'}$.

A smooth non-singular vector potential $\mathbf{A'}$ associated with the knotted field $\mathbf{B'}$ is:

$$\mathbf{A'} = F(\chi; \chi_0, \beta)\, \nabla\eta + \frac{1}{2i} F(1; \chi_0, \beta)\, \nabla \log\left(\frac{Q}{Q^*}\right) \tag{2.9}$$

where $F(\chi; \chi_0, \beta)$ is:

$$\begin{aligned} F(\chi; \chi_0, \beta) &= \int_0^{\chi} f(\chi') d\chi' \\ &= \log\left(\frac{1 + \exp(\beta(\chi - \chi_0))}{1 + \exp(-\beta\chi_0)}\right) \end{aligned} \tag{2.10}$$

To create a knotted field that abruptly vanishes outside a knotted tube $\chi = \chi_0$, the above procedure can be followed with the function f given by: $f = \Theta(\chi - \chi_0)$, where $\Theta(x)$ is the Heaviside function.

2.3.3 Knotted fields with vanishing helicity

Knotted fields $\mathbf{B}$ constructed from rational maps $\psi = P$ (i.e. $Q = 1$), have vanishing helicity despite having knotted field lines.

This because vector potential $\mathbf{A}$ in Eq. (2.2) is singularity-free, implying $\mathcal{H} = 0$. Geometrically, the lines of $\mathbf{B}$ tangent to the different knotted tori, are of different handedness, and the average linking between the lines vanishes. However, the lines of $\mathbf{B}$ in the interior of a knotted torus—such that the lines of $\mathbf{B}$ are tangent to the torus ie. the torus is a magnetic surface, so that the helicity in the torus is gauge-invariant—may have non-vanishing helicity which is difficult to compute analytically.

We will study in detail, the simple case of a knotted field constructed from $\psi = P(u, v) = u\, v$, where the lines of the knotted field $\mathbf{B}$ are linked circles as shown in Fig. 2.6, but the total helicity vanishes.

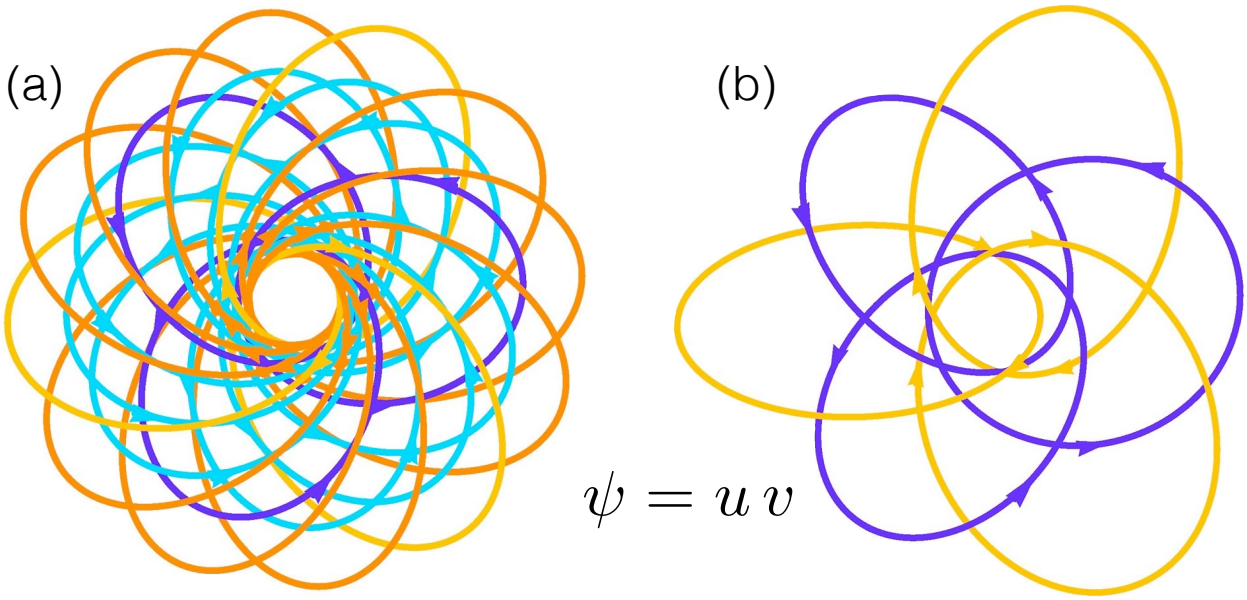

Figure 2.6: Knotted fields with vanishing helicity. (a) field lines are linked rings, forming a Hopf fibration-like structure. (b) field lines on inner tori (blue) go anticlockwise, while field lines on outer tori (yellow) go clockwise.

The knotted field $\mathbf{B}$ for the map $\psi = u\,v$ is:

$$\begin{aligned}\mathbf{B} &= \frac{1}{2\pi}\,\nabla\chi \times \nabla\eta \\ &= \frac{1}{4\pi i}\nabla\left(\frac{|u|^2\,|v|^2}{1+|u|^2\,|v|^2}\right) \times \nabla\left(\log\frac{u}{u^*} + \log\frac{v}{v^*}\right) \\ &= \frac{1}{4\pi i}\nabla\left(\frac{(1-|v|^2)\,|v|^2}{1+(1-|v|^2)\,|v|^2}\right) \times \nabla\left(\log\frac{u}{u^*} + \log\frac{v}{v^*}\right)\end{aligned} \tag{2.11}$$

where $\chi = |u|^2\,|v|^2/(1+|u|^2\,|v|^2)$, $\eta = (\log(u/u^*) + \log(v/v^*))/(2i)$, and $|u|^2 + |v|^2 = 1$ is used in the last equation. The lines of $\mathbf{B}$ are tangent to surfaces of constant χ, and therefore tangent to surfaces of constant $|v|$, i.e. tori symmetric about the z-axis.

The corresponding vector potential $\mathbf{A}$ is $\mathbf{A} = \chi\,\nabla\eta/(2\pi)$, so that $\nabla\times\mathbf{A} = \mathbf{B}$. The total helicity $\mathcal{H} = \int \mathrm{d}^3x\,\mathbf{A}\cdot\mathbf{B}$ vanishes since $\mathbf{A}\cdot\mathbf{B} = 0$. The vanishing of helicity is a result of the lines of $\mathbf{B}$ having different handedness on different tori as shown in Fig. 2.6, such that the average linking between the lines vanishes. This observation suggests that restricting the

knotted field $\mathbf{B}$ to the interior of a torus $|v| \leq v_0$ should result in non-zero average linking and non-zero helicity.

To investigate whether such knotted fields do indeed have non-vanishing helicity in the interior of tori—closed surfaces $|v| = v_0$, which are tangent to the lines of $\mathbf{B}$ (no flux penetrates the boundary of the surface)—we consider the knotted field $\mathbf{B'} = \Theta(v_0 - |v|)\,\mathbf{B}$, where $\Theta(x)$ is the Heaviside step function. On the lines of the calculation leading up to Eq. (2.9), we find that the correct vector potential $\mathbf{A'}$ which is continuous, non-singular, and satisfies $\nabla \times \mathbf{A'} = \mathbf{B'}$ is:

$$\mathbf{A'} = \begin{cases} \frac{1}{2\pi}\frac{(1-|v|^2)\,|v|^2}{1+(1-|v|^2)\,|v|^2}\nabla\eta - \frac{1}{4\pi i}\frac{(1-v_0^2)\,v_0^2}{1+(1-v_0^2)\,v_0^2}\nabla\log\frac{u}{u^*}\ , & |v| \leq v_0 \\ \\ \frac{1}{4\pi i}\frac{(1-v_0^2)\,v_0^2}{1+(1-v_0^2)\,v_0^2}\nabla\log\frac{v}{v^*}\ , & |v| > v_0 \end{cases}$$

The helicity $\mathcal{H}' = \int \mathrm{d}^3x\,\mathbf{A'}\cdot\mathbf{B'}$ can be calculated to be non-vanishing for $v_0 < 1$, demonstrating how knotted fields with vanishing total helicity can have non-vanishing helicity in a subregion of space (chosen such that there is no flux piercing the boundary of the subregion, so that helicity is gauge-invariant and well-defined).

Alternatively, the vanishing of the total helicity follows from the vanishing of the Hopf invariant [117, 81] of the map given by $\psi = P(u, u^*, v, v^*)$, since the set of (u, u^*, v, v^*) such that $\psi = \infty$ is a null set.

2.4 Summary

We have presented a general method for constructing physically viable knotted vector fields, encoding an arbitrary combination of knots woven together, and shown how to explicitly compute their helicity. Furthermore, we have shown how to construct knotted flux tubes, and calculate their helicity.

Knotted fields arising as solutions to Maxwell's equations [59] have found application in

the construction of topological solitons in magnetohydrodynamics [72] and resistive MHD flows [73]. The knotted vector fields presented here encode a much larger variety of knots, possessing a richer structure, and studying their evolution could lead to new insights about the role of helicity in fluids [49] and plasmas [98, 99], and novel topological solitons.

Finally, our systematic procedure for calculating the helicity of the knotted field $\mathbf{B}$, may help accurately determine the Hopf charge of arbitrarily knotted Skyrme-Faddeev solitons [79, 81] and help tighten the lower bound on how their minimum energy grows with their Hopf charge [119].

CHAPTER 3

TYING KNOTS IN LIGHT

This chapter is based on the work presented in [59].

3.1 Introduction

Knots and the application of mathematical knot theory to space-filling fields are enriching our understanding of a variety of physical phenomena with examples in fluid dynamics [9, 120, 121], statistical mechanics [122], and quantum field theory [123], to cite a few. Knotted structures embedded in physical fields, previously only imagined in theoretical proposals such as Lord Kelvin's vortex atom hypothesis [85], have in recent years become experimentally accessible in a variety of physical systems, for example, in the vortex lines of a fluid [63, 62, 44], the topological defect lines in liquid crystals [124, 45], singular lines of optical fields [38], magnetic field lines in electromagnetic fields [125, 27, 70] and in spinor Bose-Einstein condensates [64]. Furthermore, numerical simulations have shown that stable knot-like structures arise in the Skyrme-Faddeev model [78, 81], and consequently in triplet superconductors [83, 84] and charged Bose condensates [80]. Analytical solutions for such excitations, however, are difficult to construct owing to the inherent nonlinearity in most dynamical fields and have therefore remained elusive.

An exception is a particularly elegant solution to Maxwell's equations in free space (see Fig. 3.1), brought to light by Rañada [26], which provides an encouraging manifestation of a persistent non-trivial topological structure in a linear field theory. This solution, referred to as the Hopfion solution for the rest of the chapter, can furthermore be experimentally realized using tightly focussed Laguerre-Gaussian beams [27].

In this chapter based on [59], we present an infinite family of exact *knotted* solutions to Maxwell's equations in free space, with the electric and magnetic field lines encoding all

torus knots and links, which persist for all time. The unique combination of experimental potential and opportunity for analytical study, makes light an ideal candidate for studying knotted field configurations and furthermore, a means of potentially transferring knottedness to matter.

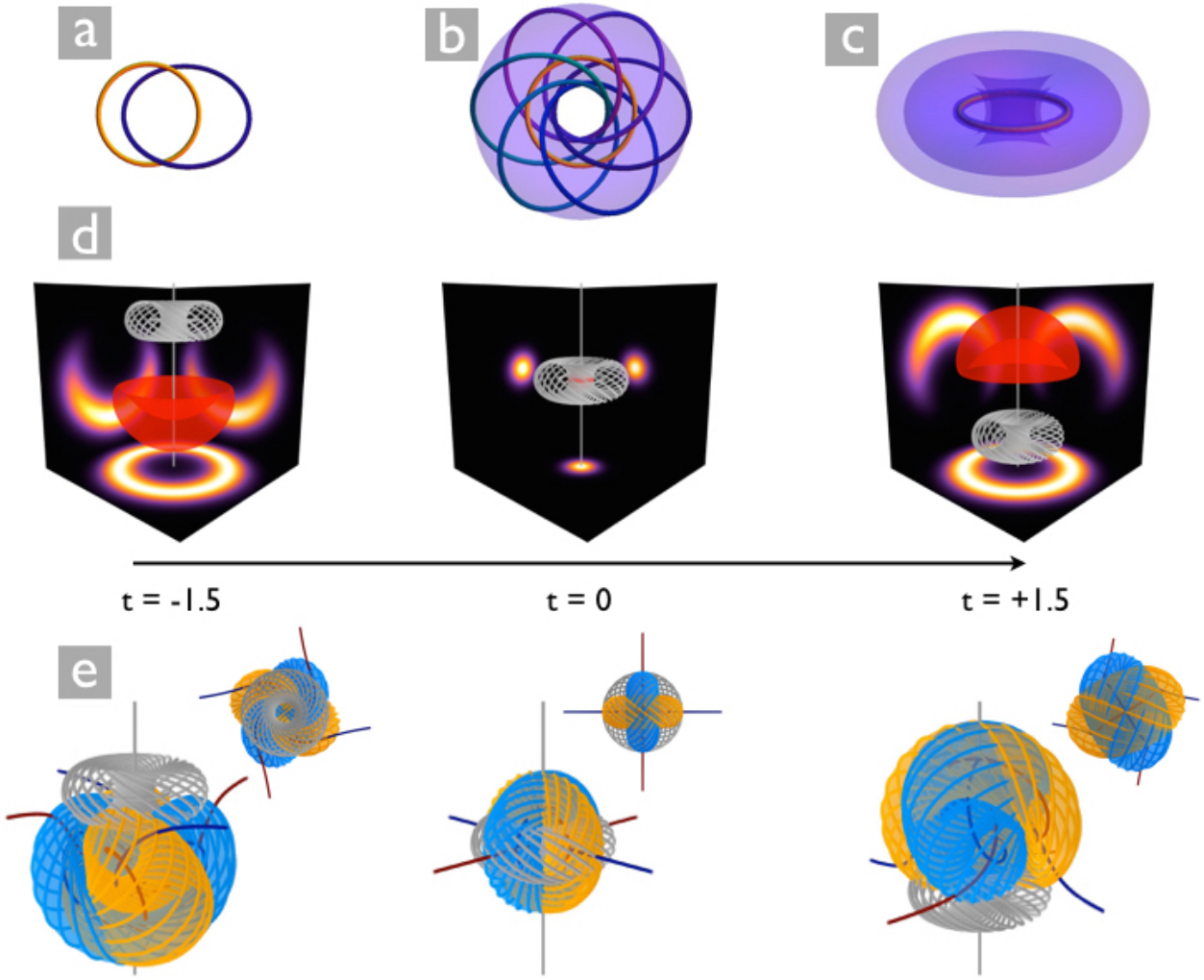

Figure 3.1: **Hopfion solution: field line structure (a-c) and time evolution (d-e)**. Field lines fill nested tori, forming closed loops linked with every other loop. **a**: Hopf link formed by the circle at the core (orange) of the nested tori, and one of the field lines (blue). **b**: The torus (purple) that the field line forming the Hopf link is tangent to. **c**: Nested tori (purple) enclosing the core, on which the field lines lie. **d**: Time evolution of the Poynting field lines (gray), an energy isosurface (red), and the energy density (shown via projections). **e**: Time evolution of the electric (yellow), magnetic (blue) and Poynting field lines (gray), with the top view shown in inset.

3.2 Hopfion solution

In case of the Hopfion solution illustrated in Fig. 3.1, the electric, magnetic and Poynting field lines exhibit a remarkable structure known as a Hopf fibration, with each field line forming a closed loop such that any two loops are linked. At time t=0, the electric, magnetic and Poynting field lines have identical structure (that of a Hopf fibration), oriented in space so that they are mutually orthogonal to each other. The topology of these structures is preserved with time, as the the electric and magnetic field lines evolve like unbreakable filaments embedded in a fluid flow, stretching and deforming while retaining their identity [70, 60]. The Poynting field lines evolve instead via a rigid translation along the z-axis. The Hopfion solution has been re-discovered and studied in several contexts [126, 26, 127, 105, 128, 27] and can be constructed in many ways: using complex scalar maps, spinors, twistors.

Despite numerous attempts at generalizing the Hopfion solution to light fields encoding more complex knots, the problem of constructing light fields encoding knots that are preserved in time has remained open until now. Attempts at generalizing Hopfions to torus knots [27, 70, 71] succeeded at constructing such solutions at an instant in time, but their structure was not preserved [70, 71], and unraveled with time. Beyond Maxwell's equations, the more general problem of finding explicit solutions to dynamical flows which embody persistent knots has also remained open.

The fluid-like topology-preserving evolution of the Hopfion solution, is closely tied to the property that the electric and magnetic fields are everywhere perpendicular and of equal magnitude (a constraint known as nullness, cf. Eq. 3.3). Nullness introduces an effective non-linearity in the problem and imposes a dynamical geometric constraint on Maxwell fields, restricting the space of possible topological configurations of field lines.

We construct knotted solutions within the space of null field configurations by making use of formalisms developed for the construction of null Maxwell fields, such as Bateman's method [129] or equivalently a spinor formalism. The combination of a null electromagnetic

field formalism with a topological construction, leading to a family of knotted null solutions is the central result of this paper. We now briefly review the key features of the evolution of null electromagnetic fields.

3.3 Null electromagnetic fields

Null electromagnetic fields have a rich history, from the early construction by Bateman [129] to Robinson's theorem [130] and Penrose's twistor theory [131]. For a null electromagnetic field, the Poynting field not only guides the flow of energy, but also governs the evolution of the electric and magnetic field lines. These field lines evolve as though embedded in a fluid, flowing at the speed of light, in the direction of the Poynting field [70, 60]. The persistence of the null conditions guarantees the continued fluid-like evolution of the electric and magnetic field lines, giving them the appearance of unbreakable elastic filaments.

The preservation of the null conditions requires the continued perpendicularity of the electric and magnetic fields as they evolve, thus requiring the flow transporting the field lines to be free of shear. Robinson's theorem [130] guarantees the existence of a shear-free family of light rays associated with every null electromagnetic field. In flat space-time, this shear-free family of light rays is given by the normalized Poynting field: the velocity field of the flow transporting the field lines.

The Hopfion solution illustrated in Fig. 3.1, beautifully demonstrates the features of a null electromagnetic field: the electric and magnetic field lines evolve smoothly, preserving the topology of the field line structure (a Hopf fibration in both cases). The shear-free family of light rays associated with the Hopfion solution, remarkably, also has the structure of a Hopf fibration, which remains unchanged as it evolves with time. This family of light rays is well known in the literature as the Robinson congruence [131].

Since the null condition makes the design of a knotted magnetic or electric field, a problem of engineering a triplet of mutually orthogonal fields that remains orthogonal under time

evolution, we start with the formalisms developed for the construction of null fields and seek to construct knotted structures within them. We now briefly summarize Bateman's method for constructing null electromagnetic fields.

3.3.1 Bateman's construction

Bateman [129] constructs all null electromagnetic fields associated with the same underlying normalized Poynting field, using two complex scalar functions of space-time. Hogan [132], has shown that all null electromagnetic fields can be constructed using Bateman's method.

According to Bateman's construction, given a pair of complex scalar functions of space-time (α, β) which satisfy:

$$\nabla\alpha \times \nabla\beta = \mathrm{i}\,(\partial_t\alpha\nabla\beta - \partial_t\beta\,\nabla\alpha) \tag{3.1}$$

there is a corresponding electromagnetic field:

$$\mathbf{F} = \mathbf{E} + \mathrm{i}\mathbf{B} = \nabla\alpha \times \nabla\beta \tag{3.2}$$

where $\mathbf{F}$ is known as the Riemann-Silberstein vector [133]. This field is null (both invariants vanish),

$$\mathbf{E}\cdot\mathbf{B} = 0\,, \quad \mathbf{E}\cdot\mathbf{E} - \mathbf{B}\cdot\mathbf{B} = 0 \tag{3.3}$$

since the scalar product $\mathbf{F}\cdot\mathbf{F}$ is zero, as can be seen by taking the dot product of the left-hand side of Eq. (3.1) with its right-hand side. For the null solutions generated by Eq. (3.2) to be non-trivial, the following conditions must be satisfied:

$$\partial_t\alpha\left((\partial_t\alpha)^2 - (\nabla\alpha)^2\right) = \partial_t\beta\left((\partial_t\beta)^2 - (\nabla\beta)^2\right) = 0$$

Each pair (α, β) satisfying Eq. (3.1) generates a whole family of fields because any vector

field of the form:

$$\mathbf{F} = h(\alpha,\beta)\,\nabla\alpha\times\nabla\beta = \nabla f(\alpha,\beta)\times\nabla g(\alpha,\beta), \tag{3.4}$$

where $h := \partial_\alpha f\,\partial_\beta g - \partial_\beta f\,\partial_\alpha g$ and f, g are arbitrary holomorphic functions of (α,β), is a null electromagnetic field. Note that all fields constructed in this way have, by construction, the same normalized Poynting field : $\frac{\mathbf{E}\times\mathbf{B}}{|\mathbf{E}\times\mathbf{B}|} = \mathrm{i}\frac{\mathbf{F}^*\times\mathbf{F}}{\mathbf{F}^*\cdot\mathbf{F}}$, where $\mathbf{F}^*$ is the complex conjugate of $\mathbf{F}$. This is made manifest, when these null fields are expressed in the equivalent language of spinors.

We list here two simple examples of this construction [128]: a circularly polarized plane wave traveling in the $+z$-direction and the Hopfion solution. They arise from the following choices of α and β. For the plane wave: $\alpha = z-t$, $\beta = x+\mathrm{i}y$, $f = \mathrm{e}^{\mathrm{i}\alpha}$, $g = \beta$, giving $\mathbf{F}^{\mathrm{pw}} = (\hat{x}+\mathrm{i}\hat{y})\mathrm{e}^{\mathrm{i}(z-t)}$. For the Hopfion we have instead: $\alpha = -d/b\,,\ \beta = -\mathrm{i}a/(2b)\,, f = 1/\alpha^2\,, g = \beta$ giving: $\mathbf{F}^{\mathrm{hp}} = d^{-3}(b^2-a^2, -\mathrm{i}(a^2+b^2), 2ab)$ where $a = x-\mathrm{i}y$, $b = t-\mathrm{i}-z$, $d = r^2-(t-\mathrm{i})^2$.

We now present a family of light-beam-like propagating solutions to Maxwell's equations in free space, in which the electric and magnetic fields encode torus knots and links that are preserved in time. We construct these solutions using complex scalar maps in the context of Bateman's framework. We then describe the knotted structure of the field lines, and compute the entire set of conserved currents, the helicity and charges for electromagnetism in free space, for this family of solutions.

3.4 Constructing knotted null electromagnetic fields

There is a natural connection between knots and singular points of complex maps from $\mathbb{S}^3$ to $\mathbb{C}$. This was used for example in recent work by Dennis et al. [38] to construct knotted optical vortices in light beams. In particular, given a pair of complex numbers (u,v) such that $|u|^2+|v|^2 = 1$ (and hence they define coordinates on $\mathbb{S}^3$), it has been shown [101, 100] that $u^p \pm v^q = 0$ is the equation of a (p,q) torus knot, when (p,q) are coprime integers.

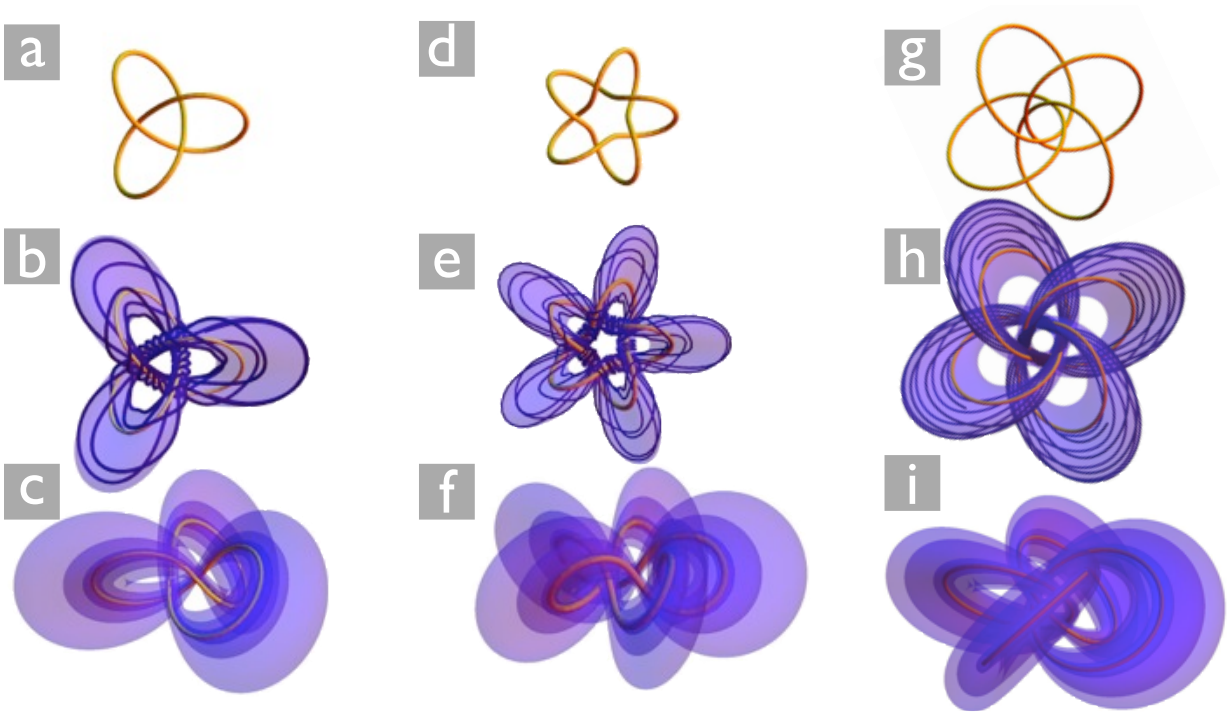

Figure 3.2: **Structure of magnetic field lines**, **a-c**: Trefoil knots ($p = 2, q = 3$), **d-f**: Cinquefoil knots ($p = 2, q = 5$), **g-i**: 4 linked rings ($p = 2, q = 2$). **a**,**d**,**g**: Core (orange) field line(s) forming (a) a trefoil knot (d) a cinquefoil knot (g) 4 linked rings. **b**,**e**,**h**: Field line(s) (blue) wrapping around the core (orange) confined to a knotted torus (purple) enclosing the core. **c**,**f**,**i**: Knotted nested tori (purple) enclosing the core, on which the field lines lie.

We note that the following choice of (α, β) in Bateman's construction:

$$\alpha = \frac{r^2 - t^2 - 1 + 2\mathrm{i}z}{r^2 - (t - \mathrm{i})^2}, \qquad \beta = \frac{2(x - \mathrm{i}y)}{r^2 - (t - \mathrm{i})^2}, \tag{3.5}$$

which satisfies Eq. (3.1), admits a natural interpretation as coordinates on $\mathbb{S}^3$ since $|\alpha|^2 + |\beta|^2 = 1$ for any t. At $t = 0$, $(\alpha, \beta) = (u, v)$, the standard stereographic coordinates on $\mathbb{S}^3$.

Hence by [101, 100], $\alpha^p \pm \beta^q = 0$ encodes a singular line tied into a (p, q) torus knot when p, q are coprime integers. Guided by this result, we make the intuitive choice of $f(\alpha, \beta) = \alpha^p$ and $g(\alpha, \beta) = \beta^q$ in (3.4), to obtain the following family of knotted null solutions:

$$\mathbf{F} = \nabla\alpha^p \times \nabla\beta^q \tag{3.6}$$

which can equivalently be expressed in terms of spinors. On inspection, we find that the electric and magnetic field lines (shown in Fig. 3.2) are grouped into knotted and linked *tori*, nested one inside the other, with (p, q)-torus knots at the core of the foliation. Being smooth, finite energy solutions to Maxwell's equations, these knotted electromagnetic fields are physically feasible, and nullness guarantees that the topology of these knotted structures is preserved in time (as shown in Fig. 3.4). The shear-free family of light rays associated with this family of solutions is the Robinson congruence.

3.4.1 Structure of knotted field lines

As illustrated in Fig. 3.2, the magnetic field lines organize around a set of *core* magnetic field lines, which form (p, q)-torus knots, and stay confined on the surfaces of nested tori, which are isosurfaces of $\Psi_B = \mathrm{Re}\{\alpha^p \beta^q\}$. The innermost core of these nested tori has zero thickness, and corresponds to the knotted core magnetic field lines. Starting from the core, the tori successively increase in thickness (as shown in Fig. 3.2), until they collide (when $\Psi_B = 0$) and extend to infinity. Since the magnetic field is divergence-free and does not vanish on any isosurface $\Psi_B \neq 0$, it follows [134] that all magnetic lines are either periodic or quasi-periodic on each toroidal surface.

As the field evolves, the nested tori along with the knotted core deform smoothly, rotating and stretching, as illustrated in Fig. 3.4.

The electric field lines are also confined on the surface of nested tori (isosurfaces of $\Psi_E = \mathrm{Im}\{\alpha^p \beta^q\}$), organizing around a set of knotted *core* electric field lines, and have exactly the same structure as the magnetic field lines, rotated in space about the z-axis by $\pi/(2q)$.

The electric and magnetic field lines organize around corresponding core electric and magnetic field lines, lying on nested tori enclosing these core field lines. Since the electric and magnetic field lines have identical structure, we begin by describing the structure of

magnetic field lines, and then go on to describe the structure of electric field lines.

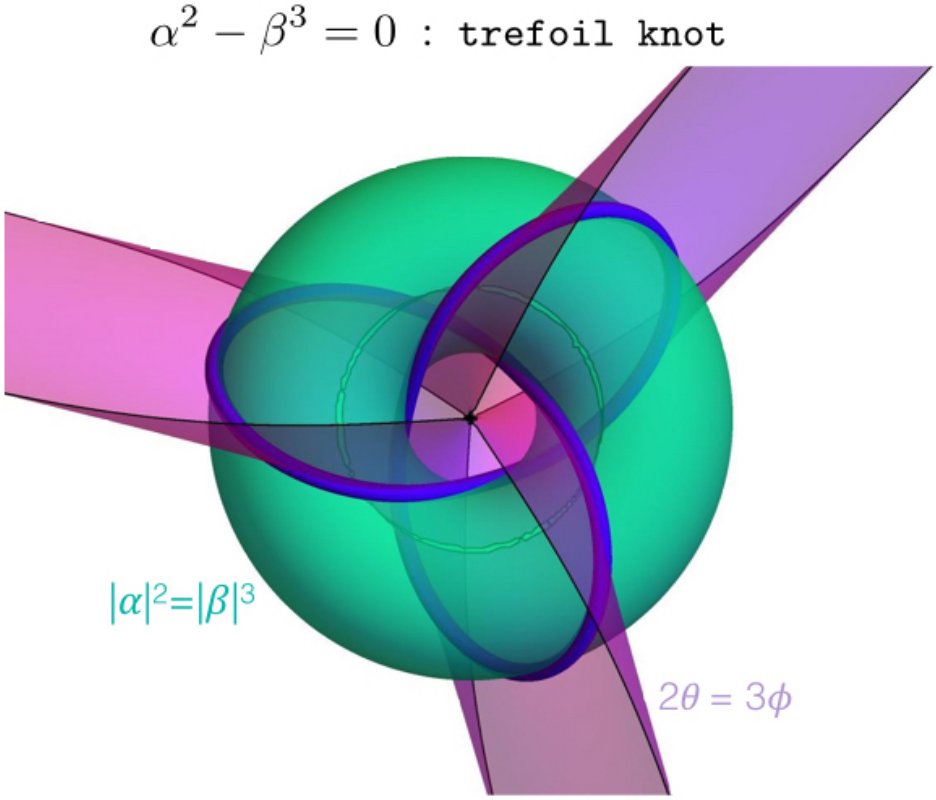

Figure 3.3: Trefoil knot (blue) as intersection of a torus (green), and a set of twisted planes (purple)

To see why the isosurfaces of Ψ_E, Ψ_B have a set of knotted field lines at their core, note that at time $t = 0$, $\alpha = \sqrt{1-\eta^2}\mathrm{e}^{\mathrm{i}\theta}$, $\beta = \eta \mathrm{e}^{\mathrm{i}\phi}$ where $\{\eta, \theta, \phi\}$ are toroidal coordinates, with their isosurfaces being nested tori, spherical bowls and half-planes respectively.

Furthermore, the intersection of a torus (η : const) with a set of twisted half-planes ($p\theta + q\phi$: const) gives a (p, q)-torus knot, as shown in Fig. 3.3. To see this for the torus knot given by $\alpha^p - \beta^q = 0$, note that :$\alpha^p = \beta^q \Rightarrow (1-\eta^2)^{p/2} = \eta^q$; $p\theta - q\phi = 0$, which is the intersection of an isosurface of η (torus) with an isosurface of $p\theta - q\phi$ (twisted half-plane) giving a (p, q)-torus knot.

The core set of knotted field lines correspond to the isosurfaces of Ψ_B, Ψ_E at their extrema. $\Psi_B = \mathrm{Re}\{\alpha^p \beta^q\} = \eta^q (1-\eta^2)^{p/2} \cos(p\theta + q\phi)$ is extremized at the intersection of

the torus $\eta = \sqrt{q/(p+q)}$ and set of twisted half-planes $p\theta + q\phi = 0, \pi$, giving (p,q)-torus knots. Similarly, $\Psi_E = \mathrm{Im}\{\alpha^p \beta^q\} = \eta^q (1-\eta^2)^{p/2} \sin(p\theta + q\phi)$ achieves its maxima at the intersection of the torus $\eta = \sqrt{q/(p+q)}$ and set of twisted half-planes $p\theta + q\phi = \pm\pi/2$, giving a (p,q)-torus knots.

The magnetic field lines are tangent to surfaces of nested tori, which are isosurfaces of $\Psi_B = \mathrm{Re}\{\alpha^p \beta^q\}$, so that: $\mathbf{B} \cdot \nabla \Psi_B = 0$. As Ψ_B is varied from its maximum and minimum values $\left(\pm\sqrt{p^p q^q/(p+q)^{p+q}}\right)$ to zero, the corresponding isosurfaces increase in size, starting from the knotted core magnetic field lines to successively bigger tori, each enveloping all previous ones, until for $\Psi_B = 0$ these tori collide, and the isosurface extends to infinity. The *core* magnetic field lines occupy the loci $K_B^{\pm}$ of maxima and minima of Ψ_B:

$$K_B^{\pm} : (\alpha, \beta) = \frac{1}{\sqrt{p+q}} \left(\mathrm{e}^{\mathrm{i}(q\theta + 2\pi k/g)} \sqrt{p}, \mathrm{e}^{\mathrm{i}(-p\theta - \pi/2q + 2\pi k/g \pm \pi/2q)} \sqrt{q} \right)$$

where $g = \gcd(p,q)$, $k \in \{0, 1, \ldots, g-1\}$ and $\theta \in [0, 2\pi/g)$ parametrizes the curve(s). The curves $K_B^{\pm}$ lie on a torus, winding p times in the toroidal direction and q times in the poloidal direction, corresponding to β and α changing phase by $-2\pi p$ and $2\pi q$ respectively, thus forming a (p,q)-torus knot for co-prime p, q.

The electric field lines have exactly the same structure, rotated in space about the z-axis by $\pi/(2q)$. The corresponding knotted tori that the electric field lines lie on, are isosurfaces of $\Psi_E = \mathrm{Im}\{\alpha^p \beta^q\}$ and the core electric field lines are given by $K_E^{\pm} : \Psi_E = \pm\sqrt{p^p q^q/(p+q)^{p+q}}$, explicitly given as follows.

$$K_E^{\pm} : (\alpha, \beta) = \frac{1}{\sqrt{p+q}} \left(\mathrm{e}^{\mathrm{i}(q\theta + 2\pi k/g)} \sqrt{p}, \mathrm{e}^{\mathrm{i}(-p\theta + 2\pi k/g \pm \pi/2q)} \sqrt{q} \right)$$

The equations for $K_E^{\pm}, K_B^{\pm}$, make it manifest that the knotted core field lines of the electric field $K_E^{\pm}$ are identical to those of the magnetic field $K_B^{\pm}$, rotated counterclockwise about the z-axis by $\frac{\pi}{2q}$. We now describe the geometry of the core field lines for all values of

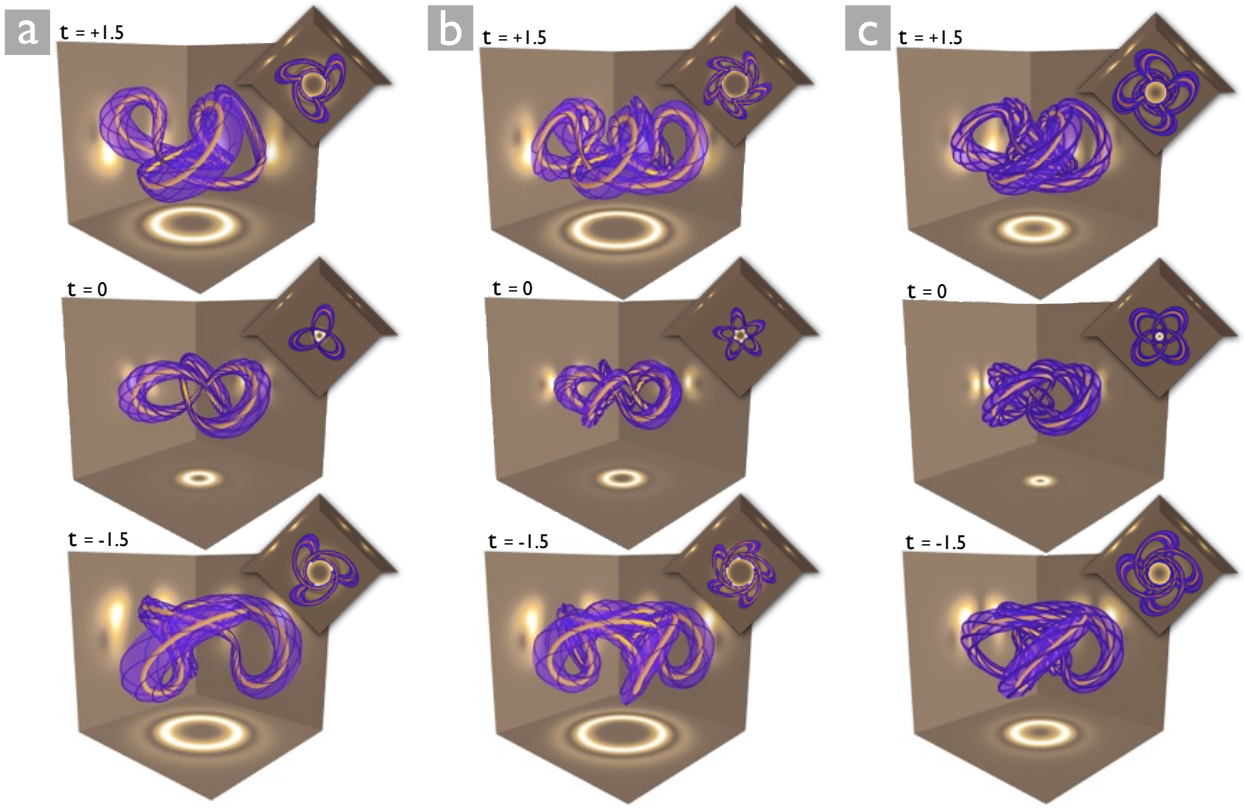

Figure 3.4: **Time evolution of magnetic field lines and energy density** for **a**: the trefoil knot ($p = 2, q = 3$), **b**: the cinquefoil knot ($p = 2, q = 5$) and **c**: the 4 Hopf-linked rings (p = 2; q = 2). Shown is the topology preserving, fluid-like evolution of the core field line(s) (orange), and field line(s) (blue) lying on tori (purple) enclosing the core.

the positive integers (p, q):

1. When $(p \neq 1, q \neq 1)$ are coprime, the core field lines are a pair of linked (p, q)-torus knots. One of the core field lines, forming trefoil and cinquefoil knots is shown in Fig. 3.2 (a).

2. When $p = 1$ (or $q = 1$), is a pair of linked rings with linking number $2q$ $(2p)$, sweeping around the torus q (p) times in the poloidal (toroidal) direction and once in the other direction.

3. In all other cases, the core field lines comprise of of $2g$ linked $(\tilde{p}, \tilde{q})$-torus knots if $\tilde{p} \neq 1, \tilde{q} \neq 1$ or $2g$ linked rings otherwise, where $g = \gcd(p, q) \neq 1$, $(p, q) = g * (\tilde{p}, \tilde{q})$.

For instance, the core magnetic field lines form 4 linked rings for $p = 2, q = 2$ as shown in Fig. 3.2(d).

This description of the knotted structure of the electric and magnetic field lines holds true for all time, conforming to our expectation of the field line structure of a null field being preserved with time.

3.4.2 Conserved charges for knotted Maxwell fields

To further characterize the physical properties of this family of knotted null fields, we compute the helicity and the full set of conserved quantities [27] corresponding to the known (conformal) symmetries of electromagnetism in free space. The non-vanishing currents and charges normalized by the energy are:

Magnetic helicity $\mathcal{H}_m$ = Electric helicity $\mathcal{H}_e = \frac{1}{p+q}$,

Momentum $\mathbf{P}$ = SCT current $\mathbf{v} = \left(0, 0, \frac{-p}{p+q}\right)$,

Angular momentum $\mathbf{L} = \left(0, 0, \frac{q}{p+q}\right)$.

The special choice of $(p, q) = (1, 1)$ yields the Hopfion solution described earlier, in which not only do the core electric and magnetic field lines form Hopf links, but all the other field lines are also closed loops, linked with every other field line.

3.5 Summary

The solutions presented here extend the space of exact, physically feasible, knotted Maxwell fields beyond the Hopfion, by encoding an entire family of both knots and links that are preserved under time evolution. Many open questions remain on the space of knotted states, such as whether solutions with each and every field line knotted and preserved by the time evolution exist with topology different from the Hopf fibration (e.g. a Seifert foliation of $\mathbb{S}^3$). Beyond electromagnetism, it remains an open question whether similar explicit solutions can be found for nonlinear evolutions such as the Euler flow of ideal fluids. From a

dynamical systems perspective, it may be interesting to explore the role of the invariant tori in the solutions we present and the conditions for which Bateman's construction give rise to electric and magnetic fields with a first integral. Finally, if realized in experiment, can these structures be imprinted on matter such as plasmas or quantum fluids?

CHAPTER 4

FLOW OF LIGHT

This chapter is based on the work presented in [60].

4.1 Introduction

Knots in physical fields, first proposed by Lord Kelvin in his vortex atom hypothesis [25], have now been observed in experiment in a wide variety of systems such as the vortex lines of a fluid [44], the topological defect lines of liquid crystals [45], singular lines of optical fields [38], and spinor Bose-Einstein condensates [65]. In recent years, much theoretical progress has been made in the study of knotted fields, and stable knot-like structures have been shown to exist as solutions of nonlinear field theories such as Euler flows [62, 135], the Skyrme-Faddeev model [78, 111, 136], and the AFZ model [137]. However, the analytical study of knotted fields remains challenging because of the inherent nonlinearity of the systems in which they emerge.

A recently discovered family of knotted light fields [59, 138], discussed in the previous chapter, has taken a significant step forward in the analytical study of knotted fields, and generated excitement as a potential tool to transfer knottedness to matter such as quantum fluids and plasmas. However, the design of such knotted light fields in which the knots persist with time has been challenging. Though it is possible to construct electromagnetic fields which encode knots in their field lines at an instant in time, [71, 58], the knots unravel at later times [70, 71]. A key ingredient in the design of knotted electromagnetic fields that persist with time has remained elusive: the initial conditions for a knot encoded in the lines of an electromagnetic field to persist with time.

In this chapter, based on [60], we present sufficient initial conditions for an initially knotted electromagnetic field to stay knotted, giving a design rule for constructing persistently

knotted electromagnetic fields.

The persistence of knots in the vortex lines of a dissipationless fluid follows from the Helmholtz laws of vortex motion [2] and served as inspiration for Lord Kelvin's vortex atom hypothesis [25]. Remarkably, the lines of the electric and magnetic field in the recently discovered family of knotted light fields evolve as if transported by the flow of the Poynting field, akin to the vortex lines in a dissipationless fluid (Euler flow). Underlying this fluid-like evolution which guarantees the persistence of knots, is a set of global $(\forall\, \mathbf{x}, t)$ geometric constraints, known as the null conditions: $\mathbf{E} \cdot \mathbf{B} = 0$; $\mathbf{E} \cdot \mathbf{E} = \mathbf{B} \cdot \mathbf{B}$.

We begin by making manifest, the equivalence between evolution by Maxwell's equations under the null conditions and transport along the flow of the normalized Poynting field, and uncover a new helicity conservation law for null electromagnetic fields. We go on to show that the null conditions are preserved by the flow of the Poynting field if and only if the flow is shear-free (4.4), giving a sufficient condition for initially knotted electromagnetic fields to stay knotted, thus enabling the design of more persistently knotted Maxwell fields. Lastly, we review an alternative global method of constructing null electromagnetic fields from complex scalar potentials [129], and establish tools for studying their topology.

4.2 Flow of null electromagnetic fields

Null electromagnetic fields have a rich mathematical structure, and are of importance in many different contexts: as radiating electromagnetic waves [129], in relation to the geometry of space-time [130, 139, 140, 141], and most recently in the context of knotted electromagnetic fields [27, 70, 59, 142]. In spite of extensive theoretical work on the existence and properties of null electromagnetic fields in curved space-time, the flow-like evolution of null electromagnetic fields in flat space-time has remained hitherto unexplored.

The null conditions are nonlinear geometric constraints on the electromagnetic field:

$$\mathbf{E} \cdot \mathbf{B} = 0 \ , \ \mathbf{E} \cdot \mathbf{E} - \mathbf{B} \cdot \mathbf{B} = 0 \tag{4.1}$$

ensuring that both scalar invariants of the electromagnetic field tensor: $F^{\mu\nu}F_{\mu\nu}$ and $*F^{\mu\nu}F_{\mu\nu}$ vanish.

A remarkable implication of the null conditions is that the evolution of the electromagnetic field is akin to a dissipationless compressible flow along the normalized Poynting field. This surprising equivalence is made manifest by the electromagnetic stress-energy tensor, which simplifies to that of a dissipationless, pressure-less fluid. Under the null conditions, the spatial part of the electromagnetic stress-energy tensor simplifies to: $T^{ij} = W V^i V^j$, where $W := \frac{1}{2}\left(\mathbf{E}^2 + \mathbf{B}^2\right)$ is the energy density, and $\mathbf{V} := (\mathbf{E} \times \mathbf{B}) / |\mathbf{E} \times \mathbf{B}|$ is the normalized Poynting field, becoming identical to the energy-momentum tensor of a dissipationless, pressure-less fluid with mass density W, and flow velocity $\mathbf{V}$.

Furthermore, under the null conditions, the electric and magnetic fields evolve as if transported by the flow of $\mathbf{V}$, analogous to the transport of vortex lines in a dissipationless flow, as proved in the Appendix.

The equivalence between the evolution of a null electromagnetic field and dissipationless fluid flow is summarized in the Table 4.1.

It is surprising that the null conditions ensure an equivalence between Maxwell's equations which are linear, and the fluid equations which are nonlinear. We note that this equivalence arises only when the equations of motion are expressed in terms of the normalized Poynting field $\mathbf{V}$, which is nonlinear in terms of the electric and magnetic fields $\mathbf{E}, \mathbf{B}$, and encodes the nonlinearity inherent in the null conditions themselves.

Interestingly, even if the null conditions are satisfied only on a time slice, the evolution of such an electromagnetic field is analogous to dissipationless fluid flow on that time slice.

Helicity—a measure of the average linking between vortex lines—is an additional con-

Null electromagnetic fields	$\leftrightarrow$	**Dissipationless flow**
Energy conservation $\partial_t W + \nabla \cdot (W\,\mathbf{V}) = 0$ energy density $W := \frac{1}{2}(\mathbf{E}^2 + \mathbf{B}^2)$	$\leftrightarrow$	Mass conservation $\partial_t \rho + \nabla \cdot (\rho\,\mathbf{u}) = 0$ mass density ρ
Momentum conservation $\partial_t \mathbf{V} + (\mathbf{V} \cdot \nabla)\,\mathbf{V} = 0$ $\mathbf{V} := (\mathbf{E} \times \mathbf{B})/W$	$\leftrightarrow$	Momentum conservation $\partial_t \mathbf{u} + (\mathbf{u} \cdot \nabla)\mathbf{u} = -\nabla p/\rho$ fluid velocity $\mathbf{u}$
Transport of $\mathbf{E}/W$, $\mathbf{B}/W$ along $\mathbf{V}$ $\partial_t\,(\mathbf{E}/W) = [\mathbf{E}/W\,,\,\mathbf{V}]$ $\partial_t\,(\mathbf{B}/W) = [\mathbf{B}/W\,,\,\mathbf{V}]$	$\leftrightarrow$	Transport of ω/ρ along $\mathbf{u}$ $\partial_t\,(\omega/\rho) = [\omega/\rho\,,\,\mathbf{u}]$ $\omega := \nabla \times \mathbf{u}$

Table 4.1: Flow of null electromagnetic fields (see appendix for detailed proofs)

served quantity in Euler flows [9], a consequence of the fact that vortex lines are transported by the flow. Since the lines of the electric and magnetic fields are transported by the flow of $\mathbf{V}$, akin to vortex lines in an Euler flow, the helicity of the electric and magnetic fields is also conserved [70]. Furthermore, since the Poynting field evolves akin to pressure-less Euler flow, the vorticity associated with the flow of the Poynting field $\Omega := \nabla \times \mathbf{V}$, is also transported by the flow of the Poynting field:

$$\partial_t \Omega = \nabla \times (\mathbf{V} \times \Omega) \tag{4.2}$$

This gives rise to a new conserved quantity for null electromagnetic fields: the Poynting helicity $\mathcal{H}_\Omega := \int \mathbf{V} \cdot \Omega \, \mathrm{d}^3x$. Though the for the Poynting helicity $\mathcal{H}_\Omega = \int \mathbf{V} \cdot \Omega \, \mathrm{d}^3x$ diverges since $|\mathbf{V}| = 1$, the corresponding local conservation law for $h_\Omega = \mathbf{V} \cdot \Omega$:

$$\partial_t h_\Omega + \nabla \cdot \left(\mathbf{V}\, h_\Omega - \frac{\Omega}{2} \right) = 0 \tag{4.3}$$

is a well-behaved new conservation law for null electromagnetic fields in flat space-time.

Hence, under the null conditions, electromagnetic fields evolve akin to transport along a pressure-less Euler flow given by the normalized Poynting field $\mathbf{V}$, and satisfy topological

conservation laws for the electric field $\mathbf{E}$, the magnetic field $\mathbf{B}$ and the Poynting vorticity field Ω.

Since the null conditions ensure that lines of the electric and magnetic fields are transported, satisfying the null conditions for all space-time is sufficient to guarantee that knots encoded in the lines of the electric and magnetic fields will persist forever. Hence, designing persistent knotted electromagnetic fields requires constructing a knotted electromagnetic field on the initial time slice that satisfies the null conditions not only on the initial time slice, but for all time. We now seek the conditions under which an electromagnetic field satisfying the null conditions on an initial time slice, satisfies the null conditions for all time.

4.3 When does an initially null electromagnetic field stay null?

Since null electromagnetic fields exhibit the topology preserving dynamics of dissipationless flows, the initial conditions that guarantee nullness for all space-time are sufficient to ensure the persistence of knots for all time. However, previous attempts at addressing the question of the initial conditions that guarantee nullness for all space-time, have either been inconclusive [143, 144] or have reached the incorrect conclusion [145] that satisfying null conditions on the initial time slice is sufficient to guarantee nullness for all space-time.

The evolution of an electromagnetic field satisfying the null conditions on the initial time slice is the transport of a triplet of mutually perpendicular vectors $\{\mathbf{E}, \mathbf{B}, \mathbf{V}\}$ along the flow of $\mathbf{V}$. For the null conditions to be satisfied by the electromagnetic field on the next time slice, the angle between the electric and magnetic fields $\{\mathbf{E}, \mathbf{B}\}$ and their magnitudes must remain invariant under the flow of $\mathbf{V}$. For the flow of $\mathbf{V}$ to preserve magnitudes and angles of two mutually perpendicular vectors $\mathbf{E}, \mathbf{B}$ everywhere in space, the flow must be free of non-uniform stretching or twisting, i.e. it must be free of shear. Furthermore, a flow that is shear-free stays shear-free when transported along itself in a flat space-time. Therefore an electromagnetic field that satisfies the null conditions on the initial time slice, with the flow

of the normalized Poynting field $\mathbf{V}$ initially free of shear, satisfies the null conditions and preserves the shear-free nature of the flow at later times (see Appendix for detailed proof).

Hence, we find that an initially null electromagnetic field, stays null for short times (until a singularity develops), if and only if the analogous flow field is initially shear-free

$$\left\{ \begin{array}{ll} \mathbf{E}\cdot\mathbf{B}=0 & \\ \mathbf{E}\cdot\mathbf{E}=\mathbf{B}\cdot\mathbf{B} & \end{array} \right. \quad \& \quad \left. \begin{array}{l} (E^i\,E^j - B^i\,B^j)\,\partial_j V_i = 0 \\ (E^i\,B^j + E^j\,B^i)\,\partial_j V_i = 0 \end{array} \right\}_{t=0} \Leftrightarrow \left\{ \begin{array}{l} \mathbf{E}\cdot\mathbf{B}=0 \\ \mathbf{E}\cdot\mathbf{E}=\mathbf{B}\cdot\mathbf{B} \end{array} \right\}_{\forall\, t<t^*} \tag{4.4}$$

where t^* is the time at which the flow field may develop singularities, since we are unable to rule out the possibility that the flow of the normalized Poynting field $\mathbf{V}$ develops finite-time singularities and lead to a violation of the null conditions.

We now review an alternative global construction of null electromagnetic fields, and develop tools for studying the topology of field lines for such electromagnetic fields.

4.4 Geometry of null electromagnetic fields

An alternative way of constructing electromagnetic fields that satisfy the null conditions for all space and time, was given by Bateman [129] in terms of complex scalar potentials (α, β). Hogan [132], has shown that all null electromagnetic fields can be expressed in terms of Bateman potentials (α, β): complex scalar functions of space-time which satisfy:

$$\nabla\alpha \times \nabla\beta = \mathrm{i}\,(\partial_t\alpha\nabla\beta - \partial_t\beta\,\nabla\alpha) \tag{4.5}$$

The corresponding null electromagnetic field is given by:

$$\mathbf{F} = \mathbf{E} + \mathrm{i}\mathbf{B} = \nabla\alpha \times \nabla\beta \tag{4.6}$$

where $\mathbf{F}$ is known as the Riemann-Silberstein vector [133].

The design of knotted null electromagnetic fields requires understanding the interplay between the topology of the lines of the electric and magnetic fields, and the complex scalar potentials (α, β). Unfortunately, describing the topology of the lines of a space-filling vector field is an intricate problem, made all the more challenging by the difficulty of analytically solving for the field lines everywhere in space. However, in the special case that the lines of a vector field are tangent to surfaces, i.e. the vector field has a first integral, the topology of the field lines is encoded in the topology of these surfaces. In the recently discovered family of knotted Maxwell fields [59], the field lines were tangent to knotted tori, and establishing the persistence of these knotted tori was key to establishing the persistence of the knots encoded in the field lines.

Sufficient conditions for the lines of a null electromagnetic field to be tangent to surfaces, in terms of the Bateman potentials (α, β), are (see Appendix for detailed proofs):

$$\nabla(\alpha\bar{\alpha}) \times \nabla\left(\beta\bar{\beta}\right) = 0 \Rightarrow \mathbf{E} \cdot \nabla(\mathrm{Im}\{\alpha\beta\}) = 0\,,\ \mathbf{B} \cdot \nabla(\mathrm{Re}\{\alpha\beta\}) = 0 \tag{4.7}$$

$$\nabla\left(\frac{\alpha}{\bar{\alpha}}\right) \times \nabla\left(\frac{\beta}{\bar{\beta}}\right) = 0 \Rightarrow \mathbf{E} \cdot \nabla(\mathrm{Re}\{\alpha\beta\}) = 0\,,\ \mathbf{B} \cdot \nabla(\mathrm{Im}\{\alpha\beta\}) = 0 \tag{4.8}$$

Constructing null electromagnetic fields which satisfy the above conditions would enable the study of the topology of their field lines in terms of the topology of the isosurfaces of Ψ_E, Ψ_B.

4.5 Summary

Our results firmly establish the connection between the evolution of null electromagnetic fields by Maxwell's equations and transport along the flow of the normalized Poynting field. We establish necessary and sufficient initial conditions for an electromagnetic field to satisfy the null conditions for all space-time, thereby giving a design rule for constructing persistently knotted solutions to Maxwell's equations.

Lastly, we give sufficient conditions for the lines of null electromagnetic fields to lie on

surfaces, enabling the study of the topology of field lines in terms of the surfaces they lie on.

CHAPTER 5

HELICITY IN SUPERFLUIDS

This chapter is based on the work presented in [61].

5.1 Introduction

Our understanding of fluid flow is built on fundamental conservation laws such as the conservation of mass, energy, and momentum [146]. In particular, these give rise to the Euler equations of dissipationless fluid mechanics which capture the essence of many fluid phenomena including vortex dynamics, formation and propagation of acoustic waves and shocks [147], instabilities [148] and play a key role in the study of turbulence [149, 150].

Hidden within the Euler equations, is a less familiar conservation law [8, 40, 9]: conservation of helicity $\mathcal{H}_{\text{Euler}} = \int \mathrm{d}^3x\, \mathbf{u}\cdot\boldsymbol{\omega}$, $\boldsymbol{\omega} = \nabla\times\mathbf{u}$. The conservation of helicity—a measure of the average linking of vortex lines in a fluid [9, 40]—places a topological constraint on the motion of vortex lines in Euler flows (classical inviscid, isentropic flows). Helicity, also conserved in infinitely conducting plasmas [8], has been central to the understanding of turbulent dynamo theory [50, 51], and has important consequences for the stability and relaxation of plasmas [52, 53, 54, 55]. Furthermore, helicity has yielded new insights into vortex reconnection events in viscous flows [56, 57], and plays an important role in the study of coherent dynamical structures generated by turbulent flow [151, 152, 153].

Superfluids display striking similarities with classical fluids in vortex dynamics [154, 155] and turbulence statistics [156, 157, 158]. Since superfluids flow without dissipation like Euler flows, it is natural to ask whether an additional conserved quantity analogous to helicity also exists in superfluid flows. The existence of such an additional conserved quantity could have far-reaching implications.

In this chapter, based on [61], we address the existence of a "superfluid helicity" using

an analytical approach based on the symmetry underlying classical helicity conservation. Furthermore, we use numerical simulations to examine whether collections of superfluid vortices that mimic the structure of a classical vortex, approach Euler flow-like behavior and instead find behavior consistent with viscous flows.

To simplify our discussion, we will consider superfluids at zero temperature—weakly interacting Bose condensates described by a complex order parameter ψ ("wave function of the condensate" [159])—obeying the Gross-Pitaevskii equation [160, 161]:

$$i\hbar\,\partial_t\psi = -\frac{\hbar^2}{2m}\nabla^2\psi + g\,|\psi|^2\,\psi \tag{5.1}$$

The Gross-Pitaevskii equation (GPE) captures qualitatively important features of superfluid behavior at low temperatures [162, 154], including the dynamics of vortices—lines where the complex order parameter ψ vanishes, and its phase winds around by a multiple of 2π (see Fig. 5.1).

Interestingly, the Gross-Pitaevskii equation can be mapped to an Euler flow in the region excluding vortices via the Madelung transformation [163, 164]: $\psi = \sqrt{\rho}\exp(i\phi/\hbar)$—rewriting Eq. (5.1) in terms of the fluid density $\rho = |\psi|^2$, and velocity $\mathbf{u} = \nabla\phi$. The mapping between superfluid flow and Euler flow makes it tempting to conclude that helicity is conserved in superfluids just as in Euler flows. However, the expression for helicity in Euler flows: $\mathcal{H}_{\text{Euler}} = \int \mathrm{d}^3x\,\mathbf{u}\cdot\boldsymbol{\omega}$, $\boldsymbol{\omega} = \nabla\times\mathbf{u}$ is not conserved in superfluid flows [56, 165, 166] since the writhe (coiling) [167] of a vortex line can change with time, causing $\mathcal{H}_{\text{Euler}}$ to change.

This is because superfluid flows differ from Euler flows in important ways. (i) Superfluids have singular vorticity distributions—concentrated on lines of singular phase (see Fig. 5.1)—and quantized circulation $\Gamma = \oint \mathbf{u}\cdot\mathrm{d}\mathbf{l} = 2\pi n$, unlike classical vortices which have smooth vorticity distributions. (ii) Vortex lines in a superfluid can reconnect as demonstrated numerically [168, 169], experimentally [170] and analytically (see Appendix). This is in contrast to vortices in Euler flows which can never cross.

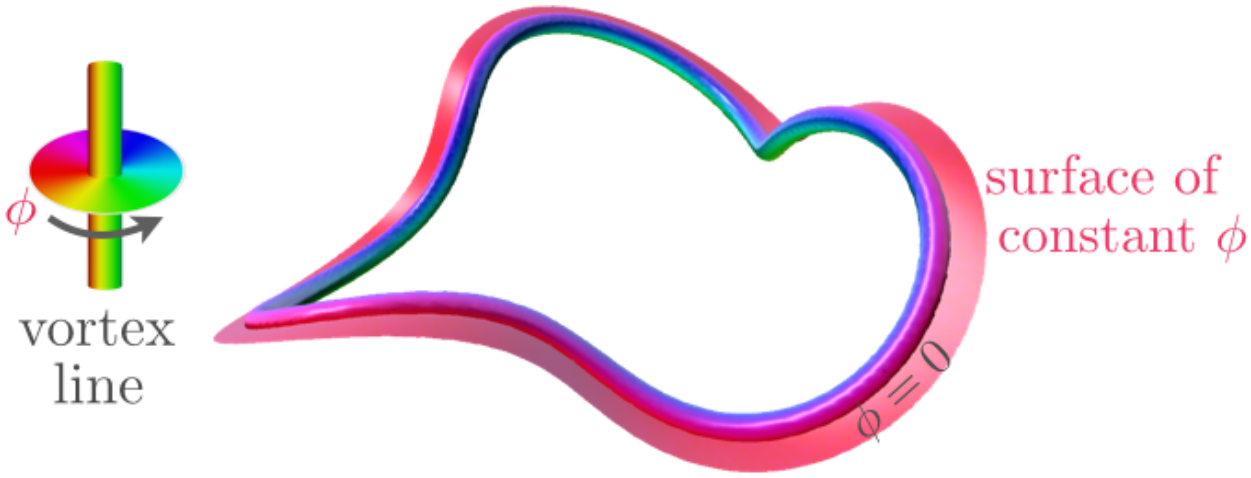

Figure 5.1: A three-fold helical superfluid vortex and a section of its phase isosurface. The volume occupied by the superfluid naturally separates into surfaces of constant phase (phase isosurfaces). Shown here is such a phase isosurface clipped at a fixed distance from the vortex.

The singular nature of superfluid vortices and the presence of vortex reconnections makes it challenging to carry over the derivation of helicity conservation [9] in Euler flows, and suggests that a fundamentally different approach is required to address the question of a "superfluid helicity". Previous approaches [165, 166, 171, 172] to seeking a conserved quantity analogous to helicity in superfluid flows have focused on adapting the expression for classical helicity $\mathcal{H}_{\text{Euler}}$ to superfluids. However, their connection to the basic notion of conservation is unclear, since classical helicity $\mathcal{H}_{\text{Euler}}$ is manifestly not conserved in superfluid flows [56].

We begin with the fundamental symmetry that gives rise to helicity conservation in Euler flows via Noether's theorem, and carry this over to superfluids. We find that there exists a conserved quantity analogous to helicity in superfluids, and that it vanishes identically. We find that the vanishing of "superfluid helicity" is a consequence of a geometric property of phase isosurfaces which was first studied in the context of magnetic flux tubes [173]. Furthermore, we consider collections of superfluid vortices that approximate the structure of a classical vortex, and ask whether in this "classical" limit, superfluids conserve the classical helicity $\mathcal{H}_{\text{Euler}}$. We find that the collective dynamics of superfluid vortex bundles are more

akin to vortices in viscous flows than Euler flows.

5.2 Helicity—as a Noether charge

Helicity conservation in Euler flows [174, 175, 176, 177, 178, 179, 180, 181, 182] can be traced back to the particle relabeling symmetry via Noether's theorem. Particle relabeling symmetry arises from an equivalence between the Lagrangian description of a flow in terms of the positions $\mathbf{x}(\mathbf{a},\tau)$ and velocities $\partial_\tau \mathbf{x}(\mathbf{a},\tau)$ of fluid particles labeled by $\mathbf{a}$ at time τ, and the Eulerian description of a flow in terms of the velocity $\mathbf{u}(\mathbf{x},t)$ and density $\rho(\mathbf{x},t)$ at each point in space. Specifically, the action for Euler flow is [176, 178, 181]:

$$S_{\text{Euler}} = \int d\tau\, d^3a \left[\frac{1}{2}\left(\partial_\tau \mathbf{x}(\mathbf{a},\tau)\right)^2 - E(\rho)\right] \tag{5.2}$$

where τ is time, $\mathrm{d}^3a = \rho\,\mathrm{d}^3x$ is the mass of a fluid element, $\partial_\tau \mathbf{x}(\mathbf{a},\tau)$ is the velocity, $E(\rho(\mathbf{a}))$ is the internal energy of the fluid element labeled by $\mathbf{a}$, and the co-ordinate frames $(\mathbf{a},\tau)$ and $(\mathbf{x},t)$ are related as follows: $\partial_\tau = \partial_t + \mathbf{u}\cdot\nabla$. Note that the Euler flow action in Eq. (5.2) depends only on the flow velocity $\mathbf{u} = \partial_\tau \mathbf{x}(\mathbf{a},\tau)$, and the density $\rho : \rho^{-1}(\mathbf{a}) = \det\left(\partial x^i(\mathbf{a})/\partial\, a^j\right)$.

Relabeling transformations are defined as changes of the particle labels: $a^i \to \tilde{a}^i = a^i + \epsilon\,\eta^i$, where η^i obeys the conditions: (i) $\partial\eta^i/\partial\tau = 0$, and (ii) $\partial\eta^i/\partial a^i = 0$, and the positions of the fluid particles remain unchanged under the relabeling transformation, i.e. $\tilde{\mathbf{x}}(\tilde{\mathbf{a}},\tau) = \mathbf{x}(\mathbf{a},\tau)$.

Particle labels can be interpreted as the initial co-ordinates of the fluid particles, and the relabeling transformation can be thought of as a smooth reshuffling (diffeomorphism) of the fluid particles, resulting in a change of initial co-ordinates, i.e. particle labels. The invariance of the action is a result of the fact that the dynamics of the fluid are independent of any particular choice of particle labels, i.e. depend only on the fluid velocity and density.

The conditions on the relabeling transformation η^i ensure that (i) the new particle labels $\tilde{\mathbf{a}}$ are independent of time τ, keeping the velocity unchanged, and (ii) the volume element $\mathrm{d}^3a = \mathrm{d}^3\tilde{a}$ is unchanged, leaving the density $\rho = \det(\partial\mathbf{x}/\partial\mathbf{a})^{-1}$ invariant. The conserved charge associated with relabeling transformations [178, 177, 183, 176, 179] is:

$$\mathcal{Q}_{\text{Euler}} = \int d^3a\, u_i \frac{\partial x^i}{\partial a^j}\, \eta^j \tag{5.3}$$

where $u_i = \partial x_i/\partial\tau$.

Kelvin's circulation theorem emerges naturally from an invariance under relabeling: conservation of circulation Γ_C along the loop C: $\Gamma_C = \oint_C \mathbf{u}\cdot\mathrm{d}\mathbf{x}(s)$ where the loop C is transported by the flow, arises from the conserved charge $\mathcal{Q}_{\text{Euler}}$ evaluated for a relabeling transformation η^j which infinitesimally translates particle labels $\mathbf{a}$ along the loop C [178, 183]. Specifically, the relabeling transformation given by $\eta^j = \oint_{C:\mathbf{a}(s)} ds\, \delta^{(3)}(\mathbf{a}-\mathbf{a}(s))\, \partial a^j(s)/\partial s$ gives via Eq. (5.3), the conserved charge: $\mathcal{Q}_{\text{Euler}} = \Gamma_C = \oint_C \mathbf{u}\cdot\mathrm{d}\mathbf{x}(s)$. Note that the conserved circulation Γ_C is intimately tied to the Lagrangian description of the flow in terms of fluid particle labels, since the loop C is transported with the flow.

Helicity conservation also arises naturally as a consequence of the relabeling symmetry: helicity is the conserved charge $\mathcal{Q}_{\text{Euler}}$ in Eq. (5.3), evaluated for a relabeling transformation η^j which infinitesimally translates the particle labels $\mathbf{a}$ along vortex lines. Specifically, such a relabeling transformation: $\eta^j = \epsilon^{jkl}(\partial u_p/\partial a^k)(\partial x^p/\partial a^l)$, is a symmetry of the action and the corresponding conserved charge (Eq. (5.3)) is the classical helicity [178, 177, 183, 176, 179]: $\mathcal{H}_{\text{Euler}} = \int \mathbf{u}\cdot\omega\, \mathrm{d}^3x$. Unlike circulation, helicity can be expressed purely in terms of Eulerian variables, and does not require tracking the flow. This is because vortex lines in Euler flows are transported by the fluid, and therefore vorticity automatically tracks the fluid elements on vortex lines, acting as a proxy for the particle labels.

Thus the particle relabeling symmetry underlies both, helicity conservation and Kelvin's circulation theorem, in Euler flows. We note that helicity conservation can be thought of as

a special case of Kelvin's circulation theorem: as the conservation of the sum of circulations along all the vortex lines in the fluid, weighted by the circulation around each vortex line.

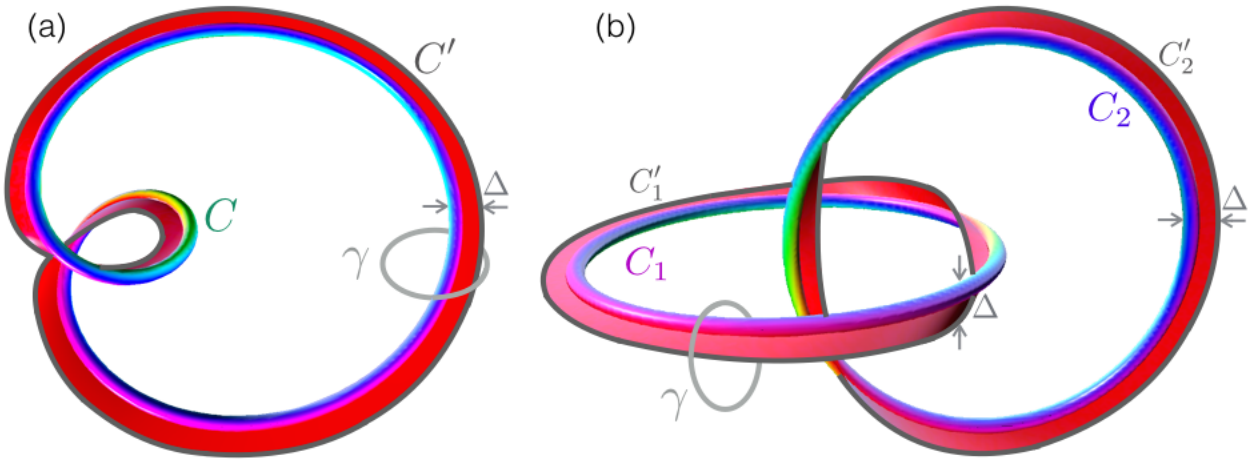

Figure 5.2: Vortex lines C, and closed curves C' obtained by offsetting vortex lines along a phase isosurface for: (a) a writhing (coiling) vortex line C, (b) a pair of linked rings C_1 , C_2. Notice that the presence of either writhing or linking in vortex lines leads to the twisting of the phase isosurface around the vortex lines. The circulation around a closed loop γ encircling a vortex line is equal to the change in phase ϕ as the loop is traversed, so that the circulation is quantized.

We seek conserved quantities analogous to helicity and circulation in superfluids, by seeking analogs of the relabeling symmetry transformations. We begin by expressing the action for the Gross-Pitaevskii superfluid in terms of the hydrodynamic variables $\rho = |\psi|^2$, and $\phi = \hbar \arg \psi$:

$$S_{\mathrm{gpe}} = -\int dt\, \rho\, d^3x \left(\partial_t \phi + \frac{1}{2m}(\nabla\phi)^2 + \frac{g}{2}\rho + \frac{\hbar^2}{2m}\left(\frac{\nabla\sqrt{\rho}}{\sqrt{\rho}}\right)^2 \right) \tag{5.4}$$

The last term in the above action: $(\nabla\sqrt{\rho}/\sqrt{\rho})^2$—known as the "quantum pressure" term—is negligible when the typical length scale of density variations is much larger [184, 185, 186]

than the "healing length" $\xi = \sqrt{\hbar^2/(2m\, g\, \rho_{\rm max})}$, and its primary effect is to regularize the size of the vortex core [186, 187, 188, 185], and enable vortex reconnections [189]. We make the Thomas-Fermi approximation [189, 159, 190, 191, 185] which neglects the "quantum pressure" term and is thought to capture well, the dynamics of superfluid vortices [189, 191, 188, 192, 193]. Within this approximation, we seek to express the action for the Gross-Pitaevskii superfluid (Eq. 5.4) in terms of the Lagrangian co-ordinates $(\mathbf{a}, \tau)$, where $\mathbf{a}$ is the particle label, and τ is time. To this end, we rewrite $\nabla\phi$ as the fluid velocity $\mathbf{u} = \partial\mathbf{x}(\mathbf{a}, \tau)/\partial\tau$, and use the relation $\partial_\tau = \partial_t + \mathbf{u}\cdot\nabla$ to rewrite $\partial_t\phi$ as $\partial_\tau\phi - \mathbf{u}\cdot\nabla\phi$. The superfluid action can then be rewritten in terms of the positions of fluid particles $\mathbf{x}(\mathbf{a}, \tau)$ and the phase associated with each fluid particle $\phi(\mathbf{a}, \tau)$ as:

$$\begin{aligned} S_{\rm gpe} &= \int d\tau\, d^3a \left[\frac{1}{2}\left(\partial_\tau \mathbf{x}(\mathbf{a},\tau)\right)^2 - E(\rho) - \partial_\tau\phi(\mathbf{a},\tau)\right] \\ &= S_{\rm Euler} + S_{\rm phase} \end{aligned} \tag{5.5}$$

where $S_{\rm phase} = \int d\tau d^3a\, (-\partial_\tau\phi(\mathbf{a},\tau))$, $S_{\rm Euler}$ is as defined in Eq. (5.2), $E(\rho) = g\,\rho/2$, $\nabla\phi = \mathbf{u} = \partial_\tau\mathbf{x}(\mathbf{a},\tau)$, we have set $m = 1$, and the Lagrangian co-ordinates $(\mathbf{a}, \tau)$ satisfy: $\rho\, {\rm d}^3x = {\rm d}^3a$, as for Euler flow. Note that the action $S_{\rm gpe}$ differs from the Euler action given in Eq. (5.2) only by $S_{\rm phase}$: an additional term associated with the phase $\phi(\mathbf{a}, \tau)$. This additional term associated with the phase $\phi(\mathbf{a}, \tau)$, is intimately tied to the Galilean invariance [194] of the action S_{gpe} and as we will see has key consequences for the conservation of helicity.

Particle relabeling transformations of the form $a^i \to \tilde{a}^i = a^i + \epsilon\,\eta^i$, $\tilde{\mathbf{x}}(\tilde{\mathbf{a}}, \tau) = \mathbf{x}(\mathbf{a}, \tau)$, $\tilde{\phi}(\tilde{\mathbf{a}}, \tau) = \phi(\mathbf{a}, \tau)$, where $\partial\eta^i/\partial\tau = 0$, $\partial\eta^i/\partial a^i = 0$, leave the velocity, the phase, and the density unchanged, and hence are symmetries of the action. Using Noether's theorem, we find the

corresponding conserved charge:

$$\begin{aligned}\mathcal{Q}_{\text{gpe}} = &\quad \mathcal{Q}_{\text{Euler}} \quad + \quad \mathcal{Q}_{\text{phase}} \\ &= \int d^3a\, u_i \frac{\partial x^i}{\partial a^j}\, \eta^j + \int d^3a \left(-\frac{\partial \phi}{\partial a^j}\right) \eta^j \end{aligned} \tag{5.6}$$

$$= \int d^3a \left(u_i \frac{\partial x^i}{\partial a^j} - \frac{\partial \phi}{\partial x^i}\frac{\partial x^i}{\partial a^j}\right) \eta^j = 0 \tag{5.7}$$

where $\mathcal{Q}_{\text{Euler}}$ is the contribution from the Euler flow part of the action S_{Euler} as defined in Eq. (5.3), and $\mathcal{Q}_{\text{phase}} = \int d^3a \left(-\partial\phi/\partial a^j\right) \eta^j$ is the contribution to the conserved charge from the additional phase term in the action S_{phase}. Since the superfluid velocity $\mathbf{u} = \nabla\phi$, the contributions $\mathcal{Q}_{\text{Euler}}$ and $\mathcal{Q}_{\text{phase}}$ cancel exactly, and the conserved charge $\mathcal{Q}_{\text{gpe}}$ vanishes identically for all relabeling transformations η^j. Note that since the phase of the complex order parameter $\phi(\mathbf{a}, \tau)$ is absent from the description of classical flow, the classical conserved charge $\mathcal{Q}_{\text{Euler}}$ is simply the superfluid conserved charge $\mathcal{Q}_{\text{gpe}}$ in the absence of the phase term: $\mathcal{Q}_{\text{phase}}$.

Since helicity and circulation emerge as conserved quantities in Euler flow from the Noether charge $\mathcal{Q}_{\text{Euler}}$ evaluated for different relabeling transformations η^j, the conserved quantities analogous to helicity and circulation in superfluid flow vanish identically. The vanishing of the conserved quantity analogous to helicity is consistent with an alternative approach based on helicity as a Casimir invariant [176, 178] (see Appendix for details). Furthermore, the vanishing of the conserved quantity analogous to circulation is consistent with the decay and collapse of a vortex ring, as observed experimentally [195, 196] and demonstrated by analytical calculations for a low-density region of the superfluid (see Appendix for details).

5.3 Superfluid helicity—a geometric interpretation

We now examine how the vanishing of "superfluid helicity" is connected to the geometry of vortex lines and phase isosurfaces in superfluids. We begin by considering the conserved charge analogous to circulation in superfluids, given by $\mathcal{Q}_{\text{gpe}}$ for a relabeling transformation $\boldsymbol{\eta}_\gamma$ that translates particle labels along an arbitrary closed loop γ encircling a vortex line (see Fig. 5.2). Such a relabeling transformation is given by $\boldsymbol{\eta}_\gamma = \oint_\gamma ds\, \delta^{(3)}(\mathbf{a} - \mathbf{a}(s))\, \mathrm{d}\mathbf{a}(s)/\mathrm{d}s$, where $\mathbf{a}(s) \in \gamma$, giving the vanishing conserved charge $\mathcal{Q}_{\text{gpe}}$:

$$\begin{aligned}\mathcal{Q}_{\text{gpe}}\Big|_{\boldsymbol{\eta}_\gamma} &= \mathcal{Q}_{\text{Euler}}\Big|_{\boldsymbol{\eta}_\gamma} \;+\; \mathcal{Q}_{\text{phase}}\Big|_{\boldsymbol{\eta}_\gamma} \\ &= \oint_\gamma \mathbf{u}\cdot \mathrm{d}\mathbf{l} + \oint_\gamma (-\nabla\phi)\cdot \mathrm{d}\mathbf{l} = 0\end{aligned}$$

In the above calculation, since the loop γ pierces phase isosurfaces as it encircles a vortex line, the circulation $\oint \mathbf{u}\cdot\mathrm{d}\mathbf{l}$ is canceled by the change in phase $\oint (-\nabla\phi)\cdot\mathrm{d}\mathbf{l}$. We note however that by judiciously choosing the shape of the loop, it is possible to make the contribution $\mathcal{Q}_{\text{phase}}$ vanish identically. This can be accomplished by choosing a loop that lies entirely on a phase isosurface as depicted in Fig. 5.2. The vanishing of $\mathcal{Q}_{\text{gpe}}$ then acquires a simple geometric interpretation.

We construct a curve C_i' by offseting the vortex line C_i along a phase isosurface by a distance Δ as shown in Fig. 5.2, and consider the relabeling transformation given by: $\boldsymbol{\eta}(\Delta) = \oint_{C_i'(\Delta)} ds\, \delta^{(3)}(\mathbf{a} - \mathbf{a}'(s))\, \mathrm{d}\mathbf{a}'(s)/\mathrm{d}s$ where $C_i'(\Delta) : \mathbf{a}'(s) = \mathbf{a}(s) + \Delta\, \hat{\mathbf{n}}(s)$, $\mathbf{a}(s) \in C_i$, $\hat{\mathbf{n}}(s)$ is perpendicular to the vortex line, and tangent to the phase isosurface. The quantum pressure term is negligible on the new closed curves $C_i'(\Delta)$ as long as the distance Δ is large compared to the healing length ξ. Since the closed curve C_i' lies on a phase isosurface, the

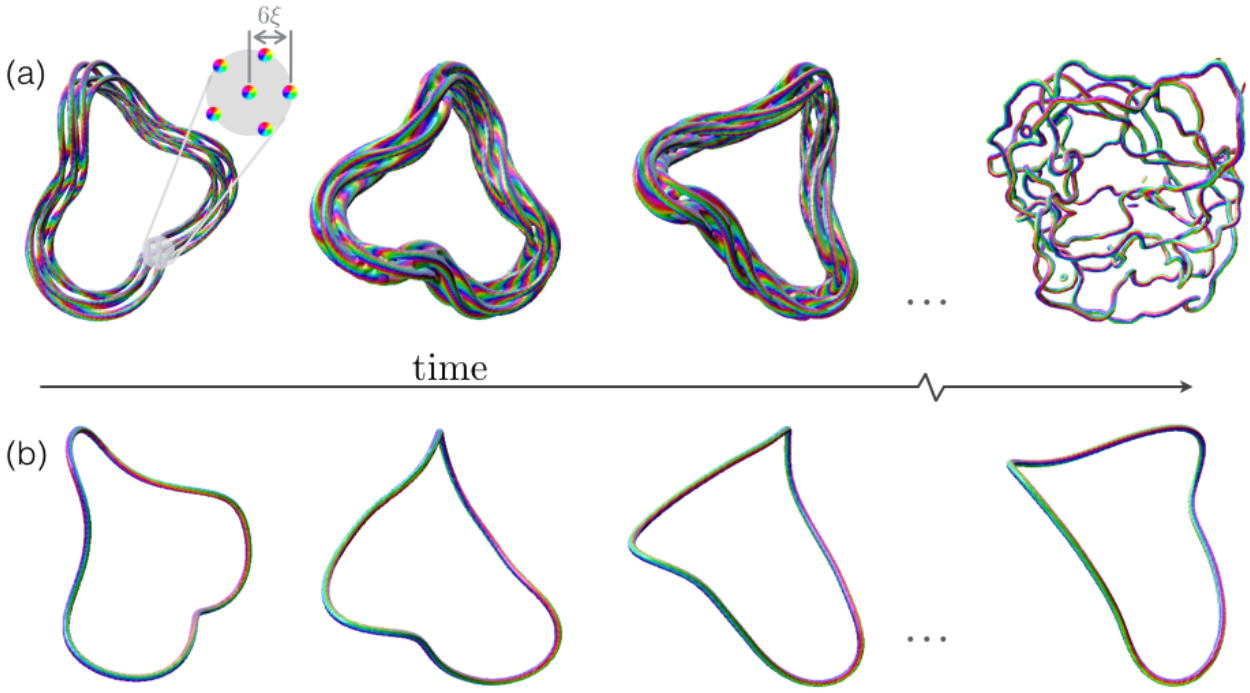

Figure 5.3: A three-fold helical superfluid vortex bundle evolving as a coherent structure, akin to a single vortex in the shape of a three-fold helix. (a) A three-fold helical superfluid vortex bundle rotates as it evolves in time, just like (b) a single three-fold helical vortex. A cross-section of the three-fold helical superfluid vortex bundle, shows a central vortex and 5 equally spaced vortices arranged around the central vortex at distance 6ξ (where ξ is the healing length). After a long time, the helical vortex bundle disintegrates (symbolized by the grey dots) and loses its bundle-like structure.

conserved charge $\mathcal{Q}_{\text{gpe}}$ in Eq. (5.6) simply becomes:

$$\mathcal{Q}_{\text{gpe}}\Big|_{\boldsymbol{\eta}(\Delta)} = \oint_{C_i'(\Delta)} \mathbf{u} \cdot \mathrm{d}\mathbf{l} = 0 \tag{5.8}$$

Following [9], we use the fact that the compressible part of $\mathbf{u}$ does not contribute to the loop integral in Eq. (5.8). It then follows from the Biot-Savart law that $\mathcal{Q}_{\text{gpe}}$ is equal to the

linking of the loop C_i' with all the vortex lines in the superfluid:

$$\begin{aligned}\mathcal{Q}_{\text{gpe}}\Big|_{\boldsymbol{\eta}=\boldsymbol{\eta}(\Delta)} &= \sum_j \frac{\Gamma_j}{4\pi} \oint_{C_i'(\Delta)} \oint_{C_j} \frac{(\mathbf{x}-\mathbf{x}')}{|\mathbf{x}-\mathbf{x}'|^3} \cdot \left(\mathrm{d}\mathbf{x} \times \mathrm{d}\mathbf{x}'\right) \\ &= \sum_j \Gamma_j \mathcal{L}_{i'j} \\ &= \sum_{j\neq i} \Gamma_j \mathcal{L}_{i'j} + \Gamma_i \mathcal{L}_{i'i} = 0\end{aligned}$$

where $\mathcal{L}_{i'j}$ denotes the linking between the vortex line C_j, and we have used the Gauss linking integral [197]. Thus, the conserved charge $\mathcal{Q}_{\text{gpe}}$ vanishes since the linking between the loop C_i' and the vortex line C_i is canceled by the linking between the loop C_i' and all the other vortex lines C_j , $j \neq i$.

Furthermore, in the case that the loop C_i' is close enough to the vortex line C_i such that the section of the phase isosurface bounded by the two loops can be considered as a smooth ribbon, we can use the Călugăreanu-White-Fuller theorem [198, 199, 200, 167] to express $\mathcal{L}_{i'i}$ as the sum of the writhe (Wr_i) and the twist (Tw_i^*) of the ribbon (see Fig. 5.2), giving:

$$\sum_{j\neq i} \Gamma_j \mathcal{L}_{ij} + \Gamma_i \mathrm{Wr}_i + \Gamma_i \mathrm{Tw}_i^* = 0 \tag{5.9}$$

This result was first studied in the context of helicity of framings of magnetic flux tubes [173], and is a consequence of the fact that a phase isosurface is an orientable surface which has as its boundary, all the vortex lines in the superfluid, i.e. it is a Seifert surface [201, 173, 202, 203] for the vortex lines in the superfluid. Moreover, this relation between linking, and writhing of vortex lines and the twisting of phase isosurfaces has been used in superfluid simulations [56] to calculate the centerline helicity (linking and writhing of vortex lines), and in recent efforts to heuristically define a superfluid helicity [166].

We have thus seen that the conserved charge associated with the particle relabeling

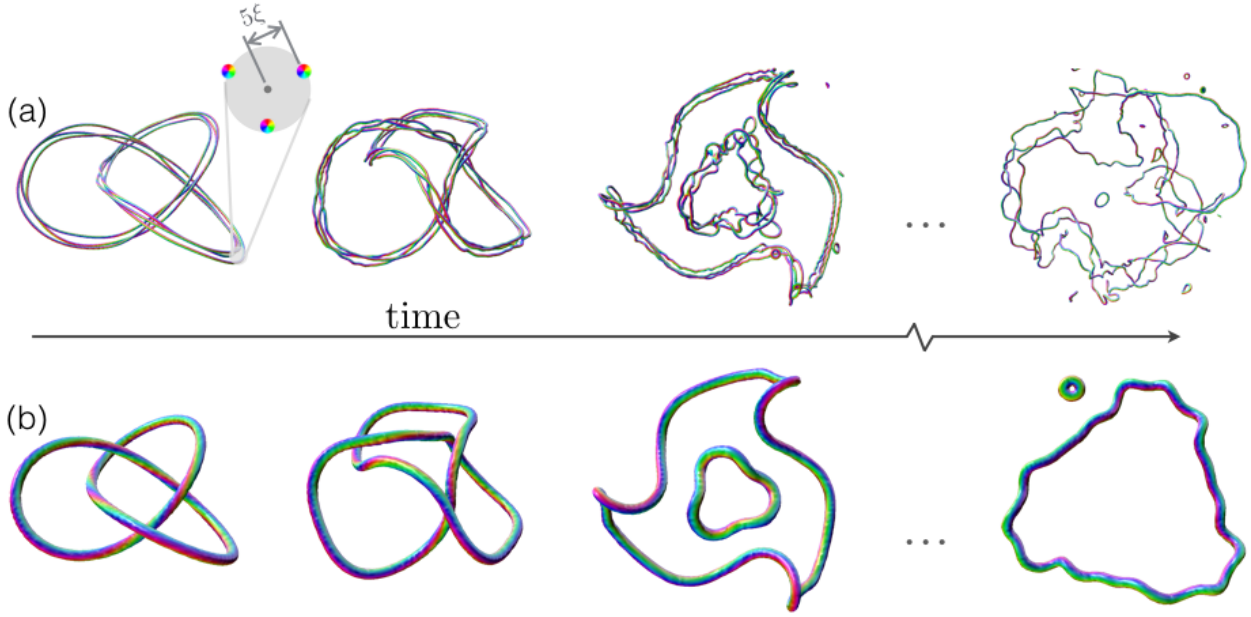

Figure 5.4: A superfluid vortex bundle in the shape of a trefoil knot evolving as a coherent structure, akin to a single trefoil knot vortex. (a) A trefoil knotted vortex bundle stretches, and reconnects to form a smaller three-fold distorted ring bundle, and a larger three-fold distorted ring bundle, which lose their bundle-like structure over time. A cross-section of the initial trefoil knotted vortex bundle, shows 3 equally spaced vortices arranged at equally spaced angles on the circumference of a disk of radius 5ξ (where ξ is the healing length). (b) A trefoil knotted superfluid vortex stretches and reconnects to form a smaller three-fold distorted ring, and a larger three-fold distorted ring, which undergoes further reconnections to give a large distorted ring at long times.

symmetry, which is the origin of helicity and circulation conservation in Euler flows, vanishes in superfluids because of a cancellation between the linking and writhing of vortex lines and the twisting of phase isosurfaces. This raises the question of whether the conservation of classical helicity $\mathcal{H}_{\text{Euler}}$ can be recovered in the "classical limit" of a collection of superfluid vortex lines mimicking a classical distribution of vorticity. To this end, we begin by reviewing the conservation of classical helicity $\mathcal{H}_{\text{Euler}}$ for a classical distribution of vorticity approached as a limit of a collection of singular vortex lines.

5.4 Classical helicity of singular vortex lines

While vorticity in superfluids is necessarily concentrated on lines of singular phase, vorticity in classical fluids can be continuously distributed, and indeed has to be, to avoid a physical singularity in the flow. Nonetheless, following Moffatt [9] and Berger [204], such a distribution can be approached from an infinite collection of intertwining singular vortex lines. For such a collection of vortex lines, the classical helicity $\mathcal{H}_{\text{Euler}} = \int \mathbf{u} \cdot \omega \, \mathrm{d}^3x$ becomes the centerline helicity $\mathcal{H}_c$ [56]:

$$\mathcal{H}_c = \sum \sum_{i \neq j} \Gamma_i \Gamma_j \mathcal{L}_{ij} + \sum_i \Gamma_i^2 \mathrm{Wr}_i \tag{5.10}$$

where Γ_i is the circulation around the i^{th} vortex line, Wr_i is the writhe of the i^{th} vortex line, and $\mathcal{L}_{ij}$ is the linking between the i^{th} and j^{th} vortex lines.

A smooth vorticity distribution is approached as the number of singular vortex lines N comprising the bundle is made larger while decreasing the circulation around each individual vortex line $\Gamma_i = \Gamma_{\text{total}}/N$, while keeping the total circulation fixed. In this limit, the centerline helicity $\mathcal{H}_c$ is:

$$\begin{aligned} \lim_{N\to\infty} \mathcal{H}_c &= \lim_{N\to\infty} \sum \sum_{i \neq j} \Gamma_i \Gamma_j \mathcal{L}_{ij} + \sum_i \Gamma_i^2 \mathrm{Wr}_i \\ &= \lim_{N\to\infty} \sum \sum_{i \neq j} \frac{\Gamma_{\text{total}}^2}{N^2} \mathcal{L}_{ij} + \sum_i \frac{\Gamma_{\text{total}}^2}{N^2} \mathrm{Wr}_i \end{aligned}$$

The contribution from the writhing ($\sum \mathrm{Wr}_i/N^2$) term scales as $O(1/N)$, and thus becomes irrelevant in the limit $N \to \infty$, leaving only a term proportional to the linking number $\mathcal{L}_{ij}$. In the case of nontrivial linking between vortex lines, the centerline helicity becomes a measure of their average linking $\mathcal{H}_c = \Gamma_{\text{total}}^2 \langle \mathcal{L}_{ij} \rangle$, which is conserved since vortex lines can not cross in Euler flows. For a thin-core vortex tube, this internal linking can be expressed

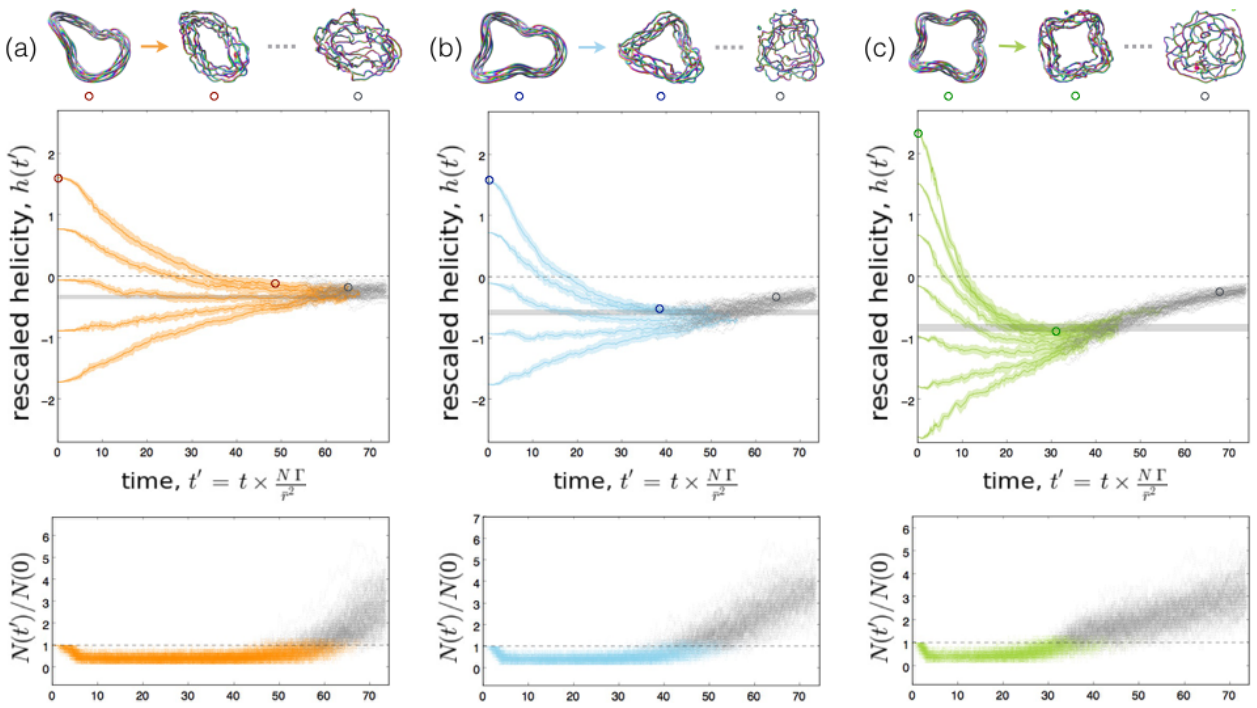

Figure 5.5: Right-handed helical vortex bundles at different stages of evolution (top row), with the corresponding points in the graph indicated by colored circles (bundle-like structure preserved), and grey circles (bundles disintegrate). The rescaled helicity h (middle row) for superfluid vortex bundles constructed with varying degrees of twist, i.e. having different initial helicity, trends towards their initial average writhe (horizontal grey band) as long as the bundle-like structure is preserved, before eventually decaying towards zero (as indicated by the grey dotted lines) for (a) 2-fold helical vortex bundles, (b) 3-fold helical vortex bundles, and (c) 4-fold helical vortex bundles. For each helical vortex bundle configuration corresponding to a given initial rescaled helicity $h(0)$, multiple simulations are performed with random Gaussian noise (r.m.s is 2% of the r.m.s. radius) added to the initial bundle. The mean rescaled helicity is indicated by the solid lines, and the width of the shaded band around the solid line indicates the standard deviation (2σ). The bottom row shows the ratio of the number of vortex filaments at time t' to the initial number of vortex filaments: $N(t')/N(0)$. After the vortex bundle disintegrates, its rescaled helicity is shown by a grey dotted line. The time at which a vortex bundle disintegrates is measured as the earliest time at which the number of vortex filaments $N(t')$ exceeds the initial number of vortex filaments $N(0)$ by more than 50%.

as the sum of the writhe of the tube, and the twist of the vortex lines in the tube [204, 205].

Note that if the distribution of vorticity was concentrated on a singular vortex line, such a limit would not apply and the classical helicity itself would not be conserved since the writhe of a vortex line can change. Hence, only for smooth vorticity distributions, i.e. in the

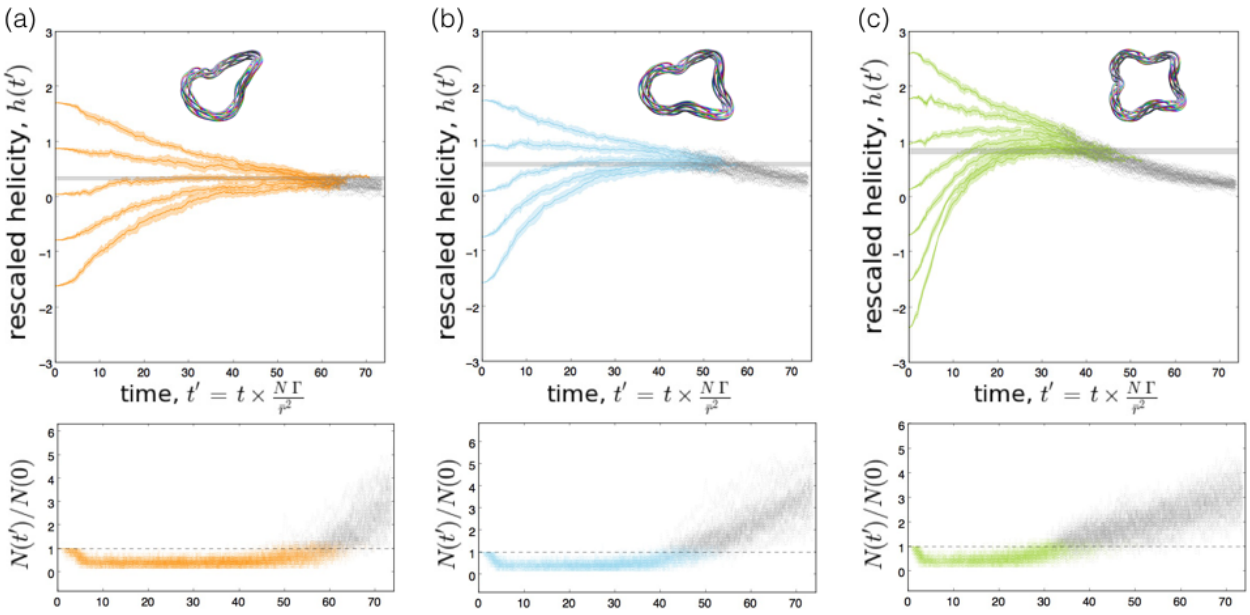

Figure 5.6: Left-handed helical vortex bundles with positive initial writhe display helicity dynamics similiar to the right-handed helical vortex bundles shown in Fig. 5.5. The rescaled helicity h for superfluid vortex bundles constructed with varying degrees of twist, i.e. having different initial helicity, trends towards their initial average writhe (horizontal grey band) as long as the bundle-like structure is preserved, before eventually decaying towards zero (as indicated by the grey dotted lines) for (a) 2-fold helical vortex bundles, (b) 3-fold helical vortex bundles, and (c) 4-fold helical vortex bundles. For each helical vortex bundle configuration corresponding to a given initial rescaled helicity $h(0)$, multiple simulations are performed with random Gaussian noise (r.m.s is 2% of the r.m.s. radius) added to the initial bundle. The mean rescaled helicity is indicated by the solid lines, and the width of the shaded band around the solid line indicates the standard deviation (2σ). After the vortex bundle disintegrates, its rescaled helicity is shown by a grey dotted line. The bottom row shows the ratio of the number of vortex filaments at time t' to the initial number of vortex filaments: $N(t')/N(0)$. The time at which a vortex bundle disintegrates is measured as the earliest time at which the number of vortex filaments $N(t')$ exceeds the initial number of vortex filaments $N(0)$ by more than 50%.

limit ($N \to \infty$) of a bundle of a large number of singular vortex lines, is the conservation of classical helicity $\mathcal{H}_{\text{Euler}}$ guaranteed.

Inspired by this, we numerically study whether a similar "classical" limit in superfluid flow, i.e. many singular vortex lines approximating a smooth distribution of vorticity, recovers the conservation of classical helicity $\mathcal{H}_{\text{Euler}}$.

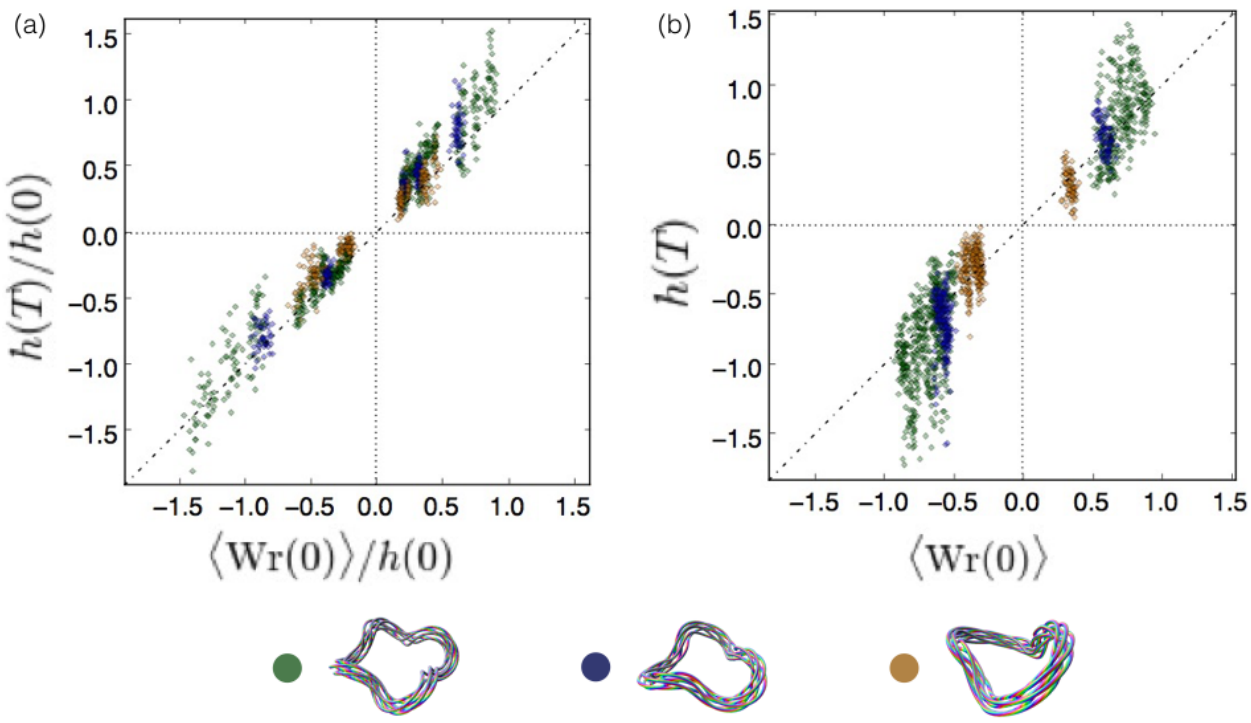

Figure 5.7: (a)The ratio of the rescaled helicity $h(T)$ to the initial rescaled helicity $h(0)$ approaches the ratio of the average initial writhe $\langle \mathrm{Wr}(0) \rangle$ to the initial rescaled helicity for a variety of helical vortex bundles in the shape of 2,3, and 4-fold helices with $N = 5$ and $N = 6$ vortex filaments. Here T is the time at which the vortex bundle disintegrates, i.e. the earliest time at which the number filaments $N(t')$ exceeds the initial number of filaments $N(0)$ by more than 50%. To divide by the initial helicity $h(0)$, we only consider vortex bundles whose initial helicity satisfies: $|h(0)| > 0.25$. Vortex bundles with lower absolute values of initial helicity $|h(0)| < 0.25$ also display similar behavior with $h(T) \to \langle \mathrm{Wr}(0) \rangle$ as shown in (b). (b) The rescaled helicity $h(T)$ trends towards the average initial writhe $\langle \mathrm{Wr}(0) \rangle$ for a variety of helical vortex bundles in the shape of 2,3, and 4-fold helices with $N = 5$ and $N = 6$ vortex filaments. Here T is the time at which the vortex bundle disintegrates, i.e. the earliest time at which the number filaments $N(t')$ exceeds the initial number of filaments $N(0)$ by more than 50%. The large spread in values of $h(T)$ comes from vortex bundles whose initial rescaled helicity $h(0)$ is far from their average initial writhe $\langle \mathrm{Wr}(0) \rangle$, and is removed on rescaling both the axes by $h(0)$, as shown in (a). The final rescaled helicity $h(T)$ trends towards the average initial writhe as shown in Fig.s 5.5,5.6, but such vortex bundles often disintegrate before the final rescaled helicity $h(T)$ becomes equal to the average initial writhe $\langle \mathrm{Wr}(0) \rangle$, giving rise to the large observed spread in $h(T)$.

5.5 Superfluid helicity—a "classical limit"

To study superfluid vortex bundles which approximate the structure of a classical vortex tube, we consider bundles of vortex lines—like the one shown in Fig. 5.3(a). Our bundles

consist of a central vortex, and a collection of neighboring vortices at equal distance from the central vortex, that wind around it. We construct vortex bundles with $N = 5$ and $N = 6$ vortex lines, with an initial inter-vortex spacing of $d \sim 6\xi$ (see Fig. 5.3) and an overall r.m.s. radius of the vortex bundle given by $\bar{r} \sim 50\xi$, where ξ is the healing length. Each vortex line in the bundle has circulation $\Gamma = 2\pi$, making the total circulation $N\,\Gamma$ and Gaussian noise (2 % of r.m.s. radius $\bar{r}$) is added to each vortex line in the transverse direction.

From these vortex bundle configurations, we construct the initial complex order parameter ψ using the methods outlined in [169, 56, 66]. To study the dynamics of superfluid vortex bundles, we solve the Gross-Pitaevskii equation (Eq. (5.1)) for the evolution of the complex order parameter ψ using a split-step method. We use grids of volume 256^3 with a grid spacing of 1ξ, and volume 512^3 with a grid spacing of $0.5\,\xi$ and obtain identical results. The superfluid vortex bundles evolve coherently (see Fig.s 5.3,5.4), with dynamics that closely resemble single vortex loops in superfluids and vortices in classical fluids. As they evolve coherently, they undergo a large number of vortex reconnections while preserving their bundle-like structure, eventually becoming unstable and disintegrating into a large number of smaller vortex loops as shown in the Supplementary movies of [61]. We restrict our attention to vortex bundles which preserve their bundle-like structure for a considerable amount of time, traveling over a distance of $6\bar{r}$ or greater.

We simulate the evolution of vortex bundles in the shape of trefoil knots and helices, and find that in all cases vortex bundles behave much like their classical vortex tube counterparts [44, 56]. Helical vortex bundles propagate coherently without a significant change in shape (see Fig. 5.3), while knotted vortex bundles stretch and reconnect (see Fig. 5.4), into disconnected loop bundles.

To investigate whether these superfluid vortex bundles recover the notion of classical

helicity conservation, we measure their rescaled centerline helicity [56]:

$$\begin{aligned} h &= \mathcal{H}_c/(N\,\Gamma)^2 \\ \Rightarrow h &= \sum\sum_{i\neq j} \mathcal{L}_{ij}/N^2 + \sum_i \mathrm{Wr}_i/N^2 \end{aligned} \tag{5.11}$$

where $\mathcal{H}_c$ is defined as in Eq. (5.10). The rescaled helicity h measures the linking between the vortex lines forming the bundle, and the writhe (coiling) of each vortex line.

We study the evolution of rescaled centerline helicity h of vortex bundles until the vortex bundle disintegrates. We measure the time T at which a vortex bundle disintegrates, by measuring the earliest time at which the number of vortex filaments N in the superfluid exceeds the initial number of vortex filaments in the vortex bundle N_0 by 50% (see Fig. 5.5. To study the long time behavior of the rescaled centerline helicity h of vortex bundles, we focus our attention on vortex bundles which evolve coherently over distances of $6\bar{r}$ or greater without disintegrating. We study the evolution of helical vortex bundles organized around a central vortex in the shape of a toroidal helix, winding in the poloidal direction 2, 3, or 4 times around tori of aspect ratios 0.35, 0.25 or 0.2, as it winds around once in the toroidal direction.

For a smooth thin-cored vortex bundle, as discussed earlier in the context of Euler flows, there are two geometrically distinct contributions to the rescaled helicity h: (i) the writhe (coiling) of the centerline of the vortex bundle which naturally induces a winding of the neighboring vortex lines around the central vortex much like a geometric phase [206, 207], and (ii) the twisting of the neighboring vortex lines around the central vortex which corresponds to an additional locally detectable winding.

Unlike in Euler flows, where the rescaled centerline helicity h of a bundle of singular vortex lines would emerge as a conserved quantity in the limit of a large number of vortex lines N, the rescaled centerline helicity h of superfluid vortex bundles appears to change with time.

As shown in Fig. 5.5, the rescaled helicity h of vortex bundles with different amounts of twist trends towards a common value as long as the vortex bundle preserves its bundle-like shape, before eventually trending towards 0 as the vortex bundle disintegrates. As demonstrated by Fig.s 5.5, and 5.7, this common value of the rescaled helicity h is well-predicted by the average initial writhe $\langle \mathrm{Wr}(0) \rangle = \sum_i \mathrm{Wr}(0)/N$ of the vortex bundle (indicated by the grey horizontal band in Fig. 5.5), suggesting the simple rule that twist is dissipated. Since twist can be positive or negative, the dissipation of twist can lead to an increase or a decrease in the value of helicity.

The untwisting of superfluid vortex bundles in our simulations has a striking resemblance to the dissipation of twist that has been experimentally observed in vortices in viscous flows [206]. It is surprising that the numerous and complex reconnections of vortex lines in superfluid vortex bundles can be simply understood as the dissipation of twist. This points to a "classical limit" in which classical behavior is recovered from quantized vortex filaments *geometrically* by replacing single vortex filaments with vortex bundles. Owing to reconnections however, the classical behavior that is recovered is not that of Euler flows, but that of the Navier-Stokes equations in which viscosity acts to dissipate twist. Our work adds a geometric lens to previous work [208] on the dissipative effects of vortex reconnections in superfluids.

5.6 Conclusion

We have addressed the question of "superfluid helicity" by generalizing the relabeling symmetry used to study helicity in Euler flows to superfluids. We find conserved quantities analogous to circulation and helicity in superfluids, however they vanish identically owing to the appearance of an additional term that comes from the phase of the superfluid order parameter, not present in Euler flows. We find a geometric interpretation for the vanishing of "superfluid helicity" in terms of a relation between the linking and writhing of vortex

lines, and the twisting of phase isosurfaces near vortex lines.

By replacing superfluid vortices with superfluid vortex *bundles*, we find that a classical notion of helicity can be recovered, whose dynamics are akin to that of classical helicity in a viscous fluid, providing further evidence for the notion that the classical limit of superfluids is attained in the limit of a large number of vortex lines [208].

The geometric origin of our results point to further implications for systems with phase defects akin to vortices in superfluids, from liquid crystals [209] to cosmic strings [171, 172].

CHAPTER 6

SUMMARY & DISCUSSION

Finally, we summarize what we have learned and list some speculative questions for future research.

In chapter 2, we presented a method for analytically constructing arbitrarily knotted fields, which can be smoothly confined to a knotted tube, and showed how their helicity could be tuned. In chapter 3, we found an infinite family of persistently knotted solutions to Maxwell's equations in vacuum, showing that a linear theory can preserve knots with time. In chapter 4, we found the sufficient initial conditions under which Maxwell's equations preserve knots encoded in the lines of the electric and magnetic fields, giving a design rule for constructing persistently knotted solutions to Maxwell's equations. In chapter 5, we analytically addressed the question of a "superfluid helicity" by defining the particle relabeling symmetry in superfluids, and found that a conserved quantity analogous to helicity exists in superfluids, but vanishes identically owing to the intrinsic geometry of complex scalar fields. Furthermore, we used numerical simulations to demonstrate that *bundles* of superfluid vortices recover a "classical limit", but evolve akin to classical vortices in viscous flows.

Some speculative questions:

- What can we learn about fluid flows via their connections with Maxwell's equations?
- Can conserved quantities analogous to helicity exist in other complex flows?
- What can we learn about viscous flows from simulations of superfluid vortex bundles?

APPENDIX A

A RECIPE FOR CONSTRUCTING KNOTTED FIELDS

Since the lines of the knotted field **B** are organized around a core set of lines corresponding to the zeros of the polynomials $P(u, u^*, v, v^*)$, $Q(u, u^*, v, v^*)$, different choices of these polynomials lead to different knotted fields. We briefly describe here the known complex polynomials $Q(u, u^*, v, v^*)$, which encode in $Q = 0$, a variety of knots and links, all of which in fact are in the family of lemniscate knots or their generalizations [108].

1. *Torus knots and links.* The entire family of (p, q)-torus knots and links is encoded in the zeros of $Q(u, v) = u^q + v^p$ [101, 100].

2. *Lemniscate knots.* This family, described in [108] is a wide family of fibred knots and links which includes both the torus knots, the figure-8 knot and many others. They are defined in terms of their braid representation, which must be equivalent to an s-strand braid where each strand executes the same $(1, l)$ Lissajous figure in the horizontal plane perpendicular to the height h of the braid; the basic permutation of the strands around the figure is repeated r times. Lemniscate knots are therefore determined by three positive integers (s, l, r); the (s, r) torus knot has $l = 1$. With the Lissajous figure (generalised lemniscate) given by $(a\cos(h), bl^{-1}\sin(lh))$, the lemniscate knot/link is the nodal set of the complex polynomial $Q(v, u, u^*)$ where, with appropriate choice of real numbers a, b,

$$Q(v,u,u^*) = \prod_{j=1}^{s} \left(v - \frac{a}{2}\left(e^{irt/s} e^{2\pi ij/s} + e^{-irt/s} e^{-2\pi ij/s} \right) - \frac{b}{2l}\left(e^{irlt/s} e^{2\pi ijl/s} - e^{-irlt/s} e^{-2\pi ijl/s} \right) \right),$$

where, after multiplying out, the replacements $e^{it} \to u, e^{-it} \to u^*$ (the coefficients of all fractional powers of u, u^* vanish due to the various roots of unity $e^{2\pi ij/s}$). An

advantage of this construction is that Q is independent of v^* (holomorphic in v), which guarantees that the helicity of the resulting vector field is an integer multiple of s, the braid index of the lemniscate knot. In [108] it is proved that, for sufficiently small a and b, the nodal set of this Q indeed is the desired lemniscate knot. With $l = 2$, and $s = 3$, $a = b = 1$ suffice, the lemniscate polynomial multiplies out: $Q(u, u^*, v) = 64v^3 - 12v(3 + 2u^r - 2u^{*r}) - (14u^r + 14u^{*r} + u^{2r} - u^{*2r})$, and $r = 2$ gives the figure-8 knot, $r = 3$ the borromean rings and $r = 4$ the Turk's head knot [38]. Explicit polynomials for many other lemniscate knots are given in [108]. Alternative polynomials are given for the figure-8 knot and its higher-r generalizations in [102, 118].

3. *Cable knots.* All cable knots $C^{n_2,m_2}_{m_1,n_1}$—(m_2, n_2)-torus knots cabled on a torus in the neighbourhood of a (m_1, n_1)-torus knot, where (m_1, n_1) and (m_2, n_2) are coprime positive integers, and $1 < m_1/n_1 < m_2/(n_1 n_2)$—are encoded in the following complex equation: $v - u^{m_1/n_1} - \eta\, u^{m_2/(n_1 n_2)} = 0$, where η is a non-zero complex number. This can also be realised from a braid construction [108]. The above equation can be transformed into a complex polynomial with positive integer powers on a case-by-case basis as outlined in [109]. For instance the $C^{2,3}_{3,2}$-cable knot is encoded in the zeros of the complex polynomial $Q(u, v) = v^4 - 2u^3\, v^2 - 2iu^3\, v + u^6 + \frac{1}{4}u^3$, and the $C^{2,7}_{3,2}$-cable knot is encoded in the complex polynomial $Q(u, v) = v^4 - 2u^3\, v^2 - 2iu^5\, v + u^6 + \frac{1}{4}u^7$.

4. *Links.* Many links arise from appropriate choice of integers as torus links, lemniscate links or cabled links. More generally, the product of any set of polynomials $Q_j(u, u^*, v, v^*)$ with non-intersecting nodal sets $\mathcal{K}_j$, $j = 1, \ldots, k$, clearly has as its overall nodal set the link $\bigcup_{j=1}^{k} \mathcal{K}_j$. This has a huge amount of freedom, since it is straightforward to transform each Q_j so $\mathcal{K}_j$ is rescaled, translated or rotated, giving rise to a range of linking topologies. As an example, the knotted field based on the linked pair of trefoil knots shown in Fig. (2.1) is realised from $Q(u, v) = Q_1(u, v)Q_2(u, v)$ where each of the trefoil factors Q_1, Q_2 starts from the polynomial $u^3 + v^2$, then Q_1

is rotated about the z-axis by $9\pi/24$ and translated by $\Delta x = -0.8, \Delta y = -1.55$, while Q_2 is rotated about the z-axis by $\pi/24$, followed by a rotation about the y-axis by $\pi/24$, and a translation by $\Delta x = 0.9\,,\ \Delta y = 1.55$.

The next step is a choice of a complex polynomial $P(u, u^*, v, v^*)$ such that the line $P = 0$ is linked with the chosen knot $Q = 0$, and does not intersect it. Different choices of $P(u, u^*, v, v^*)$, change the helicity of the knotted field $\mathbf{B}$ while keeping the knotted structure encoded in its lines unchanged, as shown in Fig. 2.4.

APPENDIX B

NULL MAXWELL FIELDS USING SPINORS

We now describe in more detail, the space of null Maxwell fields and their correspondence with null geodesic shear-free congruences (null GSF congruences), expressing them in the equivalent language of spinors.

A null GSF congruence is a family of null geodesics, described by a null vector field ξ^μ, which satisfies the geodesic and the shear-free conditions [210]. In flat space-time, these conditions are given by:

$$\text{Affine geodesic condition:} \quad \xi^\mu \partial_\mu \xi^\nu = 0 \tag{B.1}$$

$$\text{Shear-free condition:} \quad \frac{1}{2}\partial_{(\nu}\,\xi_{\mu)}\partial^\nu \xi^\mu - \left(\frac{1}{2}\partial_\mu\,\xi^\mu\right)^2 = 0 \tag{B.2}$$

where, $\partial_{(\nu}\,\xi_{\mu)} = \frac{1}{2}(\partial_\nu \xi_\mu + \partial_\mu \xi_\nu)$.

By Robinson's theorem [130], there is a shear-free family of light rays (a null GSF congruence) underlying each null electromagnetic field. In flat space-time, the null GSF congruence ξ^μ corresponding to a null electromagnetic field is explicitly given by $(1, \frac{\mathbf{E}\times\mathbf{B}}{|\mathbf{E}\times\mathbf{B}|})$.

The correspondence between a null GSF congruence and a null electromagnetic field is not one-to-one, instead a null GSF congruence corresponds to a family of null electromagnetic fields. All null electromagnetic fields can be grouped into such families of null fields, with all null fields in a family corresponding to a common underlying null GSF congruence. In Bateman's formalism, a particular choice of (α, β) determines a null GSF congruence, and the corresponding family of null fields is given by $\mathbf{F} = h(\alpha, \beta)\,\nabla\alpha \times \nabla\beta$, where h is an arbitrary holomorphic function.

This is made manifest when the above null field and its associated null GSF congruence are expressed in the equivalent language of spinors [211]. In this formalism, a null congruence ξ^μ is constructed from a spinor field ξ_A, and a null electromagnetic field $F^{\mu\nu}$ is constructed

from a symmetric spinor Φ_{AB} as:

$$\xi^{\mu} = g^{\mu AA'}\,\xi_A\,\bar{\xi}_{A'}\,;\; F^{\mu\nu} = g^{\mu AA'}g^{\nu BB'}\left(\Phi_{AB}\,\epsilon_{A'B'} + \epsilon_{AB}\,\bar{\Phi}_{A'B'}\right)$$

where $\{\bar{\Phi}_{A'B'}, \bar{\xi}_{A'}\}$ denote the complex conjugates of $\{\Phi_{AB}, \xi_A\}$, and $\epsilon_{AB} = \epsilon_{A'B'}$ is the 2×2 symplectic matrix, $g^{\mu AA'} = (\mathbb{I}, -\sigma_x, \sigma_y, -\sigma_z)/\sqrt{2}$ are the Infeld-van der Waerden symbols [211, 212], σ_i being the Pauli matrices.

A number of expressions simplify in this language: Maxwell's equations become:

$$g^{\mu AA'}\partial_{\mu}\Phi_{AB} = 0$$

and the null condition is: $\Phi_{AB}\Phi^{AB} = 0$. Finally, the geodesic and the shear-free conditions for ξ^{μ} can be combined, and simplify to: $\xi^{A}\,\xi_B\,g^{\mu BB'}\partial_{\mu}\xi_A = 0$.

A null GSF congruence ξ_A then gives rise to a null electromagnetic field $\Phi_{AB} = \kappa\,\xi_A\,\xi_B$ where the complex scalar κ is chosen to satisfy Maxwell's equations. It is easily verified that Φ_{AB} satisfies the null condition.

The Bateman field $\mathbf{F} = \nabla\alpha \times \nabla\beta$ corresponds to $\Phi_{AB} = \kappa\,\xi_A\,\xi_B$ with:

$$\kappa = \frac{\mathrm{i}}{\partial_{\bar{w}}\bar{\alpha}\,\partial_z\,\bar{\beta} - \partial_z\bar{\alpha}\,\partial_{\bar{w}}\,\bar{\beta}}\,,\; \xi_A = \begin{pmatrix} \partial_w\bar{\alpha}\,\partial_{\bar{w}}\,\bar{\beta} - \partial_{\bar{w}}\bar{\alpha}\,\partial_w\,\bar{\beta} \\ \partial_{\bar{w}}\,\bar{\alpha}\,\partial_z\,\bar{\beta} - \partial_z\,\bar{\alpha}\,\partial_{\bar{w}}\,\bar{\beta} \end{pmatrix} \tag{B.3}$$

if $\partial_{\bar{w}}\bar{\alpha}\,\partial_z\,\bar{\beta} - \partial_z\bar{\alpha}\,\partial_{\bar{w}}\,\bar{\beta} \neq 0$, otherwise

$$\kappa = \frac{\mathrm{i}}{\partial_w\,\bar{\alpha}\,\partial_z\,\bar{\beta} - \partial_z\,\bar{\alpha}\,\partial_w\,\bar{\beta}}\,,\; \xi_A = \left(\partial_w\,\bar{\alpha}\,\partial_z\,\bar{\beta} - \partial_z\,\bar{\alpha}\,\partial_w\,\bar{\beta},\, 0\right),$$

where $w = x + \mathrm{i}y$, and $\{\bar{\alpha}, \bar{\beta}, \bar{w}\}$ denote the complex conjugates of $\{\alpha, \beta, w\}$.

The entire family of null fields given by $\mathbf{F} = h(\alpha, \beta)\,\nabla\alpha \times \nabla\beta$, thus corresponds to ξ_A as given above with κ rescaled by $\bar{h}$, the complex conjugate of h.

We now give the spinor equivalents of the examples given earlier: a circularly polarized plane wave traveling in the $+z$-direction and the Hopfion solution: $\xi_A^{\rm pw} = (0, -1)$, $\kappa^{\rm pw} = -{\rm e}^{-{\rm i}(z-t)}$ and

$$\xi_A^{\rm hp} = (-\bar{b}, \bar{a}) \ , \ \kappa^{\rm hp} = \bar{d}^{-3} \tag{B.4}$$

where ξ_A, κ differ from those computed using Eq. $(B.3)$ (with κ rescaled by $\bar{h}$) by factors that leave the product $\Phi_{AB} = \kappa\, \xi_A\, \xi_B$ unchanged; $\{\bar{a}, \bar{b}, \bar{d}\}$ are complex conjugates of $\{a, b, d\}$. The null GSF congruence underlying the Hopfion solution: $\xi_A^{\rm hp}$, is referred to in the literature as the Robinson congruence.

We now express the knotted Maxwell fields presented in Chapter 3 in the language of spinors, showing that the common underlying null GSF congruence for our new family of knotted Maxwell fields is the Robinson congruence. In the spinor formalism the fields described by $\mathbf{F} = \nabla\alpha^p \times \nabla\beta^q$ arise from the same spinor as in (B.4) but different scaling factors κ:

$$\xi_A = (-\bar{b}, \bar{a}), \ \kappa = 4pq\, \bar{\alpha}^{p-1}\ \bar{\beta}^{q-1} \bar{d}^{-3} \tag{B.5}$$

where ξ_A, κ have again been simplified leaving the product $\Phi_{AB} = \kappa \xi_A \xi_B$ unchanged. Thus, the entire family of knotted solutions is constructed by simply changing the scaling factor κ, with the Robinson congruence as the underlying null GSF congruence.

APPENDIX C

FLOW OF NULL ELECTROMAGNETIC FIELDS

C.1 Null electromagnetic fields and Euler flows

We begin by considering a null electromagnetic field, i.e. an electromagnetic field satisfying $\mathbf{E}\cdot\mathbf{B}=0\,,\ \mathbf{E}\cdot\mathbf{E}=\mathbf{B}\cdot\mathbf{B}$ (in units where $c=1$), and give proofs for the equations stated in Table 4.1.

1. $\partial_t W+\nabla\cdot(W\,\mathbf{V})=0$, where $W=\frac{1}{2}\left(\mathbf{E}^2+\mathbf{B}^2\right)$ and $\mathbf{V}=(\mathbf{E}\times\mathbf{B})/W$.

   The above follows from energy conservation for an electromagnetic field in vacuum, and holds for any electromagnetic field [213].

2. $\partial_t\mathbf{V}+(\mathbf{V}\cdot\nabla)\,\mathbf{V}=0$

   Momentum conservation for an electromagnetic field in vacuum gives [213]:

$$\partial_t\left(W\,V_i\right)+\partial_j\left(W\,\delta_{ij}-E_i\,E_j-H_i\,H_j\right)=0 \tag{C.1}$$

   For null electromagnetic fields, the following special property holds $\left(W\,\delta_{ij}-E_i\,E_j-H_i\,H_j\right)=W\,V_i\,V_j$. Substituting in Eq. (C.1), and using energy conservation, we get

$$\partial_t V_i+V_j\,\partial_j\,V_i=0 \tag{C.2}$$

   as required.

3. $\partial_t\left(\mathbf{E}/W\right)=\left[\mathbf{E}/W\,,\,\mathbf{V}\right]\,,\ \partial_t\left(\mathbf{B}/W\right)=\left[\mathbf{B}/W\,,\,\mathbf{V}\right]$

   For null electromagnetic fields, $\mathbf{V}\times\mathbf{E}=\mathbf{B}\,,\ \mathbf{V}\times\mathbf{B}=-\mathbf{E}$. Substituting, we find that $\partial_t\mathbf{E}=\nabla\times(\mathbf{V}\times\mathbf{E})\,,\ \partial_t\mathbf{B}=\nabla\times(\mathbf{V}\times\mathbf{B})$ follows trivially from Maxwell's equations.

Using the definition of the Lie Bracket $[\mathbf{A}\,,\,\mathbf{B}] = (\mathbf{A}\cdot\nabla)\,\mathbf{B} - (\mathbf{B}\cdot\nabla)\,\mathbf{A}$, and energy conservation of electromagnetic fields, the above relation follows.

We note that the above statements and proofs do not assume that the null conditions are satisfied for all times, and hold true on a time slice if the null conditions are satisfied on a time-slice.

We now show the conservation of electric helicity $\mathcal{H}_e = \int \mathrm{d}^3x\,\mathbf{C}\cdot\mathbf{E}\,,\ \nabla\times\mathbf{C} = \mathbf{E}$, magnetic helicity $\mathcal{H}_m = \int \mathrm{d}^3x\,\mathbf{A}\cdot\mathbf{B}\,,\ \nabla\times\mathbf{A} = \mathbf{B}$, and Poynting helicity $\mathcal{H}_\Omega = \int \mathrm{d}^3x\,\mathbf{V}\cdot\Omega\,,\ \nabla\times\mathbf{V} = \Omega$. Since the electric $\mathbf{E}$, magnetic $\mathbf{B}$ and the Poynting vorticity Ω fields all obey an equation of type $\partial_t\mathbf{Y} = \nabla\times(\mathbf{V}\times\mathbf{Y})$, we will show how such an equation implies the conservation of the helicity of a vector field $\mathbf{Y}$, i.e. $\mathcal{H}_Y = \int \mathrm{d}^3x\,\mathbf{Z}\cdot\mathbf{Y}\,,\ \nabla\times\mathbf{Z} = \mathbf{Y}$, and the conservation of $\mathcal{H}_e\,,\ \mathcal{H}_m\,,\ \mathcal{H}_\Omega$ follow automatically.

The evolution of $\mathcal{H}_Y$ is given by:

$$\partial_t\mathcal{H}_Y = \int \mathrm{d}^3x\,\partial_t\mathbf{Z}\cdot\mathbf{Y} + \int \mathrm{d}^3x\,\mathbf{Z}\cdot\partial_t\mathbf{Y}$$

The evolution of $\mathbf{Y}$ implies an evolution equation for $\mathbf{Z}$:

$$\begin{aligned}
\partial_t\left(\nabla\times\mathbf{Z}\right) &= \nabla\times(\mathbf{V}\times\mathbf{Y}) \\
\nabla\times(\partial_t\mathbf{Z}) &= \nabla\times(\mathbf{V}\times\mathbf{Y}) \\
\partial_t\mathbf{Z} &= \mathbf{V}\times\mathbf{Y} + \nabla f \quad , \quad \text{(for some scalar function } f\text{)}
\end{aligned}$$

Substituting for the evolution of $\mathbf{Z}$ in the evolution of $\mathcal{H}_Y$, we get:

$$\begin{aligned}
\partial_t\mathcal{H}_Y &= \int \mathrm{d}^3x\ (\mathbf{V}\times\mathbf{Y} + \nabla f)\cdot\mathbf{Y} + \int \mathrm{d}^3x\,\mathbf{Z}\cdot\nabla\times(\mathbf{V}\times\mathbf{Y}) \\
&= \int \mathrm{d}^3x\ [(\mathbf{V}\times\mathbf{Y})\cdot\mathbf{Y} + \nabla f\cdot\mathbf{Y} + \nabla\cdot((\mathbf{V}\times\mathbf{Y})\times\mathbf{Z}) + (\nabla\times\mathbf{Z})\cdot(\mathbf{V}\times\mathbf{Y})] \\
&= \int \mathrm{d}^3x\,\nabla\cdot[(f\,\mathbf{Y}) + ((\mathbf{V}\times\mathbf{Y})\times\mathbf{Z})] = 0
\end{aligned}$$

C.2 Shear-free transport, Nullness and Maxwell's equations

The proof proceeds by showing that the null and shear-free conditions on the initial time slice are transported along the Poynting field. Using nullness, we then show that the divergence-less property is also transported. Finally using these, we show that $\mathbf{E}, \mathbf{B}$ satisfy Maxwell's equations in free space. By the uniqueness theorems, evolution of the initial electromagnetic field by Maxwell's equations with the given initial conditions should also give null solutions. Thus the shear-free condition is the required initial condition for an initial null electromagnetic field to stay null. The question of whether evolution by Maxwell's equations under the same initial conditions preserves nullness remains open.

Detailed proofs leading up to Eq. (4.4) are given below.

Lemma C.2.1. *Consider the initial-value problem:*

$$\partial_t \mathbf{V} + (\mathbf{V} \cdot \nabla)\, \mathbf{V} = 0\,, \quad \mathbf{V}_{t=0} = \mathbf{V}_0 \tag{C.3}$$

There exists a unique C^∞ solution $\mathbf{V}(\mathbf{r}, t)$ in a space-time region U, defined as $U := \left\{(t, \mathbf{r}) \in \mathbb{R}^4 : 0 < t < \psi(\mathbf{r})\,,\, \psi \in C^\infty(\mathbb{R}^4)\right\}$, if $\mathbf{V}_0(\mathbf{r}) \in C^\infty(\mathbb{R}^3)$.

Proof. The equation (C.3) is simply the geodesic transport of the initial vector field $\partial_t + \mathbf{V}_0$. Consider points $(0, \mathbf{x}_0)$ lying in the neighborhood N_0 of a point $(0, \mathbf{x}_0)$ in the hyperplane $\{t = 0\}$. The geodesics in $\mathbb{R}^4$ with initial point $(0, \mathbf{x}_1) \in N_0$ in the direction $(1, \mathbf{V}_0(\mathbf{x}_1))$ are straight lines (S):

$$(S) : \begin{cases} t(\lambda) &= \lambda \\ \mathbf{x}(\lambda) &= \mathbf{x}_1 + \lambda \mathbf{V}_0(\mathbf{x}_1) \end{cases}, \quad \mathbf{x}_1 \in N_0$$

The solutions to eq.(C.3) for $(0, \mathbf{x}_0) \in N_0$ are smooth in time $t \in (0, T)$ provided that the straight lines (S) do not intersect for any $\mathbf{x}_1 \in N_0$ and $\lambda \in (0, T)$.

To estimate the time of existence, we consider the intersection of two straight lines with

initial points $(0, \mathbf{x}_1) \in N_0$ and $(0, \mathbf{x}_2) \in N_0$, i.e.

$$\begin{cases} \mathbf{x}_1 + \lambda \mathbf{V}(\mathbf{x}_1) &= \mathbf{x}_2 + \lambda \mathbf{V}_0(\mathbf{x}_2) \\ \lambda &= T \end{cases}$$

$$\Rightarrow T = \frac{|\mathbf{x}_1 - \mathbf{x}_2|}{|\mathbf{V}_0(\mathbf{x}_1) - \mathbf{V}_0(\mathbf{x}_2)|}$$

It follows that if $\mathbf{V}_0(\mathbf{x})$ is locally Lipschitz continuous at $\mathbf{x}_0$, there exists a constant C_{N_0}, which depends on the neighborhood N_0 of $\mathbf{x}_0$, s.t.

$$\begin{cases} |\mathbf{V}_0(\mathbf{x}_1) - \mathbf{V}_0(\mathbf{x}_0)| &\leq C_{N_0} |\mathbf{x}_1 - \mathbf{x}_0| \\ \quad \text{for any } \mathbf{x}_1 \in N_0 \end{cases}$$

$$\Rightarrow T \geq \frac{1}{C_{N_0}}$$

Hence, on the neighborhood N_0, there exists a unique C^∞ solution to eq.(C.3) for time $t \in (0, \frac{1}{C_{N_0}})$. Considering a locally finite covering of $\mathbb{R}^3$ by open sets N_i, centred at points $\mathbf{x}_i$, we get local time existence for $t \in (0, \frac{1}{C_{N_i}})$ for each set N_i, provided $V_0(\mathbf{x})$ is locally Lipschitz continuous at each point of $\mathbb{R}^3$. One can then easily define a space-time region $U := \left\{(t, \mathbf{x}) \in \mathbb{R}^4 : 0 < t < \psi(\mathbf{x})\right\}$ such that $\psi \in C^\infty(\mathbb{R}^3)$, there exists a C^∞, and unique, solution to eq.(C.3) in the set U.

Notice that the constants C_{N_i} do not need to be uniform in i, and hence the region U may be narrower and narrower to the problem:

$$\begin{cases} \mathbf{V}_t + (\mathbf{V} \cdot \nabla)\mathbf{V} &= 0 \\ \mathbf{V}(t = 0) &= \mathbf{V}_0 \end{cases}$$

in a set $U \subset \mathbb{R}^3 \times \mathbb{R}^+$. □

Theorem C.2.2. *Let $\tilde{\mathbf{E}}(\mathbf{r}, t), \tilde{\mathbf{B}}(\mathbf{r}, t), \mathbf{V}(\mathbf{r}, t)$ be smooth solutions in $\mathbb{R}^3 \times \mathbb{R}^+$ to the initial-*

value problem :

$$\partial_t \mathbf{V} + (\mathbf{V}\cdot\nabla)\,\mathbf{V} = 0\,;\; \partial_t \tilde{\mathbf{E}} = \left[\tilde{\mathbf{E}}, \mathbf{V}\right]\;;\; \partial_t \tilde{\mathbf{B}} = \left[\tilde{\mathbf{B}}, \mathbf{V}\right] \tag{C.4}$$

$$\tilde{\mathbf{E}}_{t=0} = \frac{\mathbf{E}_0}{\rho_0}\,,\; \tilde{\mathbf{B}}_{t=0} = \frac{\mathbf{B}_0}{\rho_0}\,,\; \mathbf{V}_{t=0} = \frac{\mathbf{E}_0\times\mathbf{B}_0}{\rho_0}\,,\; \rho_0 := \frac{1}{2}\left(\mathbf{E}_0^2 + \mathbf{B}_0^2\right) \tag{C.5}$$

with the following initial conditions:

$$\nabla\cdot\mathbf{E}_0 = \nabla\cdot\mathbf{B}_0 = 0 \tag{C.6}$$

$$\mathbf{E}_0\cdot\mathbf{B}_0 = \mathbf{E}_0\cdot\mathbf{E}_0 - \mathbf{B}_0\cdot\mathbf{B}_0 = 0 \tag{C.7}$$

$$(E_0^i B_0^j) g_{0_{ij}} = (E_0^i E_0^j - B_0^j B_0^k) g_{0_{ij}} = 0\,,\; g_{0_{ij}} := \partial_i V_{0j} + \partial_j V_{0i} \tag{C.8}$$

Then the fields $\mathbf{E} := \rho\tilde{\mathbf{E}}\,,\; \mathbf{B} := \rho\tilde{\mathbf{B}}, \rho := \frac{1}{\frac{1}{2}\left(\tilde{\mathbf{E}}^2+\tilde{\mathbf{B}}^2\right)}$ *are null solutions to Maxwell's equations with the initial conditions:* $\mathbf{E}_{t=0} = \mathbf{E}_0\,,\; \mathbf{B}_{t=0} = \mathbf{B}_0$ *where* ρ *satisfies the continuity equation:* $\partial_t\rho + \nabla\cdot(\rho\mathbf{V}) = 0$, *with the initial condition* $\rho_{t=0} = \rho_0\,,\; \mathbf{V} = \frac{\mathbf{E}\times\mathbf{B}}{\rho}$. *Moreover,* $\rho = \frac{1}{2}\left(\mathbf{E}^2 + \mathbf{B}^2\right)$.

The converse also holds true, i.e. if $\mathbf{E}, \mathbf{B}$ *are null solutions to Maxwell's equations with* $\mathbf{E}_{t=0} = \mathbf{E}_0\,,\; \mathbf{B}_{t=0} = \mathbf{B}_0$, *then the fields* $\tilde{\mathbf{E}} := \frac{\mathbf{E}}{\rho}\,, \tilde{\mathbf{B}} := \frac{\mathbf{B}}{\rho}, \mathbf{V} = \frac{\mathbf{E}\times\mathbf{B}}{\rho}$ *satisfy Eq. (C.4) with the initial conditions given by Eq. (C.5) and the conditions given by Eq.s (C.6),(C.7),(C.8).*

Proof. To prove the first part of the theorem, we need to prove that if the initial normalized Poynting field $\mathbf{V}_0$ is shear-free, i.e. satisfies Eq. (C.8), then $\mathbf{E}, \mathbf{B}$ generated by solving Eq.s (C.4) with initial conditions in Eq.s (C.5),(C.6),(C.7),(C.8) are null solutions to Maxwell's equations.

Given fields $\mathbf{E}_0(\mathbf{r}), \mathbf{B}_0(\mathbf{r})$ at time $t = 0$, we define a tetrad $(k_0{}^\mu, n_0{}^\mu, \bar{m}_0^\mu, m_0{}^\mu)$:

$$k_0{}^\mu = \frac{1}{\sqrt{2}}\left(1, \mathbf{V}_0\right)\,,\; n_0{}^\mu = \frac{1}{\sqrt{2}}\left(1, -\mathbf{V}_0\right) \tag{C.9}$$

$$m_0{}^\mu = \frac{1}{\sqrt{2}}\left(0, \frac{\mathbf{E}_0 + \mathrm{i}\mathbf{B}_0}{\rho_0}\right)\,,\; \bar{m}_0^\mu = \frac{1}{\sqrt{2}}\left(0, \frac{\mathbf{E}_0 - \mathrm{i}\mathbf{B}_0}{\rho_0}\right) \tag{C.10}$$

Solving Eqs. (C.4) is akin to defining the tetrad $(k^\mu, n^\mu, \bar{m}^\mu, m^\mu)$ for all space-time by parallel transport of k, n and Lie transport of m:

$$k^\mu \partial_\mu k^\nu = 0\,,\; k^\mu \partial_\mu n^\nu = 0\,,\; [k,m]^\mu = 0 \tag{C.11}$$

with the initial conditions: $(k^\mu, n^\mu, \bar{m}^\mu, m^\mu)_{t=0} = (k_0{}^\mu, n_0{}^\mu, \bar{m}_0^\mu, m_0{}^\mu)$ and defining the fields $(\mathbf{E}/\rho, \mathbf{B}/\rho, \mathbf{V})$ by this tetrad as:

$$k^\mu = \frac{1}{\sqrt{2}}\,(1, \mathbf{V})\;,\; n^\mu = \frac{1}{\sqrt{2}}\,(1, -\mathbf{V}) \tag{C.12}$$

$$m^\mu = \frac{1}{\sqrt{2}}\left(0, \frac{\mathbf{E} + \mathrm{i}\mathbf{B}}{\rho}\right)\;,\; \bar{m}^\mu = \frac{1}{\sqrt{2}}\left(0, \frac{\mathbf{E} - \mathrm{i}\mathbf{B}}{\rho}\right) \tag{C.13}$$

We now show that the fields $\mathbf{E}, \mathbf{B}$ are null solutions to Maxwell's equations, related to $\mathbf{V}$ and ρ by: $\mathbf{V} = \mathbf{E} \times \mathbf{B}/\rho$, and $\rho = \frac{1}{2}(\mathbf{E}\cdot\mathbf{E} + \mathbf{B}\cdot\mathbf{B})$, if the initial conditions given by Eq.s (C.6),(C.7),(C.8) are satisfied.

The sequence of steps followed in the proof is as follows. We begin by showing that the null and shear-free conditions on the initial time slice, i.e. Eq.s (C.7)(C.8), are transported along k^μ. Using nullness, we then show that the divergence-free condition in Eq. (C.6) is also transported by k^μ. Finally using these, we show that $\mathbf{E}, \mathbf{B}$ satisfy Maxwell's equations in free space.

We will use the following notation:

$$k^\mu \partial_\mu = \frac{\mathrm{D}}{\mathrm{D}r_k}\;;\; m^\mu \partial_\mu = \frac{\mathrm{D}}{\mathrm{D}r_m} \tag{C.14}$$

In this notation, eq. (C.11) can be rewritten as:

$$\frac{\mathrm{D}}{\mathrm{D}r_k} k^\nu = 0\,,\; \frac{\mathrm{D}}{\mathrm{D}r_k} n^\nu = 0\,,\; \frac{\mathrm{D}}{\mathrm{D}r_k} m^\mu = \frac{\mathrm{D}}{\mathrm{D}r_m} k^\mu \tag{C.15}$$

The commutation relation of the vector fields k^μ, m^μ above can also be expressed as:

$$\frac{\mathrm{D}}{\mathrm{D}r_k}\frac{\mathrm{D}}{\mathrm{D}r_m} = \frac{\mathrm{D}}{\mathrm{D}r_m}\frac{\mathrm{D}}{\mathrm{D}r_k} \tag{C.16}$$

Note that eq. (C.15) for the evolution of k^μ, n^μ along with the initial condition eq. (C.9) implies that k^μ, n^μ can be written as in eq. (C.12): $k^\mu = \frac{1}{\sqrt{2}}\,(1, \mathbf{V})$, $n^\mu = \frac{1}{\sqrt{2}}\,(1, -\mathbf{V})$.

Also, the tetrad when transported along k^μ, remains a tetrad, i.e.

$$\frac{\mathrm{D}}{\mathrm{D}r_k}\{k\cdot k\,,\, k\cdot n\,,\, k\cdot m\,,\, n\cdot n\,,\, n\cdot m\} = 0 \tag{C.17}$$

as a consequence of eq. (C.11). From the null initial conditions it follows that:

$$k^\mu k_\mu = k^\mu m_\mu = n^\mu n_\mu = n^\mu m_\mu = 0\,,\; k^\mu n_\mu = 1 \tag{C.18}$$

In conjunction with eq. (C.12), $k\cdot k = 0 \Rightarrow \mathbf{V}\cdot\mathbf{V} = 1$. Also $k\cdot m = 0 \Rightarrow \mathbf{V} \propto \mathbf{E}\times\mathbf{B}$. This along with the initial condition eq. (C.9), and $\mathbf{V}\cdot\mathbf{V} = 1$ implies:

$$\mathbf{V} = \frac{\mathbf{E}\times\mathbf{B}}{\left|\mathbf{E}\times\mathbf{B}\right|} \tag{C.19}$$

We define ρ by the equation: $\bar{m}^\mu m_\mu = -1/\rho$ consistent with $\rho = \frac{1}{2}(\mathbf{E}\cdot\mathbf{E} + \mathbf{B}\cdot\mathbf{B})$.

To see how nullness (condition (i)) changes along the rays k^μ,

$$\begin{aligned}\frac{\mathrm{D}}{\mathrm{D}r_k}\left(m^\mu m_\mu\right) &= 2m^\mu\frac{\mathrm{D}}{\mathrm{D}r_k}m_\mu = 2m^\mu\frac{\mathrm{D}}{\mathrm{D}r_m}k_\mu = 2m^\mu\frac{\mathrm{D}}{\mathrm{D}r_m}k_\mu \\ &= 2m^\mu m^\nu\partial_\nu k_\mu = 2\tilde{\sigma}\end{aligned} \tag{C.20}$$

where $\tilde{\sigma} = m^\mu m^\nu\partial_\nu k_\mu = m^\mu\frac{\mathrm{D}}{\mathrm{D}r_m}k_\mu$.

When the tetrad $(k, n, \bar{m}, m)$ is null, $\tilde{\sigma} = \sigma/\rho$ where $|\sigma|$ is the shear of the congruence k^μ. The shear-free initial condition implies $\tilde{\sigma}_{t=0} = 0$. To see how $\tilde{\sigma}$ changes along the rays

k^μ,

$$\begin{aligned}\frac{\mathrm{D}}{\mathrm{D}r_k}\tilde{\sigma} &= \frac{\mathrm{D}}{\mathrm{D}r_k}\left(m^\mu \frac{\mathrm{D}}{\mathrm{D}r_m}k_\mu\right) = \frac{\mathrm{D}}{\mathrm{D}r_k}m^\mu \frac{\mathrm{D}}{\mathrm{D}r_m}k_\mu + m^\mu \frac{\mathrm{D}}{\mathrm{D}r_k}\left(\frac{\mathrm{D}}{\mathrm{D}r_m}k_\mu\right) \\ &= \frac{\mathrm{D}}{\mathrm{D}r_k}m^\mu \frac{\mathrm{D}}{\mathrm{D}r_m}k_\mu + m^\mu \frac{\mathrm{D}}{\mathrm{D}r_m}\left(\frac{\mathrm{D}}{\mathrm{D}r_k}k_\mu\right) \quad \text{(using eq. C.16)} \\ &= \frac{\mathrm{D}}{\mathrm{D}r_k}m^\mu \frac{\mathrm{D}}{\mathrm{D}r_m}k_\mu = \frac{\mathrm{D}}{\mathrm{D}r_m}k^\mu \frac{\mathrm{D}}{\mathrm{D}r_m}k_\mu \quad \text{(using eq. C.15)} \end{aligned} \tag{C.21}$$

Calculating the second derivative,

$$\begin{aligned}\frac{\mathrm{D}^2}{\mathrm{D}r_k^2}\tilde{\sigma} &= \frac{\mathrm{D}}{\mathrm{D}r_k}\left(\frac{\mathrm{D}}{\mathrm{D}r_m}k^\mu \frac{\mathrm{D}}{\mathrm{D}r_m}k_\mu\right) \\ &= \frac{\mathrm{D}}{\mathrm{D}r_k}\left(\frac{\mathrm{D}}{\mathrm{D}r_m}k^\mu\right)\frac{\mathrm{D}}{\mathrm{D}r_m}k_\mu + \frac{\mathrm{D}}{\mathrm{D}r_m}k^\mu \frac{\mathrm{D}}{\mathrm{D}r_k}\left(\frac{\mathrm{D}}{\mathrm{D}r_m}k_\mu\right) \\ &= \frac{\mathrm{D}}{\mathrm{D}r_m}\left(\frac{\mathrm{D}}{\mathrm{D}r_k}k^\mu\right)\frac{\mathrm{D}}{\mathrm{D}r_m}k_\mu + \frac{\mathrm{D}}{\mathrm{D}r_m}k^\mu \frac{\mathrm{D}}{\mathrm{D}r_m}\left(\frac{\mathrm{D}}{\mathrm{D}r_k}k_\mu\right) \\ &\qquad \text{(using eq. C.16)} \\ &= 0 \quad \text{(using eq. C.15)} \\ \therefore \frac{\mathrm{D}^n}{\mathrm{D}r_k^n}\tilde{\sigma} &= 0 \quad \forall\, n \geq 2,\, n \in \mathbb{N} \end{aligned} \tag{C.22}$$

Thus Eq.s (C.15),(C.16) which are equivalent to Eq. (C.4) ensure that the 2^{nd} and higher order derivatives of $\tilde{\sigma}$ vanish. The first derivative of $\tilde{\sigma}$ evaluated in eq. (C.21) can be rewritten as follows:

$$\frac{\mathrm{D}}{\mathrm{D}r_k}\tilde{\sigma} = \frac{\mathrm{D}}{\mathrm{D}r_m}k^\mu \frac{\mathrm{D}}{\mathrm{D}r_m}k_\mu = \frac{\mathrm{D}}{\mathrm{D}r_m}k^\mu\, \delta_\mu^\nu \frac{\mathrm{D}}{\mathrm{D}r_m}k_\nu \tag{C.23}$$

Since $m_0{}^\mu m_{0\mu} = 0$, $(k_0, n_0, \bar{m}_0, m_0)$ form a null tetrad and $\left(\delta_\mu^\nu\right)_{t=0}$ can be rewritten as:

$$\left(\delta_\mu^\nu\right)_{t=0} = k_{0\mu}n_0{}^\nu + n_{0\mu}k_0{}^\nu - \rho_0\left(\bar{m}_{0\mu}m_0{}^\nu + m_{0\mu}\bar{m}_0{}^\nu\right) \tag{C.24}$$

The above equation can be verified by contracting with the basis vectors $(k_0, n_0, \bar{m}_0, m_0)$.

Substituting (C.24) in the (C.23) above, we get,

$$\begin{aligned}
\left(\frac{\mathrm{D}}{\mathrm{D}r_k}\tilde{\sigma}\right)_{t=0} &= \left(\frac{\mathrm{D}}{\mathrm{D}r_m}k^\mu\right)_{t=0}\Big(k_{0\mu}{n_0}^\nu + n_{0\mu}{k_0}^\nu - \rho_0\left(\bar{m}_{0\mu}{m_0}^\nu + m_{0\mu}{\bar{m}_0}^\nu\right)\Big) \\
&\qquad\qquad \left(\frac{\mathrm{D}}{\mathrm{D}r_m}k_\nu\right)_{t=0} \\
&= \left(\frac{\mathrm{D}}{\mathrm{D}r_m}k^\mu\Big(k_\mu n^\nu + n_\mu k^\nu - \rho\left(\bar{m}_\mu m^\nu + m_\mu \bar{m}^\nu\right)\Big)\frac{\mathrm{D}}{\mathrm{D}r_m}k_\nu\right)_{t=0} \\
&= \left(\frac{\mathrm{D}}{\mathrm{D}r_m}k^\mu\left(-\rho\left(\bar{m}_\mu m^\nu + m_\mu \bar{m}^\nu\right)\right)\frac{\mathrm{D}}{\mathrm{D}r_m}k_\nu\right)_{t=0} \text{(using eq. C.18)} \\
&= -\rho_0\left(\left(m^\nu\frac{\mathrm{D}}{\mathrm{D}r_m}k_\nu\right)\bar{m}_\mu\frac{\mathrm{D}}{\mathrm{D}r_m}k^\mu + \left(m_\mu\frac{\mathrm{D}}{\mathrm{D}r_m}k^\mu\right)\bar{m}^\nu\frac{\mathrm{D}}{\mathrm{D}r_m}k_\nu\right)_{t=0} \\
&= -\rho_0\left(\tilde{\sigma}\,\bar{m}_\mu\frac{\mathrm{D}}{\mathrm{D}r_m}k^\mu + \tilde{\sigma}\,\bar{m}^\nu\frac{\mathrm{D}}{\mathrm{D}r_m}k_\nu\right)_{t=0} \\
&= -2\tilde{\sigma}_{t=0}\left(\rho\,\bar{m}_\mu\frac{\mathrm{D}}{\mathrm{D}r_m}k^\mu\right)_{t=0} \\
&= 0
\end{aligned} \tag{C.25}$$

$$\therefore \frac{\mathrm{D}^n}{\mathrm{D}r_k^n}\left(m^\mu m_\mu\right)\Big|_{t=0} = 0\,,\ \frac{\mathrm{D}^n}{\mathrm{D}r_k^n}\tilde{\sigma}\Big|_{t=0} = 0 \quad \forall\, n \geq 1,\, n \in \mathbb{N} \tag{C.26}$$

The above result along with the initial conditions: $\left(m^\mu m_\mu\right)_{t=0} = 0$, and $\tilde{\sigma}_{t=0} = 0$, implies that the null and shear-free conditions are transported along k^μ, and hold true for all space-time:

$$m^\mu m_\mu = 0\,,\ \tilde{\sigma} = 0 \tag{C.27}$$

Thus, the geodetic null congruence k^μ given by the normalized Poynting field $\mathbf{V}$ is shear-free and the fields $\mathbf{E}, \mathbf{B}$ defined by eq.s (C.13),(C.12) are null. Thus $\left|\mathbf{E}\times\mathbf{B}\right| = \rho$ and eq. (C.19) can be rewritten as:

$$\mathbf{V} = \frac{\mathbf{E}\times\mathbf{B}}{\rho} \tag{C.28}$$

Since $m^\mu m_\mu = 0$, $(k, n, \bar{m}, m)$ form a null tetrad and δ^ν_μ can be rewritten as:

$$\delta^\nu_\mu = k_\mu n^\nu + n_\mu k^\nu - \rho\left(\bar{m}_\mu m^\nu + m_\mu \bar{m}^\nu\right) \tag{C.29}$$

We now show that these fields satisfy Maxwell's equations in free space. Calculating the evolution of $1/\rho$ along the null GSF k^μ,

$$\begin{aligned}
\frac{\mathrm{D}}{\mathrm{D}r_k}\left(\frac{1}{\rho}\right) &= -\frac{\mathrm{D}}{\mathrm{D}r_k}\left(m^\mu \bar{m}_\mu\right) = -m^\mu \frac{\mathrm{D}}{\mathrm{D}r_k}\bar{m}_\mu - \bar{m}^\mu \frac{\mathrm{D}}{\mathrm{D}r_k} m_\mu \\
&= -m^\mu \bar{m}^\nu \partial_\nu k_\mu - \bar{m}^\mu m^\nu \partial_\nu k_\mu = -\partial_\nu k^\mu \left(m_\mu \bar{m}^\nu + \bar{m}_\mu m^\nu\right) \\
&= \frac{1}{\rho}\partial_\nu k^\mu \left(-\rho m_\mu \bar{m}^\nu - \rho \bar{m}_\mu m^\nu\right) \\
&= \frac{1}{\rho}\partial_\nu k^\mu \Big(k_\mu n^\nu + n_\mu k^\nu - \rho m_\mu \bar{m}^\nu - \rho \bar{m}_\mu m^\nu\Big) \quad \text{(using eq. C.18)} \\
&= \frac{1}{\rho}\partial_\nu k^\mu \delta^\nu_\mu = \frac{1}{\rho}\partial_\nu k^\nu \quad \text{(using eq. C.29)}
\end{aligned}$$

Substituting for k^μ from (C.12), we get the energy conservation equation:

$$\partial_t \rho + \nabla \cdot (\rho \mathbf{V}) = 0 \tag{C.30}$$

Rewriting Eq. (C.13) in terms of the Riemann-Silberstein vector $\mathbf{F} = \mathbf{E} + \mathrm{i}\mathbf{B}$,

$$\left(\frac{\mathbf{F}}{\rho}\right)_t = [\mathbf{F}/\rho, \mathbf{V}] \tag{C.31}$$

Using Eq. (C.30) alongwith Eq. (C.31),

$$\begin{aligned}
\mathbf{F}_t + [\mathbf{V}, \mathbf{F}] &= -\big(\nabla \cdot \mathbf{V}\big)\mathbf{F} \\
\Rightarrow \mathbf{F}_t + \nabla \times (\mathbf{F} \times \mathbf{V}) &= -\mathbf{V}\big(\nabla \cdot \mathbf{F}\big) \\
\Rightarrow \mathbf{F}_t + \mathrm{i}\nabla \times \mathbf{F} &= -\mathbf{V}\big(\nabla \cdot \mathbf{F}\big)
\end{aligned} \tag{C.32}$$

Taking the divergence of Eq. (C.32),

$$\begin{aligned}
&(\nabla\cdot\mathbf{F})_t = -\big(\nabla\cdot\mathbf{V}\big)\big(\nabla\cdot\mathbf{F}\big) - \mathbf{V}\cdot\nabla\big(\nabla\cdot\mathbf{F}\big)\\
\Rightarrow&\left(\partial_t + \mathbf{V}\cdot\nabla\right)\big(\nabla\cdot\mathbf{F}\big) = -\big(\nabla\cdot\mathbf{V}\big)\big(\nabla\cdot\mathbf{F}\big)\\
\Rightarrow&\frac{\mathrm{D}}{\mathrm{D}r_k}\left(\nabla\cdot\mathbf{F}\right) = -\left(\nabla\cdot\mathbf{F}\right)\nabla\cdot\mathbf{V}
\end{aligned} \tag{C.33}$$

Since $(\nabla\cdot\mathbf{F})_{t=0} = 0$, from eq. (C.33) above, $\nabla\cdot\mathbf{F} = 0$ for all space-time. Thus $\mathbf{E},\mathbf{B}$ are divergenceless for all space-time, satisfying one pair of Maxwell's equations in free space.

Substituting $\nabla\cdot\mathbf{F} = 0$ in eq. (C.32) above, we find that $\mathbf{F}$ also satisfies the other pair of Maxwell's equations: $\mathbf{F}_t + \mathrm{i}\nabla\times\mathbf{F} = 0$.

Thus the fields $\mathbf{E},\mathbf{B}$ are null solutions to Maxwell's equations in free space.

The converse is proved by Robinson's Theorem [130]. To see that the converse is true, i.e. a null Maxwell field satisfies the shear-free condition, note that eq.(C.20) implies that

$$\frac{D}{Dr_k}\left(m^\mu m_\mu\right) = 2\tilde{\sigma} = \frac{2\sigma}{\rho}$$

Since the electromagnetic field is null, $m^\mu m_\mu = 0$, which implies $\sigma = 0$, in particular $\sigma_{t=0} = 0$, which is equivalent to condition (iii). □

Corollary C.2.1. *: Let $\mathbf{E},\mathbf{B}$ be solutions to Maxwell's equations in free space with the initial conditions $\mathbf{E}_{t=0} = \mathbf{E}_0\,,\ \mathbf{B}_{t=0} = \mathbf{B}_0$, where $\mathbf{E}_0\,,\ \mathbf{B}_0$ are C^∞ vector fields in $\mathbb{R}^3$. The electromagnetic field $\mathbf{E},\mathbf{B}$ is null if and only if $\mathbf{E}_0,\mathbf{B}_0$ satisfy the initial conditions given by Eq.s (C.6),(C.7),(C.8).*

Proof. In the Theorem 4.4, we proved that If the electromagnetic field $\mathbf{E},\mathbf{B}$ is null, then the initial fields $\mathbf{E}_0,\mathbf{B}_0$ satisfy the conditions given by Eq.s (C.6),(C.7),(C.8).

To prove the corollary, we prove that the solution $\mathbf{E},\mathbf{B}$ to Maxwell's equations with initial conditions $\mathbf{E}_{t=0} = \mathbf{E}_0\,,\ \mathbf{B}_{t=0} = \mathbf{B}_0$ where $\mathbf{E}_0,\mathbf{B}_0$ satisfy the conditions given by

Eq.s (C.6),(C.7),(C.8), is a null electromagnetic field.

Define $\mathbf{V}_0 := \frac{\mathbf{E}_0 \times \mathbf{B}_0}{\rho_0}$, $\rho_0 := \frac{1}{2}\left(\mathbf{E}_0^2 + \mathbf{B}_0^2\right)$ and consider the initial value problem:

$$\begin{cases} \mathbf{V}_t + (\mathbf{V} \cdot \nabla)\,\mathbf{V} = 0 \\ \mathbf{V}_{t=0} = \mathbf{V}_0 \end{cases}$$

Since $\mathbf{V}_0$ is C^∞, it is locally Lipschitz continuous. By lemma (C.2.1), there exists a solution to this initial-value problem, which is C^∞, in the space-time region $U := \Big\{(t, \mathbf{r}) \in \mathbb{R}^4 : 0 < t < \psi(\mathbf{r})\,,\, \psi \in C^\infty(\mathbb{R}^4)\Big\}$.

Observe that, since $\mathbf{V}_{t=0}^2 = \mathbf{V}_0^2 = 1$, we have that $\mathbf{V}^2(\mathbf{x}, t) = 1$ in U, so that $\mathbf{V}(\mathbf{x}, t)$ defines a local flow ϕ_t in U. Accordingly there exist C^∞ solutions to the transport equations:

$$\partial_t \tilde{\mathbf{E}} = \left[\tilde{\mathbf{E}}, \mathbf{V}\right]\,,\, \partial_t \tilde{\mathbf{B}} = \left[\tilde{\mathbf{B}}, \mathbf{V}\right]$$

$\Rightarrow \tilde{\mathbf{E}}(\mathbf{x}, t) = \phi_{t*}\tilde{\mathbf{E}}_0(\mathbf{x})$ and $\tilde{\mathbf{B}}(\mathbf{x}, t) = \phi_{t*}\tilde{\mathbf{B}}_0(\mathbf{x})$, where $\tilde{\mathbf{E}}_0 = \frac{\mathbf{E}_0}{\rho_0}$, $\tilde{\mathbf{B}}_0 = \frac{\mathbf{B}_0}{\rho_0}$ and ϕ_t is the non-autonomous flow of $\mathbf{V}(\mathbf{x}, t)$ s.t. $\phi_0(\mathbf{x}) = \mathbf{x}$.

Therefore, we have C^∞ solutions in U to the initial value problem:

$$\begin{cases} \partial_t \mathbf{V} + (\mathbf{V} \cdot \nabla)\,\mathbf{V} = 0 \\ \partial_t \tilde{\mathbf{E}} = \left[\tilde{\mathbf{E}}, \mathbf{V}\right] \\ \partial_t \tilde{\mathbf{B}} = \left[\tilde{\mathbf{B}}, \mathbf{V}\right] \\ \tilde{\mathbf{E}}_{t=0} = \tilde{\mathbf{E}}_0\,,\, \tilde{\mathbf{B}}_{t=0} = \tilde{\mathbf{B}}_0\,,\, \mathbf{V}_{t=0} = \mathbf{V}_0 \end{cases}$$

such that conditions Eq.s(C.6),(C.7) and (C.8) of theorem C.2.2 hold.

Applying the theorem, we conclude that defining $\rho = \frac{1}{\frac{1}{2}\left(\tilde{\mathbf{E}}^2 + \tilde{\mathbf{B}}^2\right)}$ and $\mathbf{E} = \rho\tilde{\mathbf{E}}$, $\mathbf{B} = \rho\tilde{\mathbf{B}}$, the fields $\mathbf{E}(\mathbf{x}, t), \mathbf{B}(\mathbf{x}, t)$ solve Maxwell's equations in U, and satisfy the null conditions in U.

By the existence properties of Maxwell's equations, $\mathbf{E}(t, \mathbf{x})$ and $\mathbf{B}(t, \mathbf{x})$ can be globally

propagated, so that they provide C^∞ global solutions to the initial-value problem:

$$\begin{cases} \partial_t \mathbf{E} = \nabla \times \mathbf{B} \\ \partial_t \mathbf{B} = -\nabla \times \mathbf{E} \\ \mathbf{E}_{t=0} = \mathbf{E}_0 \, , \, \mathbf{B}_{t=0} = \mathbf{B}_0 \end{cases}$$

Moreover, since the set U satisfies a unique continuation property with respect to Maxwell's equations (since $\{t = 0\}$ is a Cauchy surface). Therefore the fact that $\mathbf{E}, \mathbf{B}$ are null in U implies that $\mathbf{E}, \mathbf{B}$ are globally null. □

C.3 First integrals of null electromagnetic fields

We now give a proof of the sufficient conditions, i.e. Eq.s (4.7),(4.8), for the existence of first integrals for null electromagnetic fields expressed in terms of the Bateman complex potentials $\{\alpha, \beta\}$.

Proof. Let us denote the magnitude and phase of α by r_α, θ_α and that of β by r_β, θ_β so that $\alpha = r_\alpha \exp(\mathrm{i}\theta_\alpha)$, $\beta = r_\beta \exp(\mathrm{i}\theta_\beta)$. Then,

$$\nabla\alpha = \alpha \left(\mathrm{i}\nabla\theta_\alpha + \frac{1}{r_\alpha}\nabla r_\alpha \right)$$
$$\nabla\beta = \beta \left(\mathrm{i}\nabla\theta_\beta + \frac{1}{r_\beta}\nabla r_\beta \right)$$

Then the electric field is given by:

$$\begin{aligned} \mathbf{E} &= \mathrm{Re}\{\nabla\alpha \times \nabla\beta\} \\ &= \mathrm{Re}\{\alpha\beta\} \left(\frac{\nabla r_\alpha}{r_\alpha} \times \frac{\nabla r_\beta}{r_\beta} - \nabla\theta_\alpha \times \nabla\theta_\beta \right) - \mathrm{Im}\{\alpha\beta\} \left(\frac{\nabla r_\alpha}{r_\alpha} \times \nabla\theta_\beta - \frac{\nabla r_\beta}{r_\beta} \times \nabla\theta_\alpha \right) \end{aligned}$$

Similarly the magnetic field is given by:

$$\begin{aligned}\mathbf{B} &= \mathrm{Im}\left\{\nabla\alpha \times \nabla\beta\right\} \\ &= \mathrm{Re}\left\{\alpha\beta\right\}\left(\frac{\nabla r_\alpha}{r_\alpha} \times \nabla\theta_\beta - \frac{\nabla r_\beta}{r_\beta} \times \nabla\theta_\alpha\right) + \mathrm{Im}\left\{\alpha\beta\right\}\left(\frac{\nabla r_\alpha}{r_\alpha} \times \frac{\nabla r_\beta}{r_\beta} - \nabla\theta_\alpha \times \nabla\theta_\beta\right)\end{aligned}$$

Similarly $\mathrm{Im}\left\{\nabla\left(\alpha\beta\right)\right\}$, $\mathrm{Re}\left\{\nabla\left(\alpha\beta\right)\right\}$ can be written as:

$$\mathrm{Im}\left\{\nabla\left(\alpha\beta\right)\right\} = \mathrm{Re}\left\{\alpha\beta\right\}\left(\nabla\theta_\alpha + \nabla\theta_\beta\right) + \mathrm{Im}\left\{\alpha\beta\right\}\left(\frac{\nabla r_\alpha}{r_\alpha} + \frac{\nabla r_\beta}{r_\beta}\right) \tag{C.34}$$

$$\mathrm{Re}\left\{\nabla\left(\alpha\beta\right)\right\} = \mathrm{Re}\left\{\alpha\beta\right\}\left(\frac{\nabla r_\alpha}{r_\alpha} + \frac{\nabla r_\beta}{r_\beta}\right) - \mathrm{Im}\left\{\alpha\beta\right\}\left(\nabla\theta_\alpha + \nabla\theta_\beta\right) \tag{C.35}$$

Using the above relations, we find:

$$\mathbf{E}\cdot\mathrm{Im}\left\{\nabla\left(\alpha\beta\right)\right\} = r_\alpha r_\beta\left(\nabla r_\alpha \times \nabla r_\beta\right)\cdot\left(\nabla\theta_\alpha + \nabla\theta_\beta\right) \tag{C.36}$$

$$\mathbf{E}\cdot\mathrm{Re}\left\{\nabla\left(\alpha\beta\right)\right\} = -r_\alpha r_\beta\left(\nabla\theta_\alpha \times \nabla\theta_\beta\right)\cdot\nabla\left(r_\alpha\, r_\beta\right) \tag{C.37}$$

$$\mathbf{B}\cdot\mathrm{Re}\left\{\nabla\left(\alpha\beta\right)\right\} = -r_\alpha r_\beta\left(\nabla r_\alpha \times \nabla r_\beta\right)\cdot\left(\nabla\theta_\alpha + \nabla\theta_\beta\right) \tag{C.38}$$

$$\mathbf{B}\cdot\mathrm{Im}\left\{\nabla\left(\alpha\beta\right)\right\} = -r_\alpha r_\beta\left(\nabla\theta_\alpha \times \nabla\theta_\beta\right)\cdot\ \nabla\left(r_\alpha\, r_\beta\right) \tag{C.39}$$

Hence, if $\nabla r_\alpha \times \nabla r_\beta = 0$, $\mathbf{E}\cdot\mathrm{Im}\left\{\nabla\left(\alpha\beta\right)\right\} = 0$, $\mathbf{B}\cdot\mathrm{Re}\left\{\nabla\left(\alpha\beta\right)\right\} = 0$, and if $\nabla\theta_\alpha \times \nabla\theta_\beta = 0$, $\mathbf{E}\cdot\mathrm{Re}\left\{\nabla\left(\alpha\beta\right)\right\} = 0$, $\mathbf{B}\cdot\mathrm{Im}\left\{\nabla\left(\alpha\beta\right)\right\} = 0$. □

APPENDIX D

SUPERFLUID VORTICES IN A LOW DENSITY REGION

Vortex lines in Euler flows are transported by the flow, and can not cross, giving rise to conservation of circulation, and helicity. Numerical simulations suggest that vortex lines in superfluids can reconnect and that circulation is not conserved. We present below, analytical calculations for superfluid vortices in a region of low density, showing violation of circulation conservation. and vortex reconnections analytically. This makes it clear that the phenomenon of vortex reconnection is intrinsic to the equations of motion for superfluid flows, and is not an artifact of numerical 'viscosity'.

We consider a weakly interacting BEC whose evolution is given by the Gross-Pitaevskii equation:

$$i\hbar\frac{\partial\psi}{\partial t} = -\frac{\hbar^2}{2m}\nabla^2\psi + g|\psi|^2\psi \tag{D.1}$$

where $\psi(\mathbf{x})$ is the wave-function describing the condensate.

We want to study the evolution of vortices contained in a low density region of the condensate i.e. $|\psi|^2 \ll 1$ so that the nonlinear term of the GPE can be neglected, giving the free particle Schrodinger equation:

$$i\hbar\frac{\partial\psi}{\partial t} = -\frac{\hbar^2}{2m}\nabla^2\psi \tag{D.2}$$

Let the length scale associated with the region of low density be r_0, so that $\rho(r) \ll 1$ for $r/r_0 \sim O(1)$, and $\rho(r) \to 1$ as $r/r_0 \to \infty$.

Rewriting the Schrodinger equation in terms of the dimensionless variables $\mathbf{R} = \mathbf{r}/r_0$, $\tau = \hbar t/(mr_0^2)$:

$$i\frac{\partial\psi}{\partial\tau} = -\frac{1}{2}\nabla_R^2\,\psi \tag{D.3}$$

The solution to the above equation is given by:

$$\psi(\mathbf{R};\tau) = \int d^3\mathbf{R}'\, K(\mathbf{R}'-\mathbf{R};\tau)\psi(\mathbf{R}';0) \tag{D.4}$$

where the propagator is $K(\mathbf{R}'-\mathbf{R};\tau) = \left(\frac{1}{2\pi i\,\tau}\right)^{3/2} \exp\left(\frac{-(\mathbf{R}'-\mathbf{R})^2}{2\,i\,\tau}\right)$.

We will now solve for the evolution of a vortex ring, and linked ring vortices in a region of low density using Eq. (D.4).

D.1 Vortex ring dissipation—analytical calculation

We now consider a single vortex ring in a low density region of the superfluid described by the following condensate wave-function:

$$\psi(\mathbf{R};0) = \frac{\frac{1}{3} + \frac{1}{35}\left(\frac{R}{10}\right)^2}{100\left(1 + \frac{1}{3}\left(\frac{R}{10}\right)^2 + \frac{1}{35}\left(\frac{R}{10}\right)^4\right)} \cdot \left(2Z + i\left(R^2 - 1\right)\right) \tag{D.5}$$

where $(X, Y, Z) = (x, y, z)/r_0$ and $R^2 = X^2 + Y^2 + Z^2$.

The density profile of the above wave-function is given below in Fig. D.1:

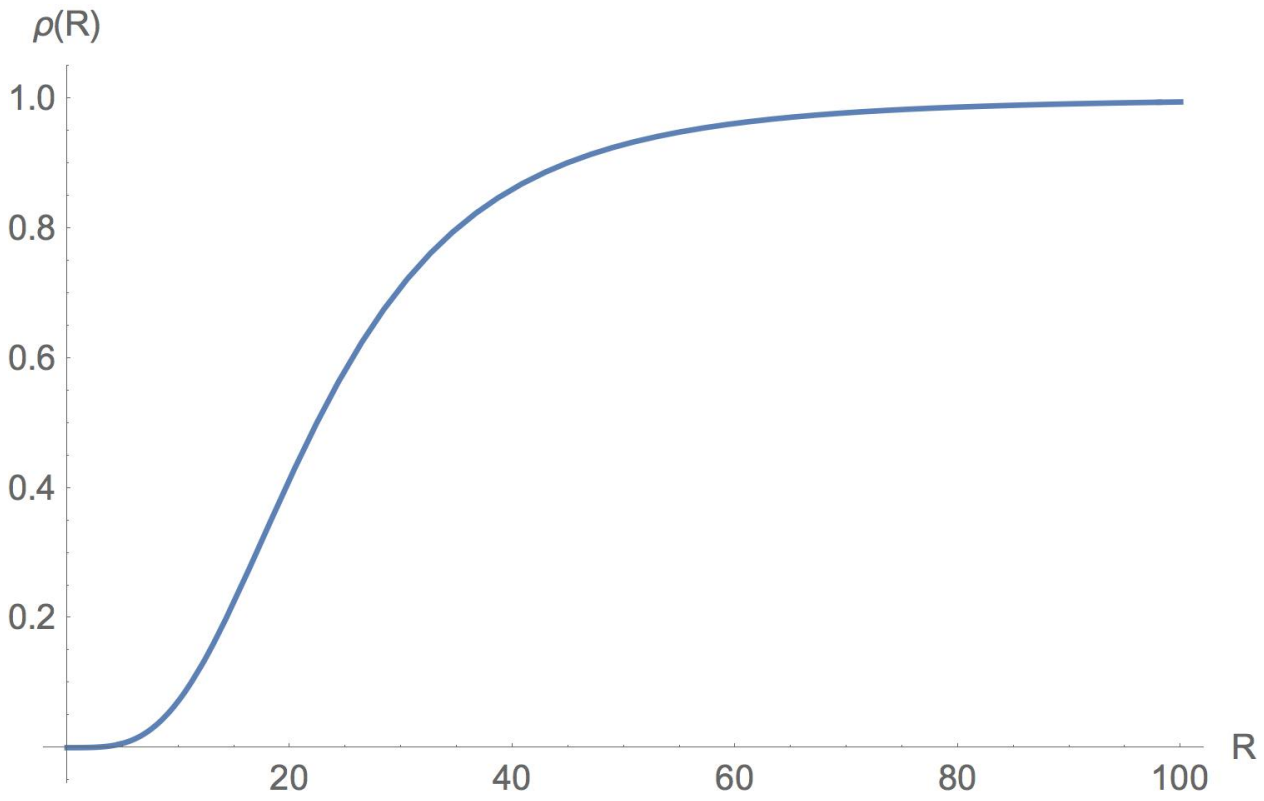

Figure D.1: Density profile of vortex ring wave-function given in Eq. (D.5), showing that the vortex ring of radius R, is indeed in a region of low density.

We approximate the initial state $\psi(\mathbf{R};0)$ in the region $R \sim O(1)$ as follows:

$$\begin{aligned}
\psi(\mathbf{R};0) &\approx \frac{1}{100}\left(\frac{1}{3}+\frac{1}{35}\left(\frac{R}{10}\right)^2\right)\left(1-\frac{1}{3}\left(\frac{R}{10}\right)^2\right)\cdot \\
&\qquad\qquad \left(2Z+i\left(R^2-1\right)\right) \\
&\approx \frac{1}{100}\left(\frac{1}{3}+\frac{1}{35}\left(\frac{R}{10}\right)^2-\frac{1}{9}\left(\frac{R}{10}\right)^2\right)\cdot \\
&\qquad\qquad \left(2Z+i\left(R^2-1\right)\right) \\
&\approx \left(1-\frac{26}{105}\left(\frac{R}{10}\right)^2\right)\frac{2Z+i\left(R^2-1\right)}{300}
\end{aligned} \tag{D.6}$$

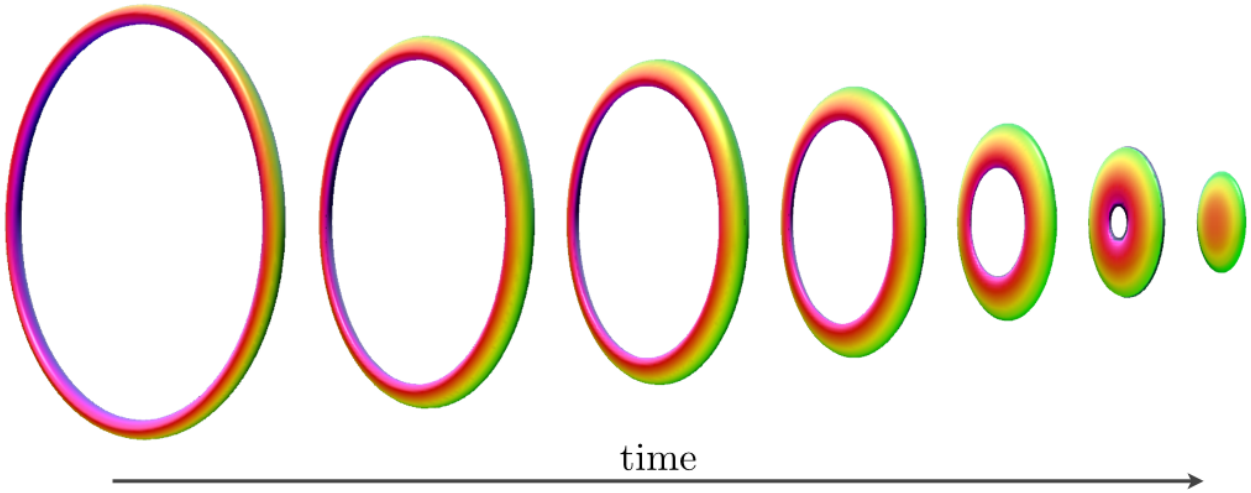

Figure D.2: Evolution of a vortex ring in a low density region of the superfluid. The vortex ring shrinks and eventually vanishes, suggesting that Kelvin's circulation theorem does not hold in superfluids.

On solving for the evolution of the above wave-function using Eq. (D.4), we find:

$$\begin{aligned}\psi(\mathbf{R};\tau) = \frac{1}{300}\Bigg(2Z - 3\tau\left(1+\frac{13}{5250}\right) \\ + \frac{13}{2625}R^2\left(5\tau - Z\right)\Bigg) + \\ \frac{i}{300}\Bigg(\left(1+\frac{13}{5250}\right)R^2 - 1 + \frac{13}{1050}\tau(3\tau - 2Z) \\ - \frac{13}{5250}R^4\Bigg)\end{aligned} \tag{D.7}$$

On solving for the evolution of the vortex ring, we find that the vortex ring shrinks and dissipates into sound at $\tau \sim 2/3$ as shown in the supplementary movie in [61]. This suggests that circulation is not conserved in a superfluid, consistent with the vanishing of the conserved quantity analogous to circulation in superfluids.

D.2 Linked vortex rings crossing—analytical calculation

Vortex lines in a superfluid can cross each other—as demonstrated numerically [168], experimentally [170]—and analytically below.

Consider a pair of linked vortex rings in a low density region of superfluid described by the following condensate wave-function:

$$\psi(\mathbf{R};0) = \frac{1}{3.5\cdot 10^5}\cdot\frac{1}{1+\frac{1}{3}\left(\frac{R}{10}\right)^2+\frac{1}{35}\left(\frac{R}{10}\right)^4}\cdot \left(\left(2Z+i\left(R^2-1\right)\right)^2-4\left(X+iY\right)^2\right) \tag{D.8}$$

where $(X,Y,Z)=(x,y,z)/r_0$ and $R^2=X^2+Y^2+Z^2$.

The density profile of the above wave-function is given below in Fig. D.3:

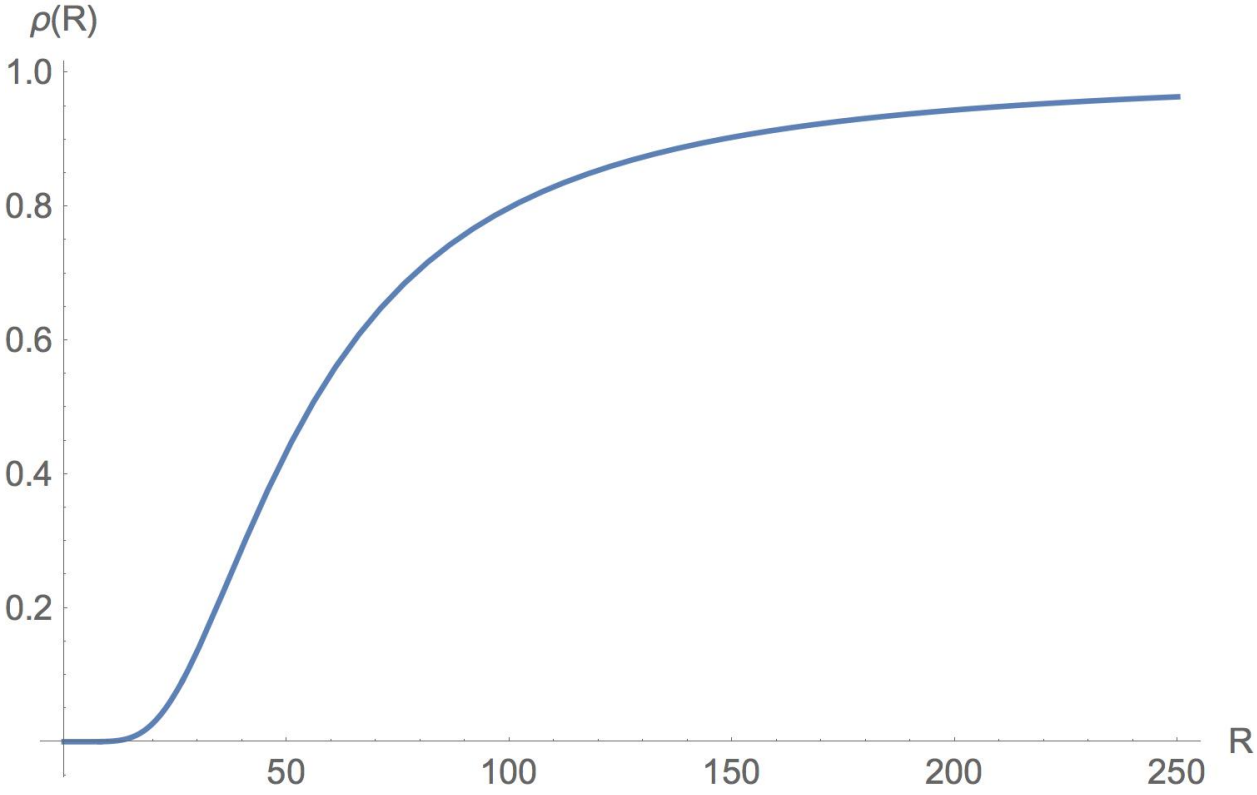

Figure D.3: Density profile of linked vortex rings wave-function given in Eq. (D.8)

We approximate the initial state $\psi(\mathbf{R};0)$ in the region $R \sim O(1)$ as follows:

$$\psi(\mathbf{R};0) \approx \frac{1}{3.5\cdot 10^5}\cdot\left(1-\frac{1}{3}\left(\frac{R}{10}\right)^2\right)\cdot \left(\left(2Z+i\left(R^2-1\right)\right)^2-4\left(X+iY\right)^2\right) \tag{D.9}$$

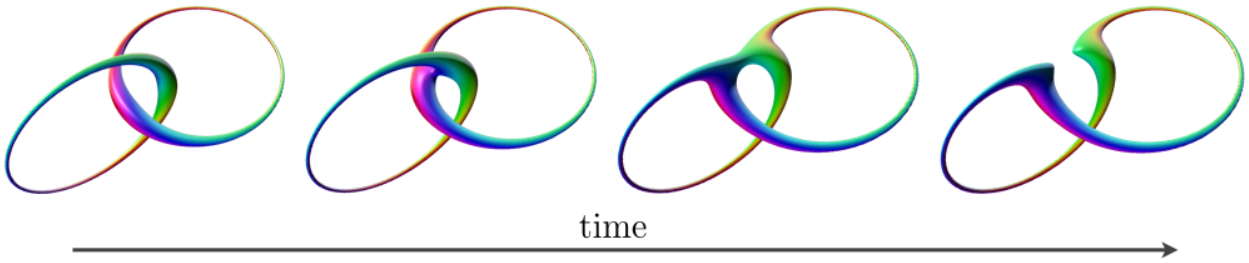

Figure D.4: The evolution of linked vortex rings in a low density region of the superfluid. We see that the linked rings reconnect to form a single writhing (coiling) loop, showing analytically that vortex lines in a superfluid can reconnect.

On solving for the evolution of the wave-function using Eq. (D.4), we find:

$$\begin{aligned}\psi(\mathbf{R};\tau) = \frac{1}{3.5\cdot 10^4}\Bigg[\Bigg(&-1+\left(6+\frac{1}{300}\right)R^2-8X^2- \\ &\left(1+\frac{1}{50}\right)R^4+\frac{2}{75}X^2R^2+\frac{R^6}{300}+ \\ &\frac{7\tau}{75}\left(Z(2R^2-215)-2XY\right)- \\ &\frac{7\tau^2}{60}\left(3R^2-130\right)\Bigg)+ \\ 4i\Bigg(&-Z-2XY+\left(1+\frac{1}{300}\right)R^2Z+ \\ &\frac{XYR^2}{150}-\frac{1}{300}R^4Z+ \\ &\frac{7\tau}{1200}\left(429-436R^2+8X^2+3R^4\right)+ \\ &\frac{7\tau^2}{60}Z-\frac{7\tau^3}{80}\Bigg)\Bigg]\end{aligned} \tag{D.10}$$

We use the above time-dependent solution of the wave-function and track the evolution of the linked vortex rings to find that the linked rings reconnect at $\tau \sim 0.25$ to form a single writhing vortex ring as shown in Fig. D.4. Our analytical calculation is further evidence that reconnections of vortex lines in superfluids are an intrinsic property of the Gross-Pitaevskii equation and do not require the presence of normal fluid or numerical 'viscosity'.

APPENDIX E

CASIMIR INVARIANTS IN SUPERFLUIDS

In Euler flows, helicity emerges a special constant of motion: a Casimir invariant [176, 178], i.e. it has a vanishing Poisson bracket with any function of the phase space variables: $\{\mathcal{H}, F(\mathbf{u}, \rho)\} = 0 \ \forall \ F$, where the density ρ and the fluid velocity $\mathbf{u}$ are the phase space variables, and $\{\,\cdot\,,\cdot\,\}$ denotes the Poisson bracket.

Solving for the Casimir invariants in Euler flow, i.e. solving $\{\mathcal{C}, F(\mathbf{u}, \rho)\} = 0 \ \forall \ F$ gives rise to helicity as an additional conserved quantity. We seek an analogous conserved quantity in superfluids by solving for the Casimir invariants for the Gross-Pitaevskii equation.

The Hamiltonian corresponding to the Gross-Pitaevskii equation is:

$$\mathbb{H} = \int d^3x \, \left[\frac{\hbar^2}{2m}|\nabla\psi|^2 + \frac{V}{2}|\psi|^4\right] \tag{E.1}$$

with the canonical Poisson bracket:

$$[F, G] = -\frac{i}{\hbar}\int d^3x \left(\frac{\delta F}{\delta\psi}\frac{\delta G}{\delta\psi^*} - \frac{\delta G}{\delta\psi}\frac{\delta F}{\delta\psi^*}\right) \tag{E.2}$$

Solving for the Casimir invariants $\{\mathcal{C}, F(\psi, \psi^*)\} = 0 \ \forall \ F$ reduces to the equations:

$$\frac{\delta\mathcal{C}}{\delta\psi} = 0\,, \quad \frac{\delta\mathcal{C}}{\delta\psi^*} = 0 \tag{E.3}$$

which gives only trivial constants as Casimir invariants. Since Casimir invariants of the Gross-Pitaevskii superfluid should yield a conserved quantity analogous to helicity in Euler flows, the above calculation suggests that the conserved quantity analogous to helicity in superfluids is a trivial constant. This is consistent with our calculation based on the relabeling symmetry which suggests that the conserved quantity analogous to helicity in superfluids vanishes identically.

We note that an alternative path to seeking Casimir invariants, by taking the phase space variables to be $\{\mathbf{j}\,,\rho\} = \{(\psi^*\nabla\psi - \psi\nabla\psi^*)\,/(2i)\,,\,\psi^*\psi\}$ instead of $\{\psi, \psi^*\}$ runs into difficulties because of the singular nature of the singular nature of vorticity: $\nabla\times(\mathbf{j}/\rho)$. This difficulty manifests as the Poisson bracket for the new phase space variables denoted by $\{\cdot\,,\,\cdot\}_{\mathbf{j},\rho}$ erroneously giving: $\partial_t\left(\nabla\times(\mathbf{j}/\rho)\right) = \{\mathbf{j}/\rho\,,\,\mathbb{H}\}_{\mathbf{j},\rho} = 0$, suggesting that vortex lines are stationary.

We now briefly review the underlying symmetry—the relabeling symmetry—that gives rise to helicity as a conserved charge via Noether's theorem, and calculate the analogous conserved charge in superfluids.

APPENDIX F

RELABELING SYMMETRY IN SUPERFLUIDS

We now consider a classical fluid which obeys the same equation of motion as the Gross-Pitaevskii superfluid, except for the quantum pressure term, and show that the relabeling symmetry which gives rise to helicity conservation via Noether's theorem in Euler fluids gives a vanishing conserved charge in such a classical fluid.

F.1 Superfluid equations of motion

On setting $\hbar = m = 1$, the Gross-Pitaevskii equation of motion for a superfluid is:

$$i\partial_t\psi = -\frac{1}{2}\nabla^2\psi + V|\psi|^2\,\psi \tag{F.1}$$

On substituting $\psi = \sqrt{\rho}\exp(i\phi)$, the above complex equation gives two real equations for the evolution of ρ and ϕ as follows:

$$\partial_t\rho + \nabla\cdot(\rho\,\nabla\phi) = 0 \tag{F.2}$$

$$\partial_t\phi + \frac{1}{2}\left(\nabla\phi\right)^2 + V\rho - \frac{1}{2}\left(\frac{\nabla^2\sqrt{\rho}}{\sqrt{\rho}}\right) = 0 \tag{F.3}$$

On applying a spatial gradient operator ∇ to Eq. (F.3), and substituting the expression for the superfluid velocity $\mathbf{u} = \nabla\phi$, we find:

$$\partial_t\mathbf{u} + \nabla\left(\frac{1}{2}\mathbf{u}^2 + V\rho - \frac{\nabla^2\sqrt{\rho}}{2\sqrt{\rho}}\right) = 0 \tag{F.4}$$

Note that the above equation contains the quantum pressure term $\frac{1}{2}\nabla\left(\nabla^2\sqrt{\rho}/\sqrt{\rho}\right)$ containing spatial derivatives of the density, is dominant only near the vortex core. Such a term is not present in classical hydrodynamics, since the pressure is assumed to depend only on the

local density, and not on the spatial derivatives of the density. We now make the Thomas-Fermi approximation [159, 185, 190, 185, 191] and neglect the quantum pressure term in the above equation, thereby considering a hypothetical classical fluid which obeys the above equation of motion without the quantum pressure term, i.e.

$$\partial_t \mathbf{u} + \nabla \left(\frac{1}{2}\mathbf{u}^2 + V\rho \right) = 0 \tag{F.5}$$

The above equation describes the superfluid well in the region excluding the vortex core. Note that the above equation is similar to the equation of motion for an irrotational Euler fluid:

$$\partial_t \mathbf{u} + \nabla \left(\frac{1}{2}\mathbf{u}^2 + e \right) = 0 \tag{F.6}$$

where $e : de = dp/\rho$ is the enthalpy per unit mass and p is the pressure.

F.2 Relabeling symmetry in a classical Euler fluid

The action for a classical (isentropic) Euler fluid is:

$$S_{\text{Euler}} = \int d^3a\, d\tau \left(\frac{1}{2} \left(\frac{\partial \mathbf{x}(\mathbf{a},\tau)}{\partial \tau} \right)^2 - E(\rho) \right) \tag{F.7}$$

where $\mathbf{x}(\mathbf{a},\tau)$ is the position of the fluid element labeled by $\mathbf{a}$ at time τ, and the fluid velocity $\mathbf{u}(\mathbf{a},\tau) = \partial_\tau \mathbf{x}(\mathbf{a},\tau)$. The label co-ordinates $\mathbf{a}$ are chosen such that $\rho\, d^3x = d^3a \Rightarrow \frac{\partial(\mathbf{x})}{\partial(\mathbf{a})} = \rho^{-1}$. It is easily verified [177, 178, 176] that extremizing the action with respect to variations in the position field $\mathbf{x}(\mathbf{a},\tau)$, gives the Euler equations of motion. Mass conservation follows from: $\frac{\partial}{\partial \tau}\rho^{-1} = \frac{\partial}{\partial \tau}\left(\frac{\partial(\mathbf{x})}{\partial(\mathbf{a})}\right)$.

As shown in [178, 177, 176, 179] and can be easily verified, the transformation $a^i \rightarrow \tilde{a}^i = a^i + \epsilon\, \eta^i$, such that $\frac{\partial}{\partial \tau}\eta^i = 0, \frac{\partial}{\partial a^i}\eta^i = 0$ is a symmetry of the action and gives the

corresponding conserved Noether charge:

$$\mathcal{Q} = \int d^3a \, u_i \, \frac{\partial x^i}{\partial a^j} \, \eta^j \tag{F.8}$$

When the fluid labels are displaced infinitesimally along a closed material curve, the conserved charge $\mathcal{Q}$ simplifies to the circulation around the material loop Γ_C, thus giving Kelvin's circulation theorem. This can be verified by substituting $\eta^j = \oint_{C:\mathbf{a}(s)} ds \, \delta^{(3)}(\mathbf{a} - \mathbf{a}(s)) \, \frac{\partial a^j(s)}{\partial s}$ in Eq. (F.8). When the fluid labels are displaced infinitesimally along vortex lines, the conserved charge $\mathcal{Q}$ is the helicity of the fluid: $\mathcal{Q} = \mathcal{H} = \int d^3x \, \mathbf{u} \cdot \nabla \times \mathbf{u}$. This can be verified by substituting $\eta^j = \epsilon^{jkl} \frac{\partial}{\partial a^k} u_p \, \frac{\partial}{\partial a^l} x^p$ in Eq. (F.8).

F.3 Relabeling symmetry in a superfluid

The action corresponding to the Gross-Pitaevskii equation is:

$$S_{\text{gpe}} = \int dt \, d^3x \left(i\psi^* \partial_t \psi - \frac{1}{2} |\nabla \psi|^2 - \frac{V}{2} |\psi|^4 \right) \tag{F.9}$$

which can be written in terms of ρ, ϕ as follows:

$$S_{\text{gpe}} = - \int dt \, d^3x \left(\rho \, \partial_t \phi + \frac{1}{2} \rho \, (\nabla \phi)^2 + \frac{V}{2} \rho^2 + \frac{1}{2} (\nabla \sqrt{\rho})^2 \right) \tag{F.10}$$

It is easy to verify that extremizing the above action in Eq. (F.10) with respect to ρ, ϕ gives the desired equations of motion: Eq.s (F.2),(F.3), and that the last term in the action: $\frac{1}{2}(\nabla\sqrt{\rho})^2$ corresponds to the quantum pressure term in Eq.s (F.3),(F.4).

We now model the superfluid in the region excluding vortex cores as a classical fluid which carries with it a phase $\phi(\mathbf{x}, t)$. We neglect the quantum pressure term (making the

Thomas-Fermi approximation), and use the relation $\mathbf{u} = \nabla\phi$ to get the following new action:

$$\tilde{S}_{\text{gpe}} = -\int dt\, d^3x \left(\frac{1}{2}\rho\, \mathbf{u}^2 + \rho\, \partial_t\phi + \frac{V}{2}\rho\right) \tag{F.11}$$

In region excluding the vortex cores, we assume that we can label the fluid particles with labels $\mathbf{a}$ where $d^3a = \rho\, d^3x$, and track the positions of these particles $\mathbf{x}(\mathbf{a}, \tau)$ over time τ. We now rewrite the above action in terms of label co-ordinates $\mathbf{a}, \tau$ using $\partial_\tau = \partial_t + \mathbf{u}\cdot\nabla$:

$$\tilde{S}_{\text{gpe}} = \int d\tau\, d^3a \left(\frac{1}{2}\mathbf{u}^2 - \partial_\tau\phi - \frac{V}{2}\rho\right) \tag{F.12}$$

It is easy to verify that extremizing the above action with respect to $\mathbf{x}(\mathbf{a}, \tau)$ gives the desired equation of motion: Eq. (F.5).

We now perform the same relabeling transformation that gives the circulation theorem and helicity conservation in Euler fluids, to seek analogous conservation laws. It is easily verified that the relabeling transformation: $a^i \to \tilde{a}^i = a^i + \epsilon\,\eta^i$, such that $\partial\eta^i/\partial\tau = 0, \partial\eta^i/\partial a^i = 0$, is a symmetry of the above action $\tilde{S}_{\text{gpe}}$. The corresponding Noether charge is found to vanish identically, independent of η^i, as shown below:

$$\begin{aligned}
\mathcal{Q}_{gpe} &= \int d^3a\, \eta^j \left(\frac{\partial x^i}{\partial\tau}\frac{\partial x^i}{\partial a^j} - \frac{\partial\phi}{\partial a^j}\right) \\
&= \int d^3a\, \eta^j \left(u^i\frac{\partial x^i}{\partial a^j} - \frac{\partial\phi}{\partial a^j}\right) \\
&= \int d^3a\, \eta^j \left(\frac{\partial\phi}{\partial x^i}\frac{\partial x^i}{\partial a^j} - \frac{\partial\phi}{\partial a^j}\right) \qquad (\because \mathbf{u} = \nabla\phi) \\
&= \int d^3a\, \eta^j \left(\frac{\partial\phi}{\partial a^j} - \frac{\partial\phi}{\partial a^j}\right) \\
&= 0
\end{aligned} \tag{F.13}$$

The above calculation suggests that the conserved charges analogous to helicity, and circu-

lation trivially vanish for superfluids.

Note that the presence of an additional phase term $(-\partial_\tau \phi)$ in addition to the terms present in the Euler action S_{Euler}, is necessary to ensure Galilean invariance (as defined in [194]) of the modified action $\tilde{S}_{\text{gpe}}$, much like the constant term $(-c^2)$ [214] is necessary to ensure Galilean invariance of the classical fluid action. The presence of the additional phase term gives rise to mass conservation in the original Gross-Pitaevskii action S_{gpe}, which is manifestly Galilean invariant. However, mass conservation is inherent to the description of the superfluid when expressed in terms of the particle label co-ordinate frame $(\mathbf{a}, \tau)$, and instead this term now has the effect of giving a vanishing conserved charge corresponding to relabeling symmetry transformations. We note that an alternative calculation due to Bretherton [215] which derives the conservation of circulation using Hamilton's principle, also yields a vanishing conserved quantity in superfluids.

APPENDIX G

TWIST OF A UNIT VECTOR FIELD

Given a unit vector field $\hat{\omega}$, we want to calculate the twist of a field line (integral curve) of $\hat{\omega}$.

The twist rate along a curve (parametrized by s) is given by:

$$\mathrm{Tw}(s) = \frac{1}{2\pi}\partial_s \hat{n} \cdot \left(\hat{t} \times \hat{n}\right) \tag{G.1}$$

where $\hat{n}$ is a unit vector defining a framing of the curve, and $\hat{n} \perp \hat{t}$ all along the curve.

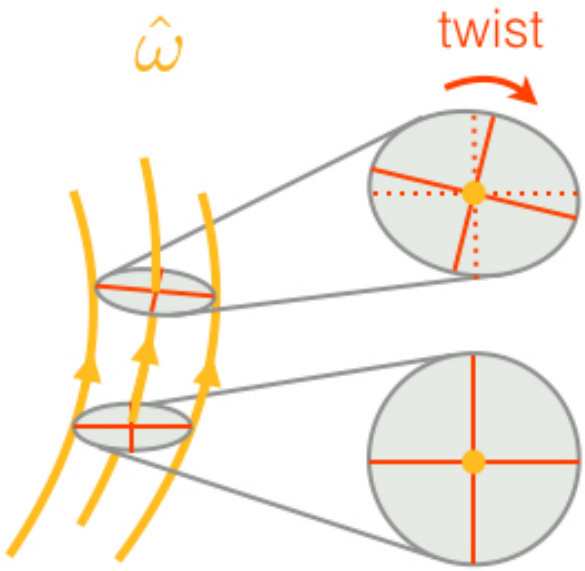

Figure G.1: Transporting a circular disk $\perp$ to $\hat{\omega}$ along a field line, rotates the disk while distorting it into an ellipse. The average rotation of the points on the periphery of the disk gives average twist of the field line.

In the neighbourhood of any given field line of $\hat{\omega}$, there is a bundle of field lines of $\hat{\omega}$. We consider an infintesimally small circular disk perpendicular to the given field line, and propagate it along this field line so that the circle on the periphery of the disk always lies on the same neighbouring field lines. The circular disk generally distorts into an elliptical

disk, and the average twist of the field line through the center of the disk is measured by the average rotation of the points lying on the circle forming the boundary of the disk, as shown in Fig. G.1.

We find that the average twist of the field lines of a unit vector $\hat{\omega}$ is given by:

$$\boxed{\langle \mathrm{Tw} \rangle = \pm \frac{1}{4\pi} \hat{\omega} \cdot (\nabla \times \hat{\omega})} \tag{G.2}$$

G.1 Twist framing

To use Eq. (G.1) to calculate the twist of an integral curve of $\hat{\omega}$, we need to define a framing of the curve locally, i.e. define $\hat{n}$ and $\partial_s \hat{n}$ such that:

(i) $\hat{\omega} \cdot \hat{n} = 0$

(ii) $\partial_s (\hat{\omega} \cdot \hat{n}) = 0$.

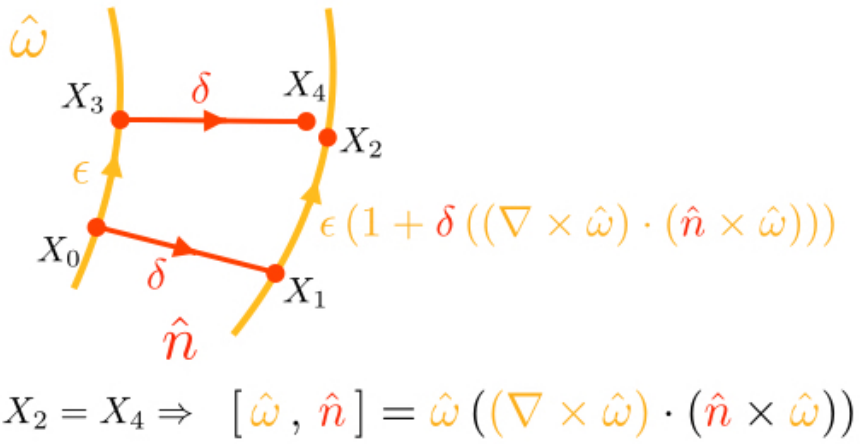

Figure G.2: Defining a frame: transport a unit vector $\hat{n} \perp \hat{\omega}$ joining neighboring field lines of $\hat{\omega}$ so that $\hat{n} \perp \hat{\omega}$ is satisfied locally.

A way to construct such a framing locally is as follows. We choose an arbitrary $\hat{n}$ such that $\hat{\omega} \cdot \hat{n} = 0$ at a point s_0 on the curve and transport $\hat{n}$ as shown in Fig. G.2, so that:

$$\partial_s \hat{n} = (\hat{n} \cdot \nabla)\,\hat{\omega} + \hat{\omega}\,((\nabla \times \hat{\omega}) \cdot (\hat{n} \times \hat{\omega})) \tag{G.3}$$

It is easily shown that Eq. (G.3) implies $\partial_s(\hat{\omega}\cdot\hat{n})=0$ as follows:

$$\begin{aligned}
\partial_s(\hat{\omega}\cdot\hat{n}) &= \partial_s\hat{n}\cdot\hat{\omega}+\hat{n}\cdot\partial_s\hat{\omega} \\
&= ((\hat{n}\cdot\nabla)\hat{\omega}+\hat{\omega}((\nabla\times\hat{\omega})\cdot(\hat{n}\times\hat{\omega})))\cdot\hat{\omega}+\hat{n}\cdot\partial_s\hat{\omega} \qquad (\because \text{Eq. (G.3)}) \\
&= ((\nabla\times\hat{\omega})\cdot(\hat{n}\times\hat{\omega}))+\hat{n}\cdot\partial_s\hat{\omega} \qquad (\because \hat{\omega} \text{ is a unit vector.}) \\
&= \hat{n}\cdot(\omega\times(\nabla\times\hat{\omega})+(\hat{\omega}\cdot\nabla)\hat{\omega}) \\
&= \hat{n}\cdot\nabla\left(\tfrac{1}{2}\hat{\omega}\cdot\hat{\omega}\right) \\
&= 0
\end{aligned}$$

Substituting for $\partial_s\hat{n}$ in Eq. (G.1), the twist rate of the above framing is given by:

$$\begin{aligned}
\mathrm{Tw} &= \frac{1}{2\pi}(\hat{n}\cdot\nabla)\hat{\omega}\cdot(\hat{\omega}\times\hat{n}) \\
&= \frac{1}{2\pi}\hat{n}^b\,(\partial_b\hat{\omega}_a)\,\hat{n}^a_\perp
\end{aligned} \tag{G.4}$$

where $\hat{n}_\perp=\hat{\omega}\times\hat{n}$.

Since $\hat{n}$ and $\hat{n}_\perp$ lie in the plane perpendicular to $\hat{\omega}$, the above expression for twist depends only on $(\partial_b\hat{\omega}_a)_\perp$: the projection of the strain tensor in the plane perpendicular to $\hat{\omega}$, as follows:

$$\mathrm{Tw}=\frac{1}{2\pi}\hat{n}^b\,(\partial_b\hat{\omega}_a)\,\hat{n}^a_\perp=\frac{1}{2\pi}\hat{n}^b\,(\partial_b\hat{\omega}_a)_\perp\,\hat{n}^a_\perp \tag{G.5}$$

The principal axes of the elliptical disk shown in Fig. G.1 correspond to the eigen directions of the projected strain tensor: $(\partial_b\hat{\omega}_a)_\perp$.

G.2 Twist in terms of optical scalars

We will now evaluate the projected strain tensor $(\partial_b \hat{\omega}_a)_\perp$ and decompose it in terms of scalars corresponding to dilation, rotation and shear [210].

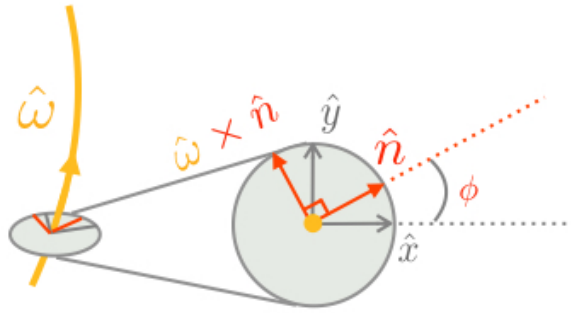

Figure G.3: Different choices of $\hat{n}$ correspond to different angles ϕ w.r.t. the reference frame given by $\hat{x}$ and $\hat{y}$ which are chosen arbitrarily.

To project the strain tensor, we construct a projection operator $h^a_b = \delta^a_b - \hat{\omega}_b \hat{\omega}^a$. This projection operator h^a_b projects onto the plane perpendicular to $\hat{w}$ as can be seen by evaluating $h^a_b \hat{\omega}^b = \hat{\omega}^a - \hat{\omega}^a = 0$. The projected strain tensor $(\partial_b \hat{\omega}_a)_\perp$ is given by:

$$\begin{aligned}(\partial_b \hat{\omega}_a)_\perp &= h^d_b \, \partial_d \hat{\omega}_c \, h^c_a \\ &= \left(\delta^d_b - \hat{\omega}_b \hat{\omega}^d\right) \partial_d \hat{\omega}_c \, (\delta^c_a - \hat{\omega}_a \hat{\omega}^c) \end{aligned} \tag{G.6}$$

To decompose this projected strain tensor in terms of dilation, shear and rotation, we need a basis in the plane perpendicular to $\hat{\omega}$. We consider a basis formed by two arbitrary perpendicular unit vectors $\hat{x}$ and $\hat{y}$. The choice of the unit vector $\hat{n}$ is parametrized by the angle ϕ it makes with $\hat{x}$ as shown in Fig. G.3 .

The decomposition of the strain tensor follows most naturally in terms of the complex null vectors $m^a = \frac{1}{\sqrt{2}}(\hat{x}^a + i\,\hat{y}^a)$, and $\bar{m}^a = \frac{1}{\sqrt{2}}(\hat{x}^a - i\,\hat{y}^a)$, which satisfy $m^a m_a = \bar{m}^a \bar{m}_a = 0$, and $m^a \bar{m}_a = 1$. In terms of the vectors $\hat{\omega}^a$, m^a, $\bar{m}^a$, the Kronecker delta and the projection

operator h^a_b can be expressed as follows:

$$\begin{aligned} \delta^a_b &= \hat{\omega}_b\,\hat{\omega}^a + m_b\,\bar{m}^a + \bar{m}_b\,m^a \\ \Rightarrow h^a_b &= m_b\,\bar{m}^a + \bar{m}_b\,m^a \end{aligned}$$

The projected strain tensor $(\partial_b\,\hat{\omega}_a)_\perp$ given by Eq. (G.6) evaluates to:

$$\begin{aligned} (\partial_b\,\hat{\omega}_a)_\perp &= \left(m_b\,\bar{m}^d + \bar{m}_b\,m^d\right)\,\partial_d\,\hat{\omega}_c\,\left(m_a\,\bar{m}^c + \bar{m}_a\,m^c\right) \\ &= m_b\left(\bar{m}^d\,\partial_d\,\hat{\omega}_c\,m^c\right)\bar{m}_a + \bar{m}_b\left(m^d\,\partial_d\hat{\omega}_c\,\bar{m}^c\right)m_a + \\ &\quad\; m_b\left(\bar{m}^d\,\partial_d\,\hat{\omega}_c\,\bar{m}^c\right)m_a + \bar{m}_b\left(m^d\,\partial_d\hat{\omega}_c\,m^c\right)\bar{m}_a \\ (\partial_b\,\hat{\omega}_a)_\perp &= \rho\,m_b\,\bar{m}_a + \bar{\rho}\,\bar{m}_b\,m_a + \bar{\sigma}\,m_b\,m_a + \sigma\,\bar{m}_b\,\bar{m}_a \end{aligned} \tag{G.7}$$

where ρ and σ are complex scalars defined so that the last equality holds.

The scalars ρ and σ encode the rotation, dilation and shear of the strain tensor in the following way.

Dilation	$\mathrm{Re}\{\rho\}$	$(=\frac{1}{2}\nabla\cdot\hat{\omega})$
Rotation	$\mathrm{Im}\{\rho\}$	$(=\pm\frac{1}{2}\,\hat{\omega}\cdot(\nabla\times\hat{\omega})$, calculation at the end)
Shear (asymmetry)	$\lvert\sigma\rvert$	(gives asymmetry in stretching of principal axes)
Shear (orientation)	$\arg(\sigma)$	(gives orientation of principal axes)

Table G.1: Expresssions for the optical scalars of a unit vector field)

Now, we are ready to calculate the twist of $\hat{\omega}$ given by Eq. (G.4).

We begin by expressing $\hat{n}$ and $\hat{n}_\perp$ in terms of m^a and $\bar{m}^a$:

$$\begin{aligned} \hat{n}^a &= \hat{x}^a\cos\phi + \hat{y}^a\sin\phi = \sqrt{2}\,\mathrm{Re}\{m^a\mathrm{e}^{-i\phi}\} \\ \hat{n}^a_\perp &= -\hat{x}^a\sin\phi + \hat{y}^a\cos\phi = \sqrt{2}\,\mathrm{Im}\{m^a\mathrm{e}^{-i\phi}\} \end{aligned}$$

We find that the twist given by Eq. (G.5) evaluates (detailed calculation given at the end) to:

$$\begin{aligned}\mathrm{Tw} &= \frac{1}{2\pi}\,\hat{n}^b\,(\partial_b\hat{\omega}_a)_\perp\,\hat{n}^a_\perp \\ &= \frac{1}{2\pi}\mathrm{Im}\{\rho + \mathrm{e}^{-2i\phi}\sigma\} \\ &= \frac{1}{2\pi}\left(\pm\frac{1}{2}\hat{\omega}\cdot(\nabla\times\hat{\omega}) + \mathrm{Im}\{\mathrm{e}^{-2i\phi}\sigma\}\right)\end{aligned} \tag{G.8}$$

Therefore the twist averaged over all ϕ, i.e. all directions of $\hat{n}$, is given by Eq. (G.2) as:

$$\boxed{\langle\mathrm{Tw}\rangle = \pm\frac{1}{4\pi}\,\hat{\omega}\cdot(\nabla\times\hat{\omega})} \tag{G.9}$$

G.3 Detailed calculations

a. Show that $\mathrm{Im}\{\rho\} = \pm\frac{1}{2}\,\hat{\omega}\cdot(\nabla\times\hat{\omega})$.

We begin by evaluating the asymmetric part of the projected strain tensor $(\partial_b\hat{\omega}_a - \partial_a\hat{\omega}_b)_\perp$ in terms of ρ using Eq. (G.7) and in terms of $\hat{\omega}$ using Eq. (G.6).

(i) Using Eq. (G.7),

$$(\partial_b\hat{\omega}_a - \partial_a\hat{\omega}_b)_\perp = (\rho - \bar{\rho})\,(m_b\,\bar{m}_a - \bar{m}_b\,m_a) \tag{G.10}$$

(ii) We can also evaluate $(\partial_b\hat{\omega}_a - \partial_a\hat{\omega}_b)_\perp$ by using Eq. (G.6), to give:

$$
\begin{aligned}
\left(\partial_b\hat{\omega}_a - \partial_a\hat{\omega}_b\right)_\perp &= \left(\delta_b^d - \hat{\omega}_b\,\hat{\omega}^d\right)\,\partial_d\hat{\omega}_c\,\left(\delta_a^c - \hat{\omega}_a\,\hat{\omega}^c\right) - (a \leftrightarrow b) \\
&= \left(\delta_b^d - \hat{\omega}_b\,\hat{\omega}^d\right)\,\partial_d\hat{\omega}_a - (a \leftrightarrow b) \\
&= \partial_b\hat{\omega}_a - \hat{\omega}_b\,(\hat{\omega}\cdot\nabla)\,\hat{\omega}_a - (a \leftrightarrow b) \\
&= \left(\partial_b\hat{\omega}_a - \partial_a\hat{\omega}_b\right) - \left(\hat{\omega}_b\,(\hat{\omega}\cdot\nabla)\,\hat{\omega}_a - \hat{\omega}_a\,(\hat{\omega}\cdot\nabla)\,\hat{\omega}_b\right) \\
&= \partial_i\omega_j\left(\delta_b^i\,\delta_a^j - \delta_b^j\delta_a^i\right) - \hat{\omega}_i\,(\hat{\omega}\cdot\nabla)\,\hat{\omega}_j\left(\delta_b^i\,\delta_a^j - \delta_b^j\delta_a^i\right) \\
&= \left(\delta_b^i\,\delta_a^j - \delta_b^j\delta_a^i\right)\left(\partial_i\omega_j - \hat{\omega}_i\,(\hat{\omega}\cdot\nabla)\,\hat{\omega}_j\right) \\
&= \epsilon_{bak}\,\epsilon_{ijk}\left(\partial_i\omega_j - \hat{\omega}_i\,(\hat{\omega}\cdot\nabla)\,\hat{\omega}_j\right) \\
&= \epsilon_{bak}\left(\nabla\times\hat{\omega} - \hat{\omega}\times(\hat{\omega}\cdot\nabla)\,\hat{\omega}\right)_k
\end{aligned}
\tag{G.11}
$$

We now contract the asymmetric projected strain tensor $\left(\partial_b\hat{\omega}_a - \partial_a\hat{\omega}_b\right)_\perp$ with itself, using the above results: Eq. (G.10) and Eq. (G.11).

(i) Using Eq. (G.10),

$$
\begin{aligned}
&\left(\partial_b\hat{\omega}_a - \partial_a\hat{\omega}_b\right)_\perp\left(\partial^b\hat{\omega}^a - \partial^a\hat{\omega}^b\right)_\perp \\
&\qquad = (\rho-\bar{\rho})^2\,(m_b\,\bar{m}_a - \bar{m}_b\,m_a)\left(m^b\,\bar{m}^a - \bar{m}^b\,m^a\right) \\
&\qquad = -2\,(\rho-\bar{\rho})^2
\end{aligned}
\tag{G.12}
$$

(ii) Using Eq. (G.11),

$$
\begin{aligned}
&\left(\partial_b\hat{\omega}_a - \partial_a\hat{\omega}_b\right)_\perp \left(\partial^b\hat{\omega}^a - \partial^a\hat{\omega}^b\right)_\perp \\
&\qquad = \epsilon_{bak}\epsilon^{bal}\left(\nabla\times\hat{\omega} - \hat{\omega}\times\left(\hat{\omega}\cdot\nabla\right)\hat{\omega}\right)_k \left(\nabla\times\hat{\omega} - \hat{\omega}\times\left(\hat{\omega}\cdot\nabla\right)\hat{\omega}\right)_l \\
&\qquad = 2\delta^l_k\left(\nabla\times\hat{\omega} - \hat{\omega}\times\left(\hat{\omega}\cdot\nabla\right)\hat{\omega}\right)_k \left(\nabla\times\hat{\omega} - \hat{\omega}\times\left(\hat{\omega}\cdot\nabla\right)\hat{\omega}\right)_l \\
&\qquad = 2\left(\nabla\times\hat{\omega} - \hat{\omega}\times\left(\hat{\omega}\cdot\nabla\right)\hat{\omega}\right)\cdot\left(\nabla\times\hat{\omega} - \hat{\omega}\times\left(\hat{\omega}\cdot\nabla\right)\hat{\omega}\right) \\
&\qquad = 2\Big(\left(\nabla\times\hat{\omega}\right)\cdot\left(\nabla\times\hat{\omega}\right) - 2\left(\nabla\times\hat{\omega}\right)\cdot\left(\hat{\omega}\times\left(\hat{\omega}\cdot\nabla\right)\hat{\omega}\right) \\
&\qquad\qquad\qquad + \left(\hat{\omega}\times\left(\hat{\omega}\cdot\nabla\right)\hat{\omega}\right)\cdot\left(\hat{\omega}\times\left(\hat{\omega}\cdot\nabla\right)\hat{\omega}\right)\Big) \\
&\qquad = 2\Big(\left(\nabla\times\hat{\omega}\right)\cdot\left(\nabla\times\hat{\omega}\right) - 2\left(\left(\nabla\times\hat{\omega}\right)\times\hat{\omega}\right)\cdot\left(\left(\hat{\omega}\cdot\nabla\right)\hat{\omega}\right) \\
&\qquad\qquad\qquad + \left(\left(\hat{\omega}\cdot\nabla\right)\hat{\omega}\right)\cdot\left(\left(\hat{\omega}\cdot\nabla\right)\hat{\omega}\right)\Big) \qquad (\because \hat{\omega} \text{ is a unit vector}) \\
&\qquad = 2\Big(\left(\nabla\times\hat{\omega}\right)\cdot\left(\nabla\times\hat{\omega}\right) - 2\left(\left(\hat{\omega}\cdot\nabla\right)\hat{\omega}\right)\cdot\left(\left(\hat{\omega}\cdot\nabla\right)\hat{\omega}\right) \\
&\qquad\qquad\qquad + \left(\left(\hat{\omega}\cdot\nabla\right)\hat{\omega}\right)\cdot\left(\left(\hat{\omega}\cdot\nabla\right)\hat{\omega}\right)\Big) \quad (\because \nabla\left(\hat{\omega}\cdot\hat{\omega}\right) = 0) \\
&\qquad = 2\Big(\left(\nabla\times\hat{\omega}\right)\cdot\left(\nabla\times\hat{\omega}\right) - \left(\left(\hat{\omega}\cdot\nabla\right)\hat{\omega}\right)\cdot\left(\left(\hat{\omega}\cdot\nabla\right)\hat{\omega}\right)\Big) \\
&\qquad = 2\Big(\left(\nabla\times\hat{\omega}\right)\cdot\left(\nabla\times\hat{\omega}\right) - \left(\left(\nabla\times\hat{\omega}\right)\times\hat{\omega}\right)\cdot\left(\left(\nabla\times\hat{\omega}\right)\times\hat{\omega}\right)\Big) \\
&\qquad\qquad\qquad\qquad\qquad\qquad (\because \nabla\left(\hat{\omega}\cdot\hat{\omega}\right) = 0) \\
&\qquad = 2\Big(\left(\nabla\times\hat{\omega}\right)\cdot\hat{\omega}\Big)^2 \qquad\qquad\qquad\qquad\qquad\qquad (G.13)
\end{aligned}
$$

From Eq. (G.12) and Eq. (G.13), we have

$$
\begin{aligned}
2\left(\left(\nabla\times\hat{\omega}\right)\cdot\hat{\omega}\right)^2 &= -2\left(\rho-\bar{\rho}\right)^2 \\
\Rightarrow \left(\left(\nabla\times\hat{\omega}\right)\cdot\hat{\omega}\right)^2 &= -\left(\rho-\bar{\rho}\right)^2 \\
\Rightarrow \left(\left(\nabla\times\hat{\omega}\right)\cdot\hat{\omega}\right)^2 &= 4\left(\frac{\rho-\bar{\rho}}{2\,i}\right)^2 \\
\Rightarrow \left(\left(\nabla\times\hat{\omega}\right)\cdot\hat{\omega}\right) &= \pm 2\,\mathrm{Im}\{\rho\} \qquad\qquad (G.14)
\end{aligned}
$$

b. Show that $\mathrm{Tw} = \frac{1}{2\pi}\mathrm{Im}\{\rho + \mathrm{e}^{-2i\phi}\sigma\}$. From Eq. (G.5), the twist is given by $\mathrm{Tw} = \frac{1}{2\pi}\,\hat{n}^b\,(\partial_b\hat{\omega}_a)_\perp\;\hat{n}^a_\perp$. We begin by calculating $\hat{n}^b\,(\partial_b\hat{\omega}_a)_\perp$ as follows:

$$\begin{aligned}
\hat{n}^b\,(\partial_b\hat{\omega}_a)_\perp &= \sqrt{2}\,\mathrm{Re}\{m^b\,\mathrm{e}^{-i\phi}\}\,(\rho\,m_b\,\bar{m}_a + \bar{\rho}\,\bar{m}_b\,m_a + \bar{\sigma}\,m_b\,m_a + \sigma\,\bar{m}_b\,\bar{m}_a)\\
&= \frac{1}{\sqrt{2}}\left(m^b\,\mathrm{e}^{-i\phi} + \bar{m}^b\,\mathrm{e}^{+i\phi}\right)(\rho\,m_b\,\bar{m}_a + \bar{\rho}\,\bar{m}_b\,m_a + \bar{\sigma}\,m_b\,m_a + \sigma\,\bar{m}_b\,\bar{m}_a)\\
&= \frac{1}{\sqrt{2}}\left(\mathrm{e}^{-i\phi}\,(\bar{\rho}\,m_a + \sigma\,\bar{m}_a) + \mathrm{e}^{+i\phi}\,(\rho\,\bar{m}_a + \bar{\sigma}\,m_a)\right)
\end{aligned}$$

$$\begin{aligned}
\Rightarrow \hat{n}^b\,(\partial_b\hat{\omega}_a)_\perp &= \frac{1}{\sqrt{2}}\left(m_a\left(\bar{\rho}\,\mathrm{e}^{-i\phi} + \bar{\sigma}\,\mathrm{e}^{+i\phi}\right) + \bar{m}_a\left(\rho\,\mathrm{e}^{+i\phi} + \sigma\,\mathrm{e}^{-i\phi}\right)\right)\\
&= \sqrt{2}\,\mathrm{Re}\left\{m_a\left(\bar{\rho}\,\mathrm{e}^{-i\phi} + \bar{\sigma}\,\mathrm{e}^{+i\phi}\right)\right\}\\
&= \sqrt{2}\,\mathrm{Re}\left\{m_a\,\mathrm{e}^{-i\phi}\left(\bar{\rho} + \bar{\sigma}\,\mathrm{e}^{+2i\phi}\right)\right\}\\
&= \sqrt{2}\left(\mathrm{Re}\left\{m_a\,\mathrm{e}^{-i\phi}\right\}\,\mathrm{Re}\left\{\bar{\rho} + \bar{\sigma}\,\mathrm{e}^{+2i\phi}\right\} - \mathrm{Im}\left\{m_a\,\mathrm{e}^{-i\phi}\right\}\,\mathrm{Im}\left\{\bar{\rho} + \bar{\sigma}\,\mathrm{e}^{+2i\phi}\right\}\right)\\
&= \sqrt{2}\left(\mathrm{Re}\left\{m_a\,\mathrm{e}^{-i\phi}\right\}\,\mathrm{Re}\left\{\bar{\rho} + \bar{\sigma}\,\mathrm{e}^{+2i\phi}\right\} + \mathrm{Im}\left\{m_a\,\mathrm{e}^{-i\phi}\right\}\,\mathrm{Im}\left\{\rho + \sigma\,\mathrm{e}^{-2i\phi}\right\}\right)\\
&= \hat{n}_a\,\mathrm{Re}\left\{\bar{\rho} + \bar{\sigma}\,\mathrm{e}^{+2i\phi}\right\} + \hat{n}^\perp_a\,\mathrm{Im}\left\{\rho + \sigma\,\mathrm{e}^{-2i\phi}\right\}
\end{aligned}$$

Therefore the twist given by Eq. (G.5) is:

$$\begin{aligned}
\mathrm{Tw} &= \frac{1}{2\pi}\,\hat{n}^b\,(\partial_b\hat{\omega}_a)_\perp\;\hat{n}^a_\perp\\
&= \frac{1}{2\pi}\,\left(\hat{n}_a\,\mathrm{Re}\left\{\bar{\rho} + \bar{\sigma}\,\mathrm{e}^{+2i\phi}\right\} + \hat{n}^\perp_a\,\mathrm{Im}\left\{\rho + \sigma\,\mathrm{e}^{-2i\phi}\right\}\right)\,\hat{n}^a_\perp\\
&= \frac{1}{2\pi}\,\mathrm{Im}\left\{\rho + \sigma\,\mathrm{e}^{-2i\phi}\right\}\\
&= \frac{1}{2\pi}\,\left(\mathrm{Im}\,\{\rho\} + \mathrm{Im}\left\{\sigma\,\mathrm{e}^{-2i\phi}\right\}\right)\\
&= \frac{1}{2\pi}\,\left(\pm\,\tfrac{1}{2}\,\hat{\omega}\cdot(\nabla\times\hat{\omega}) + \mathrm{Im}\left\{\sigma\,\mathrm{e}^{-2i\phi}\right\}\right) \qquad (\text{ as in Eq. (G.8)})
\end{aligned}$$

REFERENCES

[1] Michael Faraday. *On Lines of Magnetic Force: Their Definite Character and Their Distribution Within a Magnet and Through Space*. Royal Society, 1852.

[2] H. Helmholtz. Uber Integrale der hydrodynamischen Gleichungen, welche den Wirbelbewegungen entsprechen. *J. Reine Angew. Math.*, 55:25–55, 1858.

[3] F. C. Frank. I. Liquid crystals. On the theory of liquid crystals. *Discuss. Faraday Soc.*, 25(0):19–28, January 1958.

[4] W. M. Lomer. Defects in pure metals. *Progress in Metal Physics*, 8:255–320, 1959.

[5] N. D. Mermin. The topological theory of defects in ordered media. *Rev. Mod. Phys.*, 51(3):591–648, July 1979.

[6] Carl Friedrich Gauss. Allgemeine Theorie des Erdmagnetismus. In *Werke*, pages 119–193. Springer Berlin Heidelberg, 1877. DOI: 10.1007/978-3-642-49319-5_5.

[7] David Finkelstein and Charles W Misner. Some new conservation laws. *Annals of Physics*, 6(3):230–243, March 1959.

[8] L. Woltjer. A THEOREM ON FORCE-FREE MAGNETIC FIELDS. *Proceedings of the National Academy of Sciences of the United States of America*, 44(6):489, June 1958.

[9] H. K. Moffatt. The degree of knottedness of tangled vortex lines. *Journal of Fluid Mechanics*, 35(01):117–129, 1969.

[10] Michael Faraday. *On the magnetization of light and the illumination of magnetic lines of force*. Royal Society, 1846.

[11] Michael Faraday. XLIX. Experimental researches in electricity.Nineteenth series. *The London, Edinburgh, and Dublin Philosophical Magazine and Journal of Science*, 28(187):294–317, 1846.

[12] Michael Faraday. LVIII. On the physical character of the lines of magnetic force. *The London, Edinburgh, and Dublin Philosophical Magazine and Journal of Science*, 3(20):401–428, 1852.

[13] James Clerk Maxwell. Xxv. on physical lines of force: Part i.the theory of molecular vortices applied to magnetic phenomena. *The London, Edinburgh, and Dublin Philosophical Magazine and Journal of Science*, 21(139):161–175, 1861.

[14] J. Clerk Maxwell. On Faraday's lines of force. *Transactions of the Cambridge Philosophical Society*, 10:27, 1864.

[15] J. Clerk Maxwell. A dynamical theory of the electromagnetic field. *Philosophical transactions of the Royal Society of London*, 155:459–512, 1865.

[16] James Clerk Maxwell. *A treatise on electricity and magnetism*, volume 1. Clarendon press, 1881.

[17] C.-h Liu, S. R. Nagel, D. A. Schecter, S. N. Coppersmith, S. Majumdar, O. Narayan, and T. A. Witten. Force Fluctuations in Bead Packs. *Science*, 269(5223):513–515, July 1995.

[18] Chu-heng Liu and Sidney R. Nagel. Sound in sand. *Phys. Rev. Lett.*, 68(15):2301–2304, April 1992.

[19] Chu-heng Liu and Sidney R. Nagel. Sound in a granular material: Disorder and nonlinearity. *Phys. Rev. B*, 48(21):15646–15650, December 1993.

[20] G. I. Taylor. The Mechanism of Plastic Deformation of Crystals. Part I. Theoretical. *Proceedings of the Royal Society of London A: Mathematical, Physical and Engineering Sciences*, 145(855):362–387, July 1934.

[21] David R. Nelson. Order, frustration, and defects in liquids and glasses. *Phys. Rev. B*, 28(10):5515–5535, November 1983.

[22] J. L. Ericksen. Conservation Laws for Liquid Crystals. *Transactions of the Society of Rheology*, 5(1):23–34, March 1961.

[23] H. Alfven. Existence of Electromagnetic-Hydrodynamic Waves. *Nature*, 150:405–406, October 1942.

[24] William A Newcomb. Motion of magnetic lines of force. *Annals of Physics*, 3(4):347–385, April 1958.

[25] William Thomson Baron Kelvin. *On vortex motion*. Royal Society of Edinburgh, 1869.

[26] Antonio F. Ranada. A topological theory of the electromagnetic field. *Lett. Math. Phys.*, 18(2):97–106, August 1989.

[27] William T M Irvine and Dirk Bouwmeester. Linked and knotted beams of light. *Nature Physics*, 4:716–720, 2008. bibtex: Irvine2008.

[28] Joseph Avron. A Topological Look at the Quantum Hall Effect. *Physics Today*, 56(8):38–42, August 2003.

[29] Xiao-Liang Qi and Shou-Cheng Zhang. Topological insulators and superconductors. *Rev. Mod. Phys.*, 83(4):1057–1110, October 2011.

[30] M. Z. Hasan and C. L. Kane. Colloquium. *Rev. Mod. Phys.*, 82(4):3045–3067, November 2010.

[31] C. L. Kane and T. C. Lubensky. Topological boundary modes in isostatic lattices. *Nat Phys*, 10(1):39–45, January 2014.

[32] Lisa M. Nash, Dustin Kleckner, Alismari Read, Vincenzo Vitelli, Ari M. Turner, and William T. M. Irvine. Topological mechanics of gyroscopic metamaterials. *PNAS*, 112(47):14495–14500, November 2015.

[33] Roman Ssstrunk and Sebastian D. Huber. Classification of topological phonons in linear mechanical metamaterials. *PNAS*, 113(33):E4767–E4775, August 2016.

[34] H.-R. Trebin. The topology of non-uniform media in condensed matter physics. *Advances in Physics*, 31(3):195–254, June 1982.

[35] Mikhail V. Kurik and O. D. Lavrentovich. Defects in liquid crystals: homotopy theory and experimental studies. *Sov. Phys. Usp.*, 31(3):196, 1988.

[36] Holger Stark. Physics of colloidal dispersions in nematic liquid crystals. *Physics Reports*, 351(6):387–474, October 2001.

[37] Gareth P. Alexander, Bryan Gin-ge Chen, Elisabetta A. Matsumoto, and Randall D. Kamien. Colloquium: Disclination loops, point defects, and all that in nematic liquid crystals. *Rev. Mod. Phys.*, 84(2):497–514, April 2012.

[38] Mark R. Dennis, Robert P. King, Barry Jack, Kevin O'Holleran, and Miles J. Padgett. Isolated optical vortex knots. *Nat. Phys.*, 6(2):118–121, February 2010.

[39] Robert Paul King. *Knotting of optical vortices*. Ph.D. Thesis, University of Southampton, September 2010.

[40] J. J. Moreau. Constantes dun ilot tourbillonnaire en fluide parfait barotrope. *C.R. Acad. Sci. Paris*, 252:2810–2812, 1961.

[41] S. Chandrasekhar and L. Woltjer. On Force-Free Magnetic Fields. *PNAS*, 44, April 1958.

[42] S Chandrasekhar and PC Kendall. On force-free magnetic fields. *Proc. Nat. Acad. Sci.*, 42(1):1–5, 1956.

[43] Vladimir I. Arnold. The asymptotic Hopf invariant and its applications. In Alexander B. Givental, Boris A. Khesin, Alexander N. Varchenko, Victor A. Vassiliev, and Oleg Ya Viro, editors, *Vladimir I. Arnold - Collected Works*, number 2 in Vladimir I. Arnold - Collected Works, pages 357–375. Springer Berlin Heidelberg, 1974. DOI: 10.1007/978-3-642-31031-7_32.

[44] Dustin Kleckner and William T. M. Irvine. Creation and dynamics of knotted vortices. *Nat. Phys.*, 9(4):253–258, April 2013.

[45] Uros Tkalec, Miha Ravnik, Simon Copar, Slobodan Zumer, and Igor Musevic. Reconfigurable Knots and Links in Chiral Nematic Colloids. *Science*, 333(6038):62–65, July 2011.

[46] P. G. Tait. On links. In *Proc. Roy. Soc. Edinburgh*, volume 9, pages 321–332, 1875.

[47] Peter Guthrie Tait. On knots. *Trans. Roy. Soc. Edinburgh*, 28:145–190, 1877.

[48] Peter Guthrie Tait. *On knots:[Part II]*. Oliver & Boyd, 1885.

[49] H. Keith Moffatt. Helicity and singular structures in fluid dynamics. *PNAS*, 111(10):3663–3670, March 2014.

[50] H. K. Moffatt. *Magnetic field generation in electrically conducting fluids*. Cambridge University Press, 1978.

[51] A. Pouquet, U. Frisch, and J. Lorat. Strong MHD helical turbulence and the nonlinear dynamo effect. *J. Fluid Mech.*, 77(02):321–354, September 1976.

[52] B. C. Low. Magnetohydrodynamic processes in the solar corona: Flares, coronal mass ejections, and magnetic helicity*. *Phys. Plasmas*, 1(5):1684–1690, May 1994.

[53] J. B. Taylor. Relaxation and magnetic reconnection in plasmas. *Rev. Mod. Phys.*, 58(3):741–763, July 1986.

[54] Mitchell A. Berger. Rigorous new limits on magnetic helicity dissipation in the solar corona. *Geophys. Astrophys. Fluid Dyn.*, 30(1-2):79–104, September 1984.

[55] Jonathan Braithwaite and Hendrik C. Spruit. A fossil origin for the magnetic field in A stars and white dwarfs. *Nature*, 431(7010):819–821, October 2004.

[56] Martin W. Scheeler, Dustin Kleckner, Davide Proment, Gordon L. Kindlmann, and William T. M. Irvine. Helicity conservation by flow across scales in reconnecting vortex links and knots. *PNAS*, 111(43):15350–15355, October 2014.

[57] Y. Kimura and H. K. Moffatt. Reconnection of skewed vortices. *J. Fluid Mech.*, 751:329–345, July 2014.

[58] Hridesh Kedia, David Foster, Mark R. Dennis, and William T.M. Irvine. Weaving Knotted Vector Fields with Tunable Helicity. *Phys. Rev. Lett.*, 117(27):274501, December 2016.

[59] Hridesh Kedia, Iwo Bialynicki-Birula, Daniel Peralta-Salas, and William T. M. Irvine. Tying Knots in Light Fields. *Phys. Rev. Lett.*, 111(15):150404, October 2013.

[60] Hridesh Kedia, Daniel Peralta-Salas, and William T. M. Irvine. Flow of light. *(in preparation)*, 2017.

[61] Hridesh Kedia, Dustin Kleckner, Martin W. Scheeler, and William T. M. Irvine. Helicity in superfluids: conservation and the classical limit. *(in preparation)*, 2017.

[62] Alberto Enciso and Daniel Peralta-Salas. Knots and links in steady solutions of the Euler equation. *Annals of Mathematics*, 175(1):345–367, January 2012.

[63] Carlo F. Barenghi. Knots and Unknots in Superfluid Turbulence. *Milan J. Math.*, 75(1):177–196, May 2007.

[64] Yuki Kawaguchi, Muneto Nitta, and Masahito Ueda. Knots in a Spinor Bose-Einstein Condensate. *Phys. Rev. Lett.*, 100(18):180403, May 2008.

[65] D. S. Hall, M. W. Ray, K. Tiurev, E. Ruokokoski, A. H. Gheorghe, and M. Mttnen. Tying quantum knots. *Nat Phys*, 12(5):478–483, May 2016.

[66] Dustin Kleckner, Louis H. Kauffman, and William T. M. Irvine. How superfluid vortex knots untie. *Nat. Phys.*, 12(7):650–655, July 2016.

[67] A. M. Kamchatnov. Topological solitons in magnetohydrodynamics. *Sov. Phys. JETP*, 55(1):69, 1982.

[68] H. K. Moffatt. Magnetostatic equilibria and analogous Euler flows of arbitrarily complex topology. Part 1. Fundamentals. *J. Fluid Mech.*, 159:359–378, October 1985.

[69] A. Y. K. Chui and H. K. Moffatt. The Energy and Helicity of Knotted Magnetic Flux Tubes. *Proc. R. Soc. A*, 451(1943):609–629, December 1995.

[70] William T M Irvine. Linked and knotted beams of light, conservation of helicity and the flow of null electromagnetic fields. *Journal of Physics A: Mathematical and Theoretical*, 43:385203 1–9, 2010. bibtex: Irvine2010.

[71] Manuel Arrayas and Jose L. Trueba. A class of non-null toroidal electromagnetic fields and its relation to the model of electromagnetic knots. *J. Phys. A: Math. Theor.*, 48(2):025203, 2015.

[72] Amy Thompson, Joe Swearngin, Alexander Wickes, and Dirk Bouwmeester. Constructing a class of topological solitons in magnetohydrodynamics. *Phys. Rev. E*, 89(4):043104, April 2014.

[73] C. B. Smiet, S. Candelaresi, A. Thompson, J. Swearngin, J. W. Dalhuisen, and D. Bouwmeester. Self-Organizing Knotted Magnetic Structures in Plasma. *Phys. Rev. Lett.*, 115(9):095001, August 2015.

[74] Antonio F. Ranada, Mario Soler, and Jos L. Trueba. Ball lightning as a force-free magnetic knot. *Phys. Rev. E*, 62(5):7181–7190, November 2000.

[75] Thomas Machon and Gareth P. Alexander. Knots and nonorientable surfaces in chiral nematics. *PNAS*, 110(35):14174–14179, August 2013.

[76] Angel Martinez, Miha Ravnik, Brice Lucero, Rayshan Visvanathan, Slobodan Zumer, and Ivan I. Smalyukh. Mutually tangled colloidal knots and induced defect loops in nematic fields. *Nat. Mat.*, 13(3):258–263, March 2014.

[77] M. V. Berry and M. R. Dennis. Phase singularities in isotropic random waves. *Proc. R. Soc. A*, 456(2001):2059–2079, September 2000.

[78] L. Faddeev and Antti J. Niemi. Stable knot-like structures in classical field theory. *Nature*, 387(6628):58–61, May 1997.

[79] Richard A. Battye and Paul M. Sutcliffe. Solitons, links and knots. *Proceedings of the Royal Society of London A: Mathematical, Physical and Engineering Sciences*, 455(1992):4305–4331, December 1999.

[80] Egor Babaev, Ludvig D. Faddeev, and Antti J. Niemi. Hidden symmetry and knot solitons in a charged two-condensate Bose system. *Phys. Rev. B*, 65(10):100512, February 2002.

[81] Paul Sutcliffe. Knots in the SkyrmeFaddeev model. *Proceedings of the Royal Society of London A: Mathematical, Physical and Engineering Sciences*, 463(2087):3001–3020, November 2007.

[82] Alexander J. Taylor and Mark R. Dennis. Vortex knots in tangled quantum eigenfunctions. *Nature Communications*, 7:12346, July 2016.

[83] Egor Babaev. Dual Neutral Variables and Knot Solitons in Triplet Superconductors. *Phys. Rev. Lett.*, 88(17):177002, April 2002.

[84] Egor Babaev. Non-Meissner electrodynamics and knotted solitons in two-component superconductors. *Phys. Rev. B*, 79(10):104506, March 2009.

[85] William Thomson. On Vortex Atoms. *Proceedings of the Royal Society of Edinburgh*, 6:94–105, 1869.

[86] Romain Monchaux, Michael Berhanu, Sbastien Aumatre, Arnaud Chiffaudel, Franois Daviaud, Brengre Dubrulle, Florent Ravelet, Stephan Fauve, Nicolas Mordant, Franois Ptrlis, Mickael Bourgoin, Philippe Odier, Jean-Franois Pinton, Nicolas Plihon, and Romain Volk. The von Krmn Sodium experiment: Turbulent dynamical dynamos. *Phys. Fluids*, 21(3):035108, March 2009.

[87] M. Steenbeck, F. Krause, and K.-H. Rdler. Berechnung der mittleren Lorentz-Feldstrke fr ein elektrisch leitendes Medium in turbulenter, durch Coriolis-Krfte beeinfluter Bewegung. *Z. Naturforsch. A Phys. Sci.*, 21(4):369–376, 2014.

[88] Michael H. Freedman. A note on topology and magnetic energy in incompressible perfectly conducting fluids. *J. Fluid Mech.*, 194:549–551, September 1988.

[89] H. K. Moffatt. Magnetic relaxation and the Taylor conjecture. *Journal of Plasma Physics*, 81(6), December 2015.

[90] Michael M. Rogers and Parviz Moin. Helicity fluctuations in incompressible turbulent flows. *Physics of Fluids (1958-1988)*, 30(9):2662–2671, 1987.

[91] James M. Wallace, Jean-Louis Balint, and Lawrence Ong. An experimental study of helicity density in turbulent flows. *Phys. Fluids A: Fluid Dyn.*, 4(9):2013–2026, September 1992.

[92] H. K. Moffatt. The energy spectrum of knots and links. *Nature*, 347(6291):367–369, September 1990.

[93] Vsevolod Katritch, Jan Bednar, Didier Michoud, Robert G. Scharein, Jacques Dubochet, and Andrzej Stasiak. Geometry and physics of knots. *Nature*, 384(6605):142–145, November 1996.

[94] P. Pieranski and S. Przybyl. Ideal trefoil knot. *Phys. Rev. E*, 64(3):031801, August 2001.

[95] Roman V. Buniy and Thomas W. Kephart. A model of glueballs. *Physics Letters B*, 576(12):127–134, December 2003.

[96] Roman V. Buniy and Thomas W. Kephart. Glueballs and the universal energy spectrum of tight knots and links. *Int. J. Mod. Phys. A*, 20(06):1252–1259, March 2005.

[97] Roman V. Buniy, Jason Cantarella, Thomas W. Kephart, and Eric J. Rawdon. Tight knot spectrum in QCD. *Phys. Rev. D*, 89(5):054513, March 2014.

[98] H. K. Moffatt. Helicity and celestial magnetism. *Proc. R. Soc. A*, 472(2190):20160183, June 2016.

[99] S. R. Hudson, E. Startsev, and E. Feibush. A new class of magnetic confinement device in the shape of a knot. *Physics of Plasmas (1994-present)*, 21(1):010705, January 2014.

[100] J. Milnor. *Singular Points of Complex Hypersurfaces.* Annals of Mathematics Studies. Princeton University Press, 1969.

[101] Karl Brauner. Das verhalten der funktionen in der umgebung ihrer verzweigungsstellen. *Abh.Math.Semin.Univ.Hambg.*, 6(1):1–55, 1928.

[102] B. Perron. Le noeud huit est algebrique rel. *Inv. Math.*, 65(3):441–451, 1982.

[103] A. J. Taylor and M. R. Dennis. Geometry and scaling of tangled vortex lines in three-dimensional random wave fields. *J. Phys. A: Math. Theor.*, 47(46):465101, 2014.

[104] David W. Lyons. An Elementary Introduction to the Hopf Fibration. *Math. Magazine*, 76(2):87–98, 2003.

[105] H. K. Urbantke. The Hopf fibrationseven times in physics. *J. Geom. Phys.*, 46(2):125–150, May 2003.

[106] Rmy Mosseri and Jean-Francois Sadoc. Hopf fibrations and frustrated matter. *Struct. Chem.*, 23(4):1071–1078, May 2012.

[107] J. F. Sadoc and J. Charvolin. 3-sphere fibrations: a tool for analyzing twisted materials in condensed matter. *J. Phys. A: Math. Theor.*, 42(46):465209, 2009.

[108] Benjamin Bode, Mark R. Dennis, David Foster, and Robert P. King. Knotted fields and explicit fibrations for lemniscate knots. *arXiv:1611.02563*, November 2016.

[109] Paul Jennings. Cabling in the SkyrmeFaddeev model. *J. Phys. A: Math. Theor.*, 48(31):315401, 2015.

[110] Mitchell A. Berger and George B. Field. The topological properties of magnetic helicity. *Journal of Fluid Mechanics*, 147:133–148, 1984.

[111] Conor J. Houghton, Nicholas S. Manton, and Paul M. Sutcliffe. Rational maps, monopoles and skyrmions. *Nucl. Phys. B*, 510(3):507–537, January 1998.

[112] David Stern. Geomagnetic Euler potentials. *J. Geophys. Res.*, 72(15):3995–4005, August 1967.

[113] David P. Stern. Euler Potentials. *American Journal of Physics*, 38(4):494–501, April 1970.

[114] M. Hesse and K. Schindler. A theoretical foundation of general magnetic reconnection. *J. Geophys. Res.*, 93(A6):5559–5567, June 1988.

[115] Krishan K. Khurana. Euler potential models of Jupiter's magnetospheric field. *J. Geophys. Res.*, 102(A6):11295–11306, June 1997.

[116] R. Rosner, B. C. Low, K. Tsinganos, and M. A. Berger. On the relationship between the topology of magnetic field lines and flux surfaces. *Geophys. Astrophys. Fluid Dyn.*, 48(4):251–271, November 1989.

[117] J. H. C. Whitehead. An Expression of Hopf's Invariant as an Integral. *PNAS*, 33(5):117–123, 1947.

[118] Lee Rudolph. Isolated critical points of mappings from R4 to R2 and a natural splitting of the Milnor number of a classical fibered link. Part I: Basic theory; examples. *Commentarii Mathematici Helvetici*, 62(1):630–645, 1987.

[119] R. S. Ward. Hopf solitons on S3 and 3. *Nonlinearity*, 12(2):241, March 1999.

[120] H. K. Moffatt. Some developments in the theory of turbulence. *J. Fluid Mech.*, 106:27–47, May 1981.

[121] RL Ricca and MA Berger. Topological ideas and fluid mechanics. *Physics Today*, 49(12):28–34, 1996.

[122] F. Y. Wu. Knot theory and statistical mechanics. *Rev. Mod. Phys.*, 64(4):1099–1131, 1992.

[123] Edward Witten. Quantum field theory and the Jones polynomial. *Commun. Math. Phys.*, 121(3):351–399, 1989.

[124] Ivan I Smalyukh, Yves Lansac, Noel A Clark, and Rahul P Trivedi. Three-dimensional structure and multistable optical switching of triple-twisted particle-like excitations in anisotropic fluids. *Nature Materials*, 9(2):139–145, 2010.

[125] A. F. Raada. Knotted solutions of the Maxwell equations in vacuum. *Journal of Physics A: Mathematical and General*, 23:L815–L820, 1990.

[126] Andrzej Trautman. Solutions of the Maxwell and Yang-Mills equations associated with hopf fibrings. *International Journal of Theoretical Physics*, 16(8):561–565, August 1977.

[127] A. F. Raada and J. L. Trueba. Electromagnetic knots. *Physics Letters A*, 202(July):337–342, 1995.

[128] Iwo Bialynicki-Birula. Electromagnetic vortex lines riding atop null solutions of the Maxwell equations. *Journal of Optics A: Pure and Applied Optics*, 6(5):S181–S183, May 2004.

[129] Harry Bateman. *The Mathematical Analysis of Electrical and Optical Wave-Motion*. Dover Publications Inc., 1915.

[130] Ivor Robinson. Null Electromagnetic Fields. *Journal of Mathematical Physics*, 2(3):290, 1961.

[131] R Penrose. Twistor algebra. *Journal of Mathematical Physics*, 345, 1967.

[132] Patrick Hogan. Bateman electromagnetic waves. *Proc. R. Soc. Lond. A*, 396(1810):199–204, 1984.

[133] Iwo Bialynicki-Birula. *\rmPhoton wave function in \em Progress in Optics*, volume XXXVI, ed. E. Wolf. Elsevier, Amsterdam, 1996.

[134] Shlomo Sternberg. On differential equations on the torus. *American Journal of Mathematics*, 79:397–402, 1957.

[135] Alberto Enciso and Daniel Peralta-Salas. Existence of knotted vortex tubes in steady Euler flows. *Acta Math.*, 214(1):61–134, 2015.

[136] Nicholas Manton and Paul M. Sutcliffe. *Topological solitons*. Cambridge University Press, 2004.

[137] H. Aratyn, L. A. Ferreira, and A. H. Zimerman. Exact Static Soliton Solutions of $(3+1)$-Dimensional Integrable Theory with Nonzero Hopf Numbers. *Phys. Rev. Lett.*, 83(9):1723–1726, August 1999.

[138] M. Arrays, D. Bouwmeester, and J. L. Trueba. Knots in electromagnetism. *Physics Reports*, 667:1–61, January 2017.

[139] Asher Peres. Null Electromagnetic Fields in General Relativity Theory. *Phys. Rev.*, 118(4):1105–1110, May 1960.

[140] Asher Peres. On geometrodynamics and null fields. *Annals of Physics*, 14(0):419 – 439, 1961.

[141] R. P. Geroch. Electromagnetism as an aspect of geometry?: Already unified field theoryThe null field case. *Annals of Physics*, 36(2):147 – 187, 1966.

[142] Carlos Hoyos, Nilanjan Sircar, and Jacob Sonnenschein. New knotted solutions of Maxwell's equations. *J. Phys. A: Math. Theor.*, 48(25):255204, 2015.

[143] Franco Bampi. The shear-free condition in Robinson's theorem. *General Relativity and Gravitation*, 9(9):779–782, 1978.

[144] Bartolom Coll and JoanJosep Ferrando. On the permanence of the null character of Maxwell fields. *General Relativity and Gravitation*, 20(1):51–64, 1988.

[145] Louis Mariot. Le champ lectromagntique singulier. *CR Acad. Sci. Paris*, 322(2):62543, 1954.

[146] Lev D. Landau and E. M. Lifshitz. *Fluid Mechanics*, volume 6 of *Landau and Lifshitz course of theoretical physics*. Elsevier, 2nd edition, 1987.

[147] Demetrios Christodoulou. The Euler Equations of Compressible Fluid Flow. *Bull. Amer. Math. Soc.*, 44(4):581–602, 2007.

[148] Peter Constantin. On the Euler equations of incompressible fluids. *Bull. Amer. Math. Soc.*, 44(4):603–621, 2007.

[149] T. Dombre, U. Frisch, J. M. Greene, M. Hnon, A. Mehr, and A. M. Soward. Chaotic streamlines in the ABC flows. *J. Fluid Mech.*, 167:353–391, June 1986.

[150] J. T. Beale, T. Kato, and A. Majda. Remarks on the breakdown of smooth solutions for the 3-D Euler equations. *Commun. Math. Phys.*, 94(1):61–66, March 1984.

[151] E. Levich and A. Tsinober. On the role of helical structures in three-dimensional turbulent flow. *Phys. Lett. A*, 93(6):293–297, January 1983.

[152] A. K. M. Fazle Hussain. Coherent structures and turbulence. *J. Fluid Mech.*, 173:303–356, December 1986.

[153] Nobumitsu Yokoi and Akira Yoshizawa. Statistical analysis of the effects of helicity in inhomogeneous turbulence. *Phys. Fluids A: Fluid Dyn.*, 5(2):464–477, February 1993.

[154] C. F. Barenghi, R. J. Donnelly, and W. F. Vinen, editors. *Quantized Vortex Dynamics and Superfluid Turbulence*. Springer Berlin Heidelberg, 2001.

[155] M. S. Paoletti, Michael E. Fisher, K. R. Sreenivasan, and D. P. Lathrop. Velocity Statistics Distinguish Quantum Turbulence from Classical Turbulence. *Phys. Rev. Lett.*, 101(15):154501, October 2008.

[156] W. F. Vinen. Classical character of turbulence in a quantum liquid. *Phys. Rev. B*, 61(2):1410–1420, January 2000.

[157] W. F. Vinen and J. J. Niemela. Quantum Turbulence. *J. Low Temp. Phys.*, 128(5):167–231, 2002.

[158] Jeffrey Yepez, George Vahala, Linda Vahala, and Min Soe. Superfluid Turbulence from Quantum Kelvin Wave to Classical Kolmogorov Cascades. *Phys. Rev. Lett.*, 103(8):084501, August 2009.

[159] Franco Dalfovo, Stefano Giorgini, Lev P. Pitaevskii, and Sandro Stringari. Theory of Bose-Einstein condensation in trapped gases. *Rev. Mod. Phys.*, 71(3):463–512, April 1999.

[160] Eugene P. Gross. Hydrodynamics of a Superfluid Condensate. *J. Math. Phys.*, 4(2):195–207, February 1963.

[161] L. P. Pitaevskii. Vortex lines in an imperfect Bose gas. *Sov. Phys. JETP*, 13:451, 1961.

[162] Russell J. Donnelly. *Quantized Vortices in Helium II*. Cambridge University Press, 1 edition, 1991.

[163] E. Madelung. Eine anschauliche Deutung der Gleichung von Schrdinger. *Naturwissenschaften*, 14(45):1004–1004, 1926.

[164] E. Madelung. Quantentheorie in hydrodynamischer Form. *Z. Physik*, 40(3-4):322–326, 1927.

[165] P. Clark di Leoni, P. D. Mininni, and M. E. Brachet. Helicity, topology, and Kelvin waves in reconnecting quantum knots. *Phys. Rev. A*, 94(4):043605, October 2016.

[166] R. Hnninen, N. Hietala, and H. Salman. Helicity within the vortex filament model. *Sci. Rep.*, 6:37571, November 2016.

[167] F. Brock Fuller. The Writhing Number of a Space Curve. *PNAS*, 68(4):815–819, April 1971.

[168] Joel Koplik and Herbert Levine. Vortex reconnection in superfluid helium. *Phys. Rev. Lett.*, 71(9):1375–1378, August 1993.

[169] Davide Proment, Miguel Onorato, and Carlo F. Barenghi. Vortex knots in a Bose-Einstein condensate. *Phys. Rev. E*, 85(3):036306, March 2012.

[170] Gregory P. Bewley, Matthew S. Paoletti, Katepalli R. Sreenivasan, and Daniel P. Lathrop. Characterization of reconnecting vortices in superfluid helium. *PNAS*, 105(37):13707–13710, September 2008.

[171] Jacob D. Bekenstein. Conservation law for linked cosmic string loops. *Phys. Lett. B*, 282(1):44–49, May 1992.

[172] Tsippy R. Mendelson. Cosmic String Helicity: Constraints on Loop Configurations, and the Quantization of Baryon Number. *arXiv:hep-th/9908194*, August 1999.

[173] Peter Akhmetev and Alexander Ruzmaikin. Borromeanism and Bordism. In *Topological Aspects of the Dynamics of Fluids and Plasmas*, pages 249–264. Springer Netherlands, 1992.

[174] Jerrold E. Marsden and Tudor S. Ratiu. *Introduction to Mechanics and Symmetry*. Springer New York, 1999.

[175] Jerrold E. Marsden, Tudor S. Ratiu, and Jrgen Scheurle. Reduction theory and the LagrangeRouth equations. *J. Math. Phys.*, 41(6):3379–3429, June 2000.

[176] P. J. Morrison. Hamiltonian description of the ideal fluid. *Rev. Mod. Phys.*, 70(2):467–521, April 1998.

[177] Nikhil Padhye and P. J. Morrison. Fluid element relabeling symmetry. *Phys. Lett. A*, 219(5):287–292, August 1996.

[178] Yuhji Kuroda. Symmetries and Casimir invariants for perfect fluid. *Fluid Dyn. Res.*, 5(4):273, March 1990.

[179] Yasuhide Fukumoto. A Unified View of Topological Invariants of Fluid Flows. *Topologica*, 1(1):003–003, 2008.

[180] Yasuhide Fukumoto and Hirofumi Sakuma. A Unified View of Topological Invariants of Barotropic and Baroclinic Fluids and their Application to Formal Stability Analysis of Three-Dimensional Ideal Gas Flows. *Procedia IUTAM*, 7:213–222, January 2013.

[181] R. Salmon. Hamiltonian Fluid Mechanics. *Ann. Rev. Fluid Mech.*, 20(1):225–256, 1988.

[182] C. J. Cotter and D. D. Holm. On Noethers Theorem for the EulerPoincar Equation on the Diffeomorphism Group with Advected Quantities. *Found. Comput. Math.*, 13(4):457–477, June 2012.

[183] Nikhil Padhye and P. J. Morrison. Relabeling symmetries in hydrodynamics and magnetohydrodynamics. *Plasma Phys. Rep.*, 22:869–877, October 1996.

[184] Carlo F. Barenghi and Nick G. Parker. Gross-Pitaevskii Model of the Condensate. In *A Primer on Quantum Fluids*, SpringerBriefs in Physics, pages 33–52. Springer International Publishing, 2016. DOI: 10.1007/978-3-319-42476-7_3.

[185] R. Kaiser, C. Westbrook, and F. David. *Coherent atomic matter waves - Ondes de matiere coherentes*. Springer-Verlag Berlin Heidelberg, 2001.

[186] Christian Miniatura, Leong-Chuan Kwek, Martial Ducloy, Benot Grmaud, Berthold-Georg Englert, Leticia Cugliandolo, Artur Ekert, and Kok Khoo Phua. *Ultracold Gases and Quantum Information*. Oxford University Press, 2011.

[187] Tanja Rindler-Daller and Paul R. Shapiro. Angular momentum and vortex formation in BoseEinstein-condensed cold dark matter haloes. *MNRAS*, 422(1):135–161, May 2012.

[188] Paul H. Roberts and Natalia G. Berloff. The Nonlinear Schrdinger Equation as a Model of Superfluidity. In *Quantized Vortex Dynamics and Superfluid Turbulence*, pages 235–257. Springer Berlin Heidelberg, 2001.

[189] Carlo F. Barenghi and Nick G. Parker. Vortices and Rotation. In *A Primer on Quantum Fluids*, SpringerBriefs in Physics, pages 79–110. Springer International Publishing, 2016. DOI: 10.1007/978-3-319-42476-7_5.

[190] Xian Zhi Wang. Cold Bose stars: Self-gravitating Bose-Einstein condensates. *Phys. Rev. D*, 64(12):124009, November 2001.

[191] Lev P. Pitaevskii and S. Stringari. *Bose-Einstein Condensation*. Clarendon Press, 2003.

[192] Robert L. Jerrard. Vortex filament dynamics for Gross-Pitaevsky type equations. *Ann. Scuola Norm-Sci.*, 1(4):733–768, 2002.

[193] Fernando Lund. Defect dynamics for the nonlinear Schrdinger equation derived from a variational principle. *Phys. Lett. A*, 159(4):245–251, October 1991.

[194] Catherine Sulem and Pierre-Louis Sulem, editors. *The Nonlinear Schrdinger Equation: Self-Focusing and Wave Collapse*, volume 139 of *Applied Mathematical Sciences*. Springer New York, New York, NY, 2004.

[195] G. P. Bewley and K. R. Sreenivasan. The Decay of a Quantized Vortex Ring and the Influence of Tracer Particles. *J Low Temp Phys*, 156(3-6):84–94, September 2009.

[196] Gregory P. Bewley. The generation of particles to observe quantized vortex dynamics in superfluid helium. *Cryogenics*, 49(10):549–553, October 2009.

[197] Renzo L. Ricca and Bernardo Nipoti. Gauss' linking number revisited. *J. Knot Theory Ramifications*, 20(10):1325–1343, October 2011.

[198] George Calugareanu. Lintgrale de Gauss et lanalyse des n euds tridimensionnels. *Rev. Math. pures appl*, 4(5), 1959.

[199] G. Calugareanu. Sur les classes d'isotopie des noeuds tridimensionnels et leurs invariants. *Czechoslovak Mathematical Journal*, 11(4):588–625, 1961.

[200] James H. White. Self-Linking and the Gauss Integral in Higher Dimensions. *Am. J. Math.*, 91(3):693–728, 1969.

[201] H. Seifert. ber das Geschlecht von Knoten. *Math. Ann.*, 110(1):571–592, December 1935.

[202] Alexander Ruzmaikin and Peter Akhmetiev. Topological invariants of magnetic fields, and the effect of reconnections. *Phys. Plasmas*, 1(2):331–336, February 1994.

[203] J. J. van Wijk and A. M. Cohen. Visualization of Seifert surfaces. *IEEE Trans. Vis. Comput. Graphics*, 12(4):485–496, July 2006.

[204] Mitchell A. Berger. Introduction to magnetic helicity. *Plasma Phys. Control. Fusion*, 41(12B):B167, 1999.

[205] H. K. Moffatt and Renzo L. Ricca. Helicity and the Calugareanu Invariant. *Proc. R. Soc. A*, 439(1906):411–429, November 1992.

[206] Martin W. Scheeler, Wim M. van Rees, Hridesh Kedia, Dustin Kleckner, and William T. M. Irvine. Complete measurement of helicity and its dynamics in vortex tubes. *(submitted)*, 2017.

[207] M. R. Dennis and J. H. Hannay. Geometry of Clugreanu's theorem. *Proc. R. Soc. A*, 461(2062):3245–3254, October 2005.

[208] Carlo F. Barenghi. Is the Reynolds number infinite in superfluid turbulence? *Physica D: Nonlinear Phenomena*, 237(1417):2195–2202, August 2008.

[209] Randall D. Kamien and Ricardo A. Mosna. The topology of dislocations in smectic liquid crystals. *New J. Phys.*, 18(5):053012, 2016.

[210] Hermann Bondi, Felix Arnold Edward Pirani, and Andrzej Trautman. *Lectures on general relativity, Vol. I.* Brandeis Summer Institute in Theoretical Physics, Prentice-Hall, Englewood Cliffs, NJ, 1965.

[211] R. Penrose and W. Rindler. *Spinors and Space-Time: Volume 1, Two-Spinor Calculus and Relativistic Fields*. Cambridge University Press, 1987.

[212] E. T. Infeld and B. L. van der Waerden. Die Wellengleichung des Elektrons in der allgemeinen Relativittstheorie. *Sitzungber. Preuss. Akad. Wiss.*, 9:380–402, 1933.

[213] L.D Landau and E.M. Lifshitz. *The Classical Theory of Fields*. Course of theoretical physics, Vol. 2. Butterworth-Heinemann, 1975.

[214] Tsutomu. Kambe. *Elementary fluid mechanics*. World Scientific, Hackensack, N.J.; London, 2007.

[215] Francis P. Bretherton. A note on Hamilton's principle for perfect fluids. *Journal of Fluid Mechanics*, 44(01):19–31, October 1970.